

AERITALIA
LABORATORIES
GROUP

TETHERED GRAVITY LABORATORIES STUDY

CONTRACT NAS 9-17877

ACTIVE CENTER OF
 GRAVITY CONTROL

TASK 1 FINAL REPORT

NOVEMBER 1989

(NACA-CR-185656) TETHERED GRAVITY
 LABORATORIES STUDY Final Report (Aeritalia
 S.p.A.) 149 p CSCL 22A

Unclas
 G3/29 0264773

A E R I T A L I A
societa'
aerospaziale
italiana
SPACE SYSTEMS GROUP

TETHERED
GRAVITY LABORATORY STUDY

DOC. : TG-RP-AI-021
ISSUE : 01
DATE : 15/NOV/89
PAGE : 1 OF 38

REPORT

TITLE : ACTIVE CENTER OF GRAVITY CONTROL
TASK REPORT

D.R.D. No : SE 1111 T

----- SIGNATURES AND APPROVALS ON ORIGINAL -----

PREPARED : F. LUCCHETTI *F. Lucchetti*
CHECKED :
APPROVED : I. BARRACO *I. Barraco*
AUTHORIZED : F. BEVILACQUA *F. Bevilacqua*

APPROVALS : on

STUDY MANAGER

P. MERLINA

P. Merlina 5.01.89

DATA MANAGEMENT : *Micelata* 11/12/88

DOCUMENT CHANGE RECORD

ISSUE-DATE	REASONS FOR CHANGE	AFFECTED PARAGRAPHS
01 15/NOV/89		

All information contained in this document are property of AERITALIA
S.A.I.p.A.. All rights reserved.

AERITALIA S.A.I.p.A. CAP. LIT. 337.500.000.000 INT. VERS.

A E R I T A L I A
societa'
aerospaziale
italiana
SPACE SYSTEMS GROUP

TETHERED
GRAVITY LABORATORY STUDY

DOC. : TG-RP-AI-021
ISSUE : 01
DATE : 15/NOV/89
PAGE : 2 OF 38

TABLE OF CONTENTS

1.0	FOREWORD, SCOPE AND PURPOSE
2.0	STATEMENT OF THE PROBLEM
2.1	SCIENCE MICROGRAVITY REQUIREMENTS
2.2	ISS ENVIRONMENT
3.0	TETHER C.O.G. CONTROL RATIONALE
3.1	BASIC EQUATIONS
3.2	TETHERED SYSTEMS SIZING
3.3	TETHER MASS
4.0	CONFIGURATION ANALYSIS
4.1	ASSUMPTIONS AND CRITERIA
4.2	CONFIGURATIONS RATIONALE AND RESULTS
5.0	OVERALL CONSIDERATIONS
5.1	SPACE STATION IMPACTS
5.2	CONFIGURATIONS TRADE-OFF
5.3	MAJOR FINDINGS AND RECOMMENDATIONS

REFERENCES

APPENDIX A PADUA UNIVERSITY FINAL REPORT

APPENDIX B SAO TASK 1 REPORT

A E R I T A L I A
societa'
aerospaziale
italiana
SPACE SYSTEMS GROUP

TETHERED
GRAVITY LABORATORY STUDY

DOC. : TG-RP-AI-021
ISSUE : 01
DATE : 15/NOV/89
PAGE : 3 OF 38

1.0 FOREWORD, SCOPE AND PURPOSE

This document is submitted in compliance with the requirements of contract NAS 9-17877. It constitutes the Task Report for Task 1 of the related Statement of Work, as per DRL: T-2067, DRD: SE 1111 T.

The focus of this document is on the utilization of Tether systems to improve the lowest possible steady-gravity level on the Space Station. In fact particular emphasis is placed by the microgravity community on the achievement of high quality microgravity conditions.

The purpose of this study is to explore the tether capability for active control of the center of gravity and to analyse possible tethered configurations.

The study on the acceleration environment of the Space Station has been performed by University of Padua, Principal Investigator - Prof. S. Bergamaschi, and it is reported in Appendix A.

The analysis of acceleration noise related to possible tether configurations has been performed by SAO, Principal Investigator - E. Lorenzini and it is reported in Appendix B.

2.0 STATEMENT OF THE PROBLEM

2.1 SCIENCE MICROGRAVITY REQUIREMENTS

The availability of an environment with a very low level of acceleration is one of the reasons for building the Space Station from the science point of view. This is even more true for future industrial and commercial use of space. The most severe requirements on the acceptable acceleration level come from the material processing community which regards a steady or low frequency acceleration of 1 micro-g as acceptable and one of 0.01 micro-g as desirable (in the frequency range 0 to 0.01 Hz). This very strict requirements are largely exceeded by the ISS specification which is 10 micro-g at all frequencies. The requirements drop quickly at higher frequencies and are 10 micro-g at 1 Hz and 1 millig at 100 Hz (see fig. 1, from Ref. 1).

Sensitive experiments can be mechanically insulated from the high frequencies acceleration sources with the proper devices. Steady or very low frequency accelerations are rather difficult to deal with in this manner so the only possible way of obtaining a good experimental environment lies in reducing the causes of the accelerations.

2.2 ISS ENVIRONMENT

From the phased program assembly configuration data it was possible to extract the relevant information for a definition of the actual steady or quasi-static micro-g environment on the ISS. Some assumptions were made in order to compute the forces. The two main ones are:

- Space Station in the nominal attitude position with all the solar panels perpendicular to flight direction (worst case for drag).
- Max attitude motion amplitude of 5 degrees and 0.02 degree/second max rate (worst case within the Space Station requirements).

For a detailed mathematical formulation please refer to appendix A.

The main sources of accelerations were found to be:

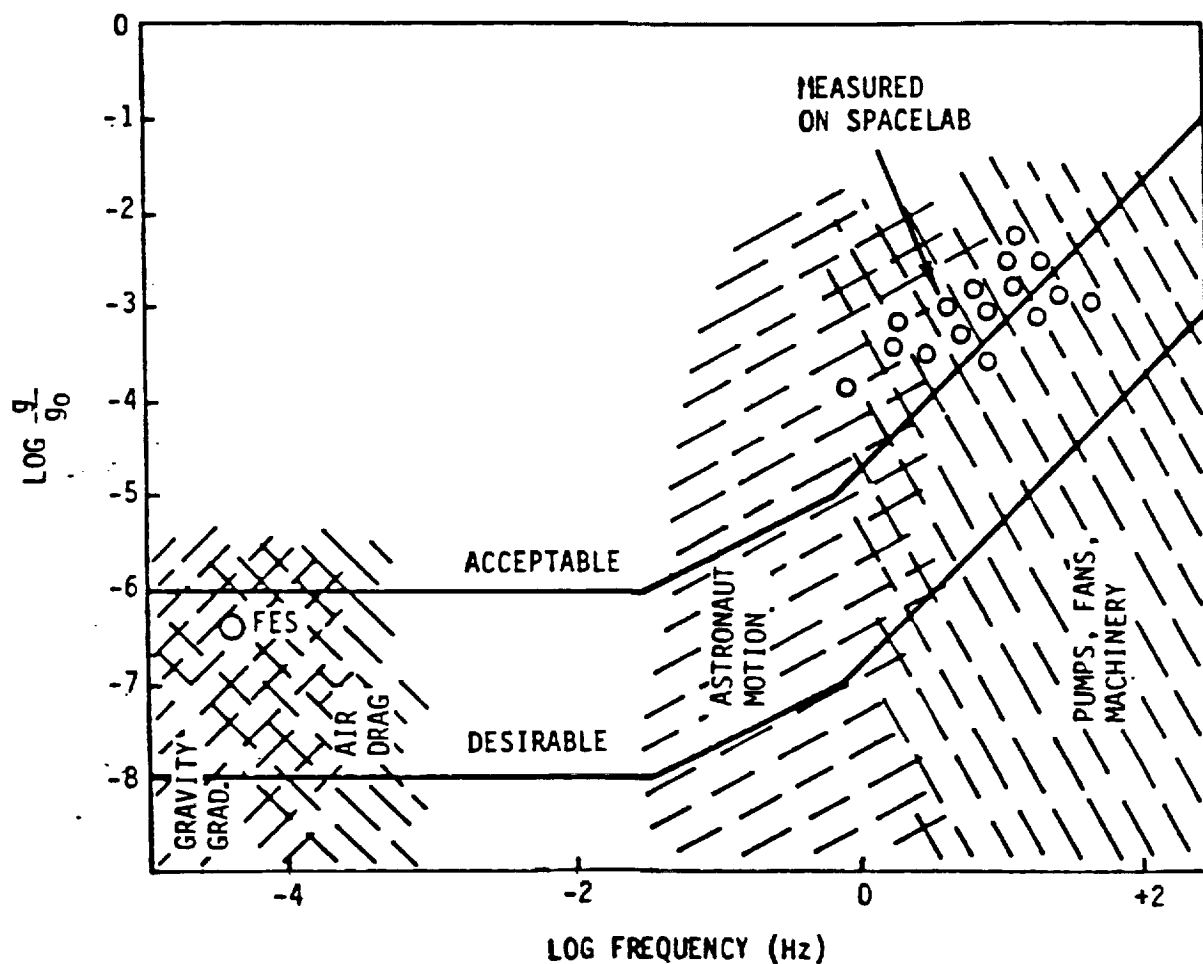


FIG. 1 - NAUMANN PROPOSED ACCELERATION LIMITS

- atmospheric drag which causes a steady acceleration equal on all the points of the ISS directed approximately along the flight direction (X axis);
- gravity gradient. The acceleration caused by the gravity gradient is almost steady (with little variations due to the orbital eccentricity) and depends on the distance from the ISS center of gravity (C.o.G.) along the local vertical and out of orbital plane direction. On the lab modules this acceleration is directed mainly along the local vertical.

In figure 2 the relative positions of the U.S. lab and C.o.G. are shown. The elliptical line is the envelope of the room within which the C.o.G. should lie in order to limit the value of gravity gradient acceleration to 1 micro-g in the whole laboratory.

The two dash lines limit the portion of the laboratory which is within the 1 micro-g requirements in OF2 and MB16 flights.

- Attitude motion. The acceleration due to the attitude motion assumed has a period which is a fraction of the orbital period (approximately one third) and depends on the distance from the C.o.G. being so rather large on the European and Japanese modules.

All these disturbances are approximately of the same order of magnitude in the U.S. module being of the order of 0.3 to 1 micro-g.

The accelerations depend on the Space Station configuration and location examined. Two configurations of the Space Station were singled out as important:

- 1) flight OF2 (end of phase 1);
- 2) flight MB16 (end of phase 2).

The main features of these configurations are reported in table 1. Two locations were thought to be particularly significant:

- a) center of the U.S. lab (which is one of the positions where the disturbances are lower)
- b) end of the European module (which is almost the worst case).

The four graphs reported in the following pages summarize the accelerations along the three axes as a function of time (fig. 3, 4, 5, 6).

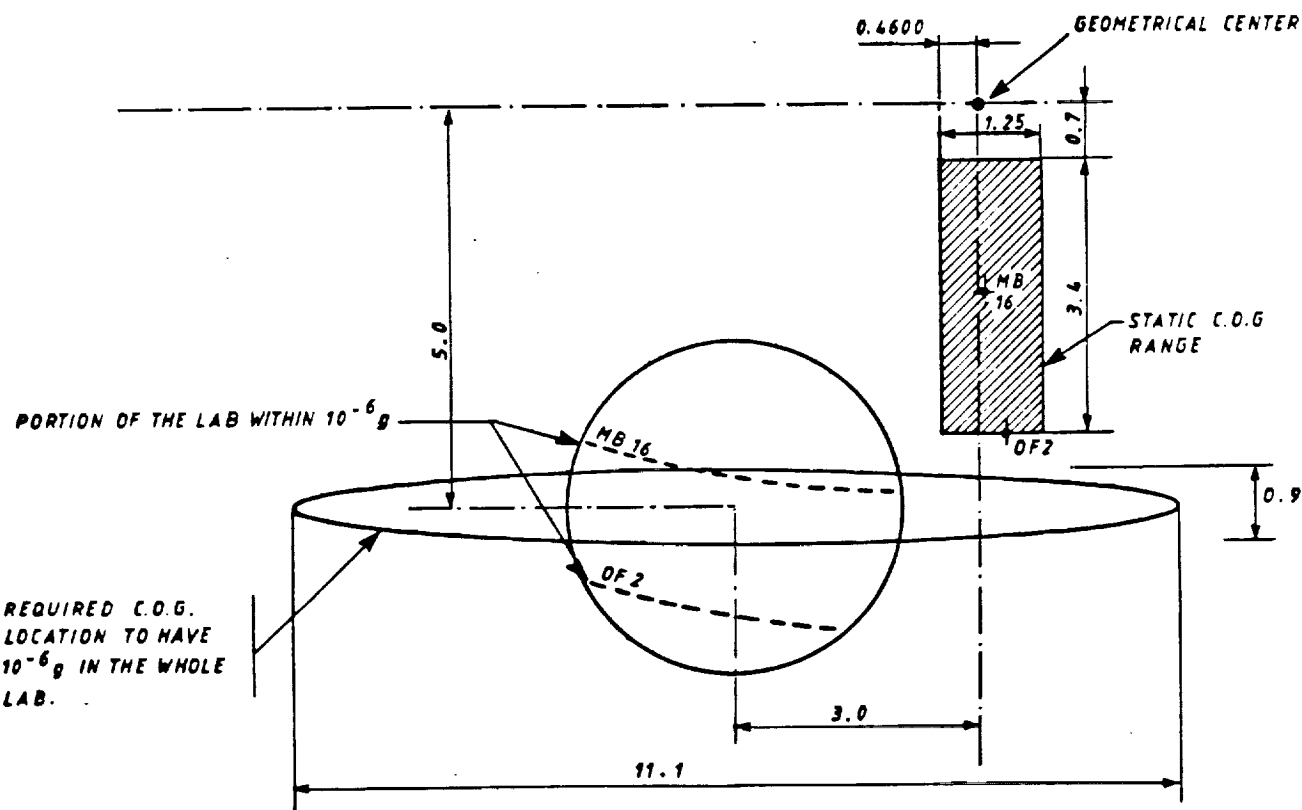


FIG. 2 - GRAVITY GRADIENT 1 MICRO-G ENVELOPES (U.S. LAB)

A E R I T A L I A
societa'
aerospaziale
italiana
SPACE SYSTEMS GROUP

TETHERED
GRAVITY LABORATORY STUDY

DOC. : TG-RP-AI-021
ISSUE : 01
DATE : 15/NOV/89
PAGE : 8 OF 38

Some observations can be made from the graphs:

- 1) mean value of the accelerations along X (which is due to the drag) does not change much between the four cases;
- 2) mean values of accelerations along Z, which are due to gravity gradient, are distinctly higher in the two MB16 cases;
- 3) the amplitude of acceleration oscillations is markedly higher on the end of the European lab (this is due to the effects of attitude motion).

The maximum overall acceleration is something of the order of 1 to 4 micro-g.

Other effects could increase the level of steady or quasi static accelerations but were not included mainly for lack of sufficient information. Among them there is, for instance, the effects of solar inertial pointing mode of the solar arrays which will cause a periodic torque on the ISS. Another example can be the low frequency components of the random disturbances interesting the Space Station. Obviously the analysis of these effects would require a detailed knowledge of the ISS which was not available.

In synthesis the accelerations due to deterministic causes are near the 1 micro-g level in all the cases considered and well above that on the European and Japanese modules.

A E R I T A L I A
societa'
aerospaziale
italiana
SPACE SYSTEMS GROUP

TETHERED
GRAVITY LABORATORY STUDY

DOC. : TG-RP-AI-021
ISSUE : 01
DATE : 15/NOV/89
PAGE : 9 OF 38

o DATA ON SPACE STATION

CONFIGURATION	OF2	MB16
MASS (KG)	204.5 10^3	258.8 10^3
ZCOG (M)	4.108	2.33

FROM
"PHASED PROGRAM
CONFIGURATION DATA"

- o MEAN ORBITAL RATE: $1.14 \cdot 10^{-3}$ RAD/SEC (366 KM)
- o TETHER SIZE DICTATED BY IMPACT PROBLEMS
- o MAX AMPLITUDE OF TETHER IN PLANE LIBRATIONS: $\pm 3^\circ$
- o DISTURBANCE CHARACTERISTICS: AMPLITUDE $\pm 5 \mu\text{G}$; FREQUENCY = n
- o SYSTEM DIMENSION OPTIMIZED WITH REFERENCE TO SYSTEM MASS AND SIZE
- o TETHER MATERIAL: ALUMINIUM

TABLE 1 - REFERENCE DATA AND ASSUMPTIONS

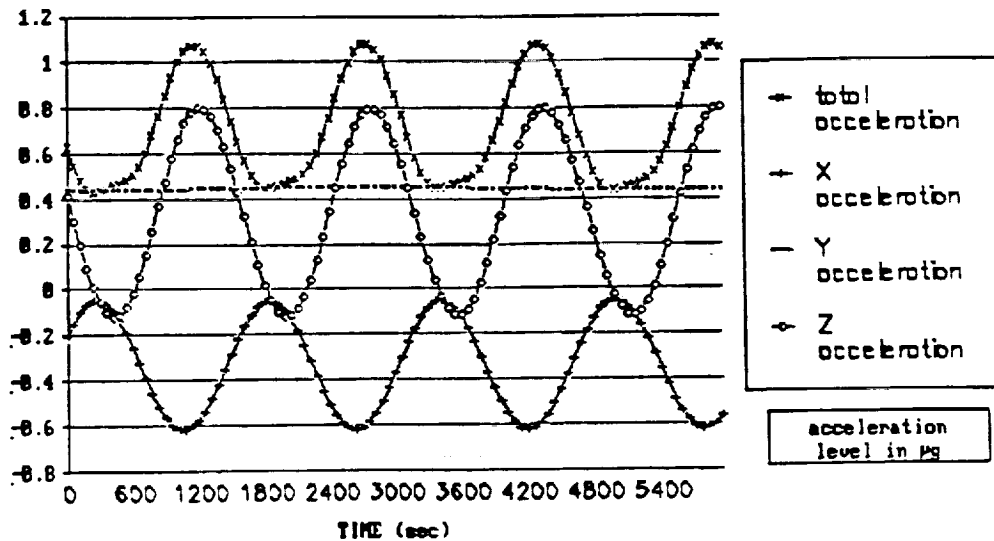


FIG. 3 - PHASE 1 (OF2) ACCELERATIONS DUE TO EXTERNAL SOURCES AND ROTATIONS. CENTER OF THE U.S. LAB

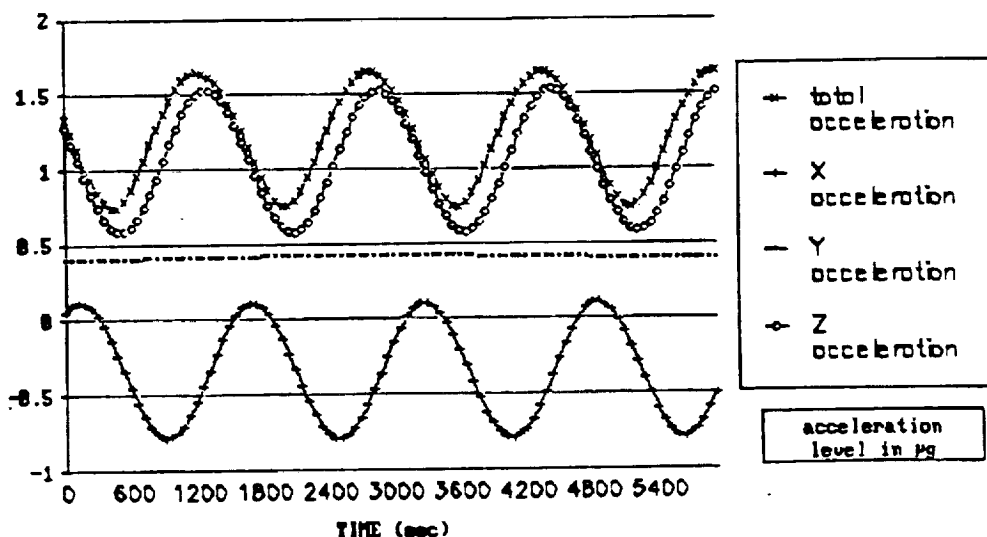


FIG. 4 - PHASE 2 (MB16) ACCELERATIONS DUE TO EXTERNAL SOURCES AND ROTATIONS. CENTER OF THE U.S. LAB

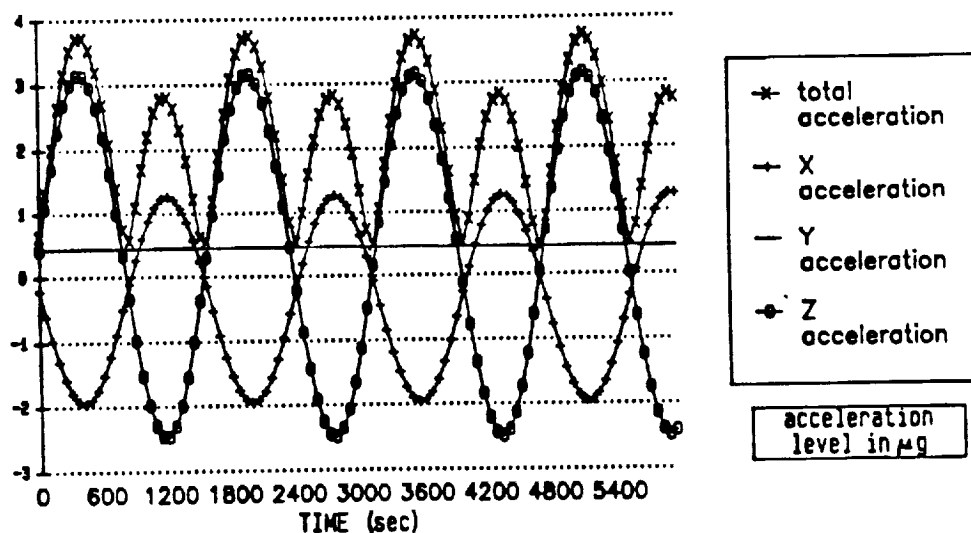


FIG. 5 - PHASE 1 (OF2) ACCELERATIONS DUE TO EXTERNAL SOURCES AND ROTATIONS. COLUMBUS END

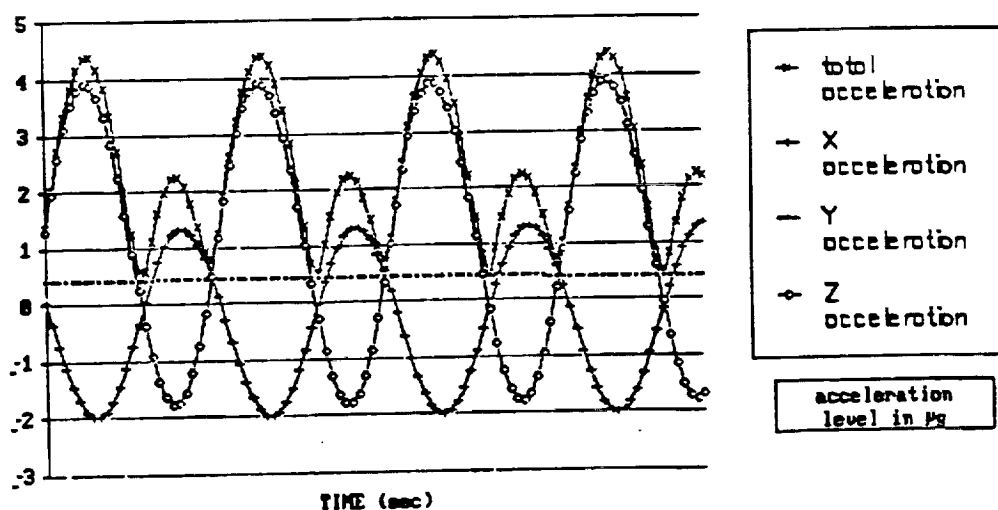


FIG. 6 - PHASE 2 (MB16) ACCELERATIONS DUE TO EXTERNAL SOURCES AND ROTATIONS. COLUMBUS END

3.0 TETHER C.O.G. CONTROL RATIONALE

The presence of a tethered system causes, in general, a displacement of the C.o.G. along the local vertical. This can be used to reduce the value of the gravity gradient acceleration along Z to an arbitrarily small value in a given point. Moreover with a periodic variation of tether length, periodic accelerations along Z axis can be counteracted. The effect of tethered system on accelerations along X and Y is, in general, quite small and was not examined in detail. Tether length variations can be used to damp attitude motion of the Space Station so reducing the g level due to centrifugal forces. This was not analyzed as it involves the general issue of Space Station attitude control which is beyond the scope of this study.

3.1. BASIC EQUATIONS

The basic method to reduce gravity gradient effects is to shift the C.o.G. until it is the nearest possible to the micro-g lab.

In the following a simple tether system with its tether attachment point placed in the geometrical center of the truss is assumed. The tether is aligned with the local vertical.

Assuming a static tether the C.o.G. shift is:

$$z = m_{cw} l / (m_{cw} + m_s) \text{ (assuming a mass-less tether)}$$

where:

l = tether length
z = C.o.G. shift along z
m_{cw} = mass of the counterweight
m_s = station mass

This means, in our case, that assuming:

$$\begin{aligned} z &= 2 \text{ m} \\ m_{cw} &= 500 \text{ kg} \\ m_s &= 100 \cdot 10^3 \text{ kg} \end{aligned}$$

Then

$$l = 400 \text{ m}$$

With these values (roughly applicable to MB-7) we reduce the gravity gradient along z to a nominal zero but we still have a gravity gradient effect due to the C.o.G. shift along y which is approx

$$a_y = 0.6 \mu g$$

A few calculations show that with

tether length 100 to 200 meters
counterweight mass 150 to 750 kg

we could be able to make null the gravity gradient along
z. In this way we could reduce the value of overall
gravity gradient from a range
1.2 ÷ 0.4 μ g without tethers
to the range
0.6 ÷ 0.4 μ g with tethers

C.o.G. shift along y would involve extremely large masses
(order of 5 to 10% of Space Station mass).
The periodic perturbations can be compensated with a
periodically varying tether length.
In fact let
 z_1 = position of the laboratory along z from the C.o.G.
of the Space Station + tethered mass

z_s = position of the C.o.G. of the Space Station alone

z_{cw} = position of the tethered mass

then:

$$z_1 = z_s + d$$

d = distance between Space Station C.o.G. and laboratory
= constant

$$z_{cw} = z_s + l$$

$$l = \text{tether length} = l_0 - l_c \sin(\omega t)$$

$$l_0 = \text{mean tether length}$$

$$l_c = \text{varying portion of tether length}$$

$$\omega = \text{frequency of the motion} = \text{disturbance frequency}$$

It can be shown that with a periodic acceleration

$$a = a_0 \sin(\omega t)$$

it has to be

$$\ddot{z}_1 - 3n^2 z_1 = a_0 \sin(\omega t) \quad 1)$$

to obtain a null value of residual acceleration along z.
From 1) it can be found

$$l_o = \frac{m_s + m_{cw}}{m_{cw}} d \quad 2)$$

$$l_c = \frac{a_o}{w^2 + 3n^2} * \frac{m_s + m_{cw}}{m_s} \quad 3)$$

Another important consideration which has to be done when one is dealing with varying length tethers is about their inherent coupling between longitudinal and pendular motion.

Let

θ = in-plane angle between the tether and local vertical

I = moment of inertia of the system around its C.o.G.

$$= \frac{m_s * m_{cw} l^2}{(m_s + m_{cw})}$$

Then from the conservation of angular momentum

$$\frac{\delta (I \dot{\alpha})}{\delta t} = 3 n^2 I \theta \quad 4)$$

for small value of θ with

$$\dot{\alpha} = \dot{\theta} + n$$

Expanding equation 4) for

$$l_o \gg l_c \quad \text{and} \quad \theta \ll n \quad \text{and} \quad l = l_o - l_c \sin(w t)$$

$$\theta_{max} = 2 \frac{l_c}{l_o} \frac{w n}{3n^2 - w^2} \quad 5)$$

which for $n = w$ it reduces to

$$\theta_{max} = l_c / l_o$$

where θ_{max} is the max angle between tether and local vertical.

If we want to keep θ small (<2.5 deg.) for $w = n$ it has to be

$$l_o > 20 l_c \quad 6)$$

This is an heavy constraint on the tether length.
Combining equations 2,3 and 5 we obtain

$$a_0 = 4 d n^2 \theta_{\max} \quad \text{if } w = n \quad 7)$$

This means that to be able to compensate large values of environmental periodic disturbances we need a large value of d (if θ is small).

Summarizing:

In the case of periodic variation of tether length another constraint appears due to the fact that changes of the tether length cause deviation of the tether direction from the local vertical. In the case of harmonic variations of tether length, the tether will librate in the orbital plane around its nominal position with angular amplitude which is proportional to the ratio between tether length variation and tether average length. So, given that it is desirable that these oscillations are limited, a constraint is imposed on the ratio between average length and its variation.

3.2 TETHERED SYSTEM SIZING

Four tethered configurations have been analysed and found applicable to the phase 1 Space Station.

1) Single tether configuration

The simplest possible tethered system is one with

- a) only one tether (deployed downwards)
- b) tether attachment point (T.A.P.) on the yaw axis of the Space Station.

Using the previously introduced symbology it has to be

$$m_{cw} (1 - d) = m_s d$$

The main advantage of this system is its extreme simplicity.

The disadvantages are:

- Low tether tension
[the tether tension is $T = 3 n^2 m_{cw} (1-d)$]
- Clearance problem for the presence of the tether in the core Space Station zone.
- Low level of periodic accelerations which can be counteracted (equation 7))

2) Double tether centered configuration

This system is made by two tethers (one deployed upwards and the other downwards) with their T.A.P.'s located along the local vertical. In order to zero the gravity gradient along z axis it has to be

$$m_1 (l_1 - D) = m_2 (l_2 + D) + m_s * D \quad 8)$$

m_1, l_1 for the downward tether

m_2, l_2 for the upward tether

D = distance of μg lab from S.S. C.o.G.

This is the simplest system which is able to counteract large value of periodically varying acceleration with only one mobile tether.

Equation 7) can now in fact be written as

$$a_o = \frac{4 n^2 \theta_{\max} [m_2 (l_2 + D) + m_s D]}{m_s} \quad 9)$$

Again a big disadvantage of this configuration is the fact that all the space near the local vertical (both downwards and upwards) is of problematic use for clearance problems.

3) Double tethered shifted configuration

The system is made by two tethers (one upward and the other downward with their T.A.P. shifted orthogonally to the orbital plane.

Equation 8) and 9) still hold but added constraints are present.

In fact, to avoid undesired torques around Y and x axis it has to be

$$m_1 l_1 x_1 = m_2 l_2 x_2 \quad 10)$$

$$m_1 l_1 y_1 = m_2 l_2 y_2$$

being

x_1, y_1 coordinate of the downward tether T.A.P.

x_2, y_2 coordinate of the upward T.A.P.

The big benefit of this system is that in this way the space wear the local vertical can be freed from clearance problems.

With only one mobile tether (for periodic disturbances) the T.A.P. of one of the tether has to be moved according to equation 9) to avoid undesired torquers. If y is the coordinate of the mobile system it has to be:

$$2 \frac{y_{\max} - y_{\min}}{y_{\max} + y_{\min}} = 2 \frac{l_c}{l_o}$$

that is:

$$\frac{y_{\max} - y_{\min}}{y_{\text{average}}} = 0.05 \text{ if equation 6 applies}$$

and for a system with $y_{\text{average}} = 40 \text{ m}$

$$y_{\max} - y_{\min} = 2 \text{ m.}$$

4) Elevator configuration

This configuration is made by two fixed (centered) tether along one of which a mobile mass (called elevator) can move.

In this case

$$m_1 (l_1 - d) + m_e (l_e - d) = m_2 (l_2 + d) + m_s d$$

where

m_e, l_e apply to the mobile mass

This configuration is inherently more stable than the others but a big increase in complexity is called for the elevator design.

3.3. TETHER MASS

All considerations up to this point do not include the effects of tether mass. In reality tether mass has a profound impact on tethered systems configuration and behaviour.

First of all it can now be considered what happens in a single tether static system.

The C.o.G. shift is

$$m_s z_s = \mu \frac{l^2}{2} + m_{cw} l$$

with μ = linear tether density

The total tethered system mass is instead

$$M = \mu l + m_{cw}$$

For a given value of z_s the total tethered mass is then

$$M = \frac{m_s z_s}{l} + \frac{\mu l}{2}$$

and the minimum M can be found to be (if μ is constant w.r.t. l) with:

$$l = 2 \frac{m_s z_s}{\mu}^{1/2}$$

$$M = 2 \frac{m_s z_s}{\mu}^{1/2} * \mu$$

$$m_{cw} = 0$$

This conclusion, although surprising, can be better understood if we think to the extreme case in which $\mu = 0$. In this case the minimum mass system would be one with counterweight mass extremely small and extremely far from Space Station.

On one hand it can be shown that for any desired value of z_s a minimum mass tethered system can be defined; this choice leads to rather long system (near to maximum possible tether length) in which the end mass is only a small fraction of the overall tethered system mass.

On the other hand, the tether will be a costly and delicate component of the system, whereas the end mass can be relatively cheap as it can be made by disposable items and it can even pay for itself as suitable experiment can be conceivably placed as end mass. Even from the pure dynamic standpoint a light end mass is not desirable as it implies very low tether tension near the end and this is a condition which it is better to avoid.

The tether section is determined, more than by structural consideration, by the problem of meteoroids and debris impacts. A complete assessment of the problem is not within the scope of this study, but some evaluations were made with the following assumptions:

a) Meteoroids distribution

$$\log_{10} N_{\text{met}} = -14.7 - 1.213 \log_{10} m_{\text{met}}$$

N_{met} = meteoroids per second per square meter

m_{met} = meteoroid mass

b) Debris distribution

$$\log_{10} N_{\text{debris}} = -2.52 \log_{10} D_{\text{deb}} - 5.46$$

N_{debris} = number of debris for square meter for year

D_{deb} = debris diameter (centimeters)

c) Tether cut

The tether is assumed to be cut when is completely penetrated by the impacting mass.

Here it can be said that, for a long duration tether system, tether masses of the order of hundreds of kg per km are expected.

4.0 CONFIGURATION ANALYSIS

4.1 ASSUMPTIONS AND CRITERIA

The main assumptions used are reported in table 1. The rationale for these assumptions are:

- mean orbital rate = $1.14 \cdot 10^{-3}$. An average value is used which is adequate for orbital rate at minimum and maximum Space Station height;
- tether size as already said is dictated by impact problem. In our study a survival probability of 95% over a year was considered acceptable. The meteoroids and debris distribution are excerpted from ref. 2 and 3. See fig. 7 for the values used for tether diameter as a function of tether length. The tether rupture condition was assumed to be tether complete penetration. The one wall structure Equation of Fish and Summers (NASA SP9013) was used for assessment of meteoroids penetration;
- max. amplitude of tether in plane librations is an arbitrary value which is thought to be reasonable. This value of 3 degrees leads to a ratio between average tether length and tether length variation near to 20;
- the amplitude of disturbance is again a reasonable arbitrary value (possibly greater than the actual value). The frequency of this harmonic disturbance equal to the mean orbital rate was selected as many source of disturbance have this frequency (solar panel motion, night - day density variation, eccentricity of the orbit). The disturbance is assumed to be only along the Z axis and of 5 micro-g amplitude;
- system dimension optimization criteria. The criteria used is: choice of the minimum length system which has a mass at most 20% greater than the minimum mass system. This was done to reduce tether length (approx by 40%) to reasonable values;
- tether material choice: aluminum. In many studies and in the foreseen actual flight the adopted tether material is Kevlar basically for its good stiffness to weight and strength to weight ratios; in our case the choice of aluminum was made as we are interested to the problem of meteoroids impact.

MINIMUM TETHER DIAMETER REQUIRED BY IMPACT PROBLEMS

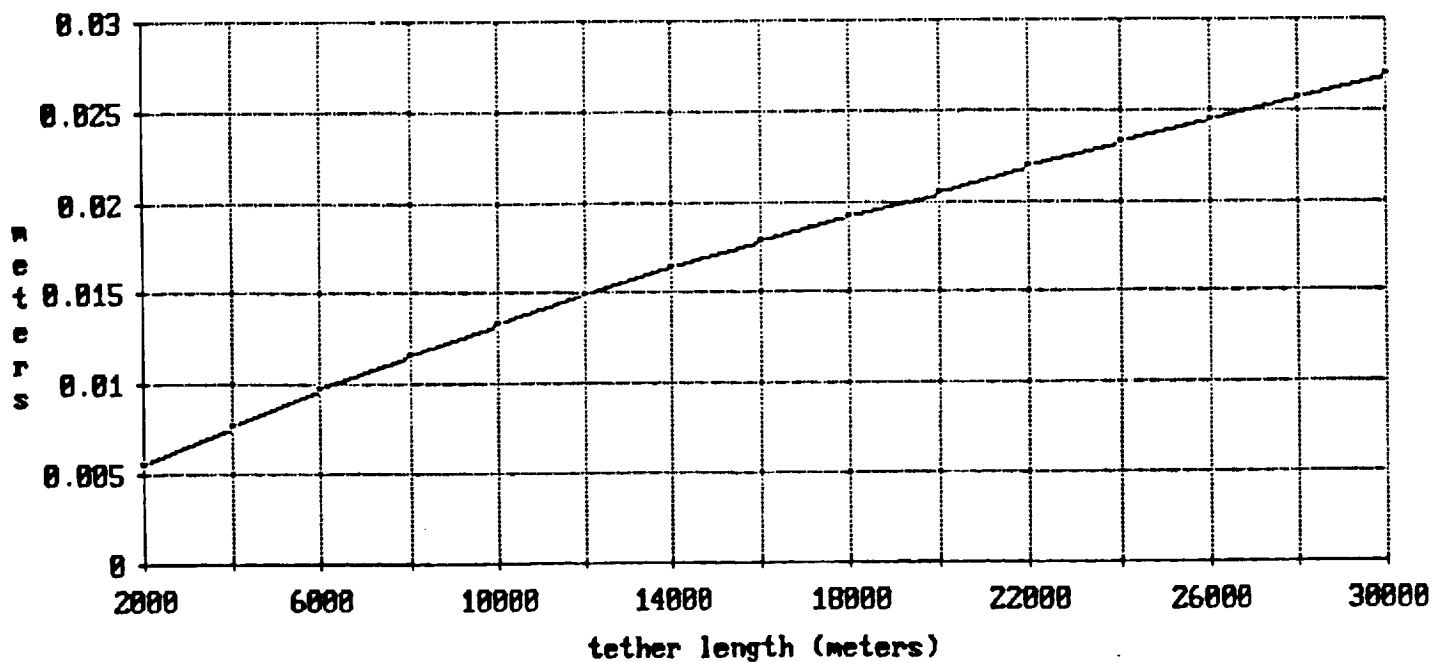


FIG. 7 - MINIMUM ALUMINUM TETHER DIAMETER REQUIRED BY IMPACT PROBLEMS (95% SURVIVAL PROBABILITY OVER A YEAR)

Material endurance against meteoroids impacts grows with Young's module and density. Kevlar and other composite materials have the problem that, although their Young's module is quite high along the fiber direction (which will be the tether direction), this is not so (being lower by an order of magnitude) in the direction orthogonal to the fibers, which is the direction which will be interested by most of the hits. Aluminum has instead a reasonable isotropic Young's module and the relatively large amount of data on hypervelocity impacts on aluminum makes its choice a sensible one as relevant equations are available.

4.2 CONFIGURATIONS RATIONALE AND RESULTS

Four tethered system configurations were selected as basis for our analysis at the end of phase 1 and phase 2 Space Station.

Except for the double tether shifted configuration (of which more will be said later) the tether attachment point coordinates have to have the same values of X and Y of the C.o.G. in order to avoid undesired torques. This implies two things:

- 1) In phase 1 the tether attachment point (henceforth T.A.P.) should be between the two U.S. modules, shifted along the - X direction with respect to the geometrical center of the middle boom. During phase 2 the T.A.P. should be placed on the upper and lower booms.
- 2) The T.A.P. would have to be moved with every major C.o.G. shift along X and Y direction.

The tethered system configurations were dimensioned assuming that we want to achieve a nominal zero value of gravity gradient acceleration along Z in the center of the U.S. laboratory.

a) Single tether configuration

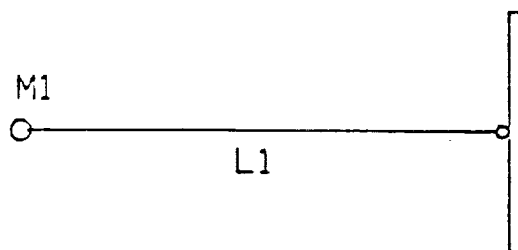
The simplest system is made by a single tether pointing downwards. This system has an intrinsically low capability of dealing with dynamic disturbances, but can make null the steady acceleration along Z in a given point. The main features of this configuration at the end of the two phases are in table 2. As it can be seen light and relatively small systems are sufficient. In the phase 1 the resulting length is lower than 2 km and the end mass falls so inside the zone where Space Station full control of every moving object is assumed.

A E R I T A L I A
societa'
aerospaziale
italiana
SPACE SYSTEMS GROUP

TETHERED
GRAVITY LABORATORY STUDY

DOC. : TG-RP-AI-021
ISSUE : 01
DATE : 15/NOV/89
PAGE : 23 OF 38

SINGLE TETHER



	END MASS M_1 (KG)	TETHER LEN. L_1 (m)	TETHER MASS M_T (KG)
PHASE I (OF2)	70.4	1660	79
PHASE II (MB16)	134.8	2766	230

TABLE 2 - SINGLE TETHER CONFIGURATION DATA

This can not be accomplished in case of tether severage unless dedicated hardware is placed on the end mass. Bigger tether length would lead to extremely low end masses complicating so tether dynamics. In phase 1 the C.o.G. shift due to tether would reduce the accelerations along z only by few tenths of micro-g so it does not seem worthwhile to implement such a system for such a small result. A big disadvantage of this configuration is that in phase 1 the T.A.P. has to be placed between the U.S. modules with the consequent clearance problems. In phase 2 the gravity gradient acceleration along Z is nearly 1 micro-g so the use of a tethered system is more interesting, furthermore payloads placed on the upper and lower booms can shift sensibly the C.o.G. and this can be counteracted easily by changing tether length by a fraction. In summary the use of a single tether appears to be appropriate only in the phase 2.

b) Double tether centered system

The system is made by two tethers with their T.A.P.'s placed along the local vertical through the C.o.G. The tether pointing downward is the mobile system and the fixed one is pointing upward (this is only an assumption. There is no need to have the downward system as the mobile one). A sketch of the configuration and the numerical result are reported in table 3.

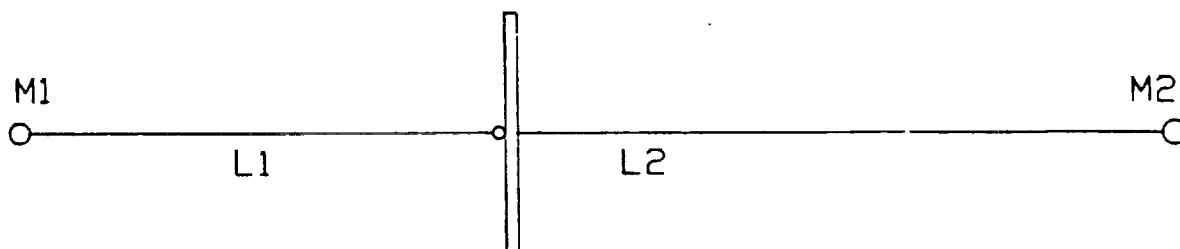
The two tethers are not identical as in the dimensioning of the mobile system a big length is an advantage in reducing the tether in-plane librations. This configuration is the simplest which can counteract both static and dynamic disturbances to a significant degree. In fact, for the single tether configuration, given that a small static C.o.G. shift is sufficient, a relatively short system is required. This implies, given that the ratio between tether length variation and average tether length is constrained to be $\ll 1$, that only small variations of the C.o.G. position are achievable with periodic elongations of the tether. The use of a tether long enough to be able to cope with the assumed dynamic disturbances would cause a large average C.o.G. shift. This can be counteracted by a second tether (fixed) which balances the average effect of the mobile one.

A E R I T A L I A
societa'
aerospaziale
italiana
SPACE SYSTEMS GROUP

TETHERED
GRAVITY LABORATORY STUDY

DOC. : TG-RP-AI-021
ISSUE : 01
DATE : 15/NOV/89
PAGE : 25 OF 38

DOUBLE TETHER CENTERED CONFIGURATION



	MOBILE TETHER SYSTEM			FIXED TETHER SYSTEM		
	END MASS M_1 (KG)	TETHER LEN. L_1 (m)	TET. MASS M_{T1} (KG)	END MASS M_2 (KG)	TET. LEN. L_2 (m)	TET. MASS M_{T2} (KG)
PHASE I (OF2)	3044	8305	2473	5388	5919	1175
PHASE II (MB16)	3649	8877	2866	6311	6350	1370

TABLE 3 - DOUBLE TETHER CENTERED CONFIGURATION DATA

From the numerical results it can be seen that the tethered systems are rather similar in the two cases at the end of phase 1 and phase 2, so possibly the same hardware could be used in both cases. The biggest problem of this configuration is that of clearance. In fact, during phase 1, the zone in proximity of the core Space Station is interested by tethers both in downward and upward directions.

With reference to the other configurations this one is massive, large and of medium complexity.

c) Double tethered shifted configuration

In the intent of overcoming the clearance problem of the double tether configuration a shift of the T.A.P.'s along Y direction is possible. The double tether shifted configuration is almost identical to the centered one (see table 4) except that the T.A.P.'s are shifted along Y axis by approx 30 m from the middle point of the transverse boom. This configuration is not applicable to phase 2 Space Station where in any case the clearance problem in the immediate proximity of the U.S. lab. does not exist being the T.A.P.'s on the lower and upper booms. A problem which affects this configuration is the fact that to avoid undesired torques one T.A.P. has to be shifted periodically in phase with tether length variations.

The average distances of the T.A.P.'s from the C.o.G. are slightly different as they do not balance each other exactly in order to place the overall C.o.G. in the center of the U.S. labs. The increase in complexity of the system due to the mobile T.A.P. issue probably outweighs the elimination of the clearance problems.

d) Elevator configuration

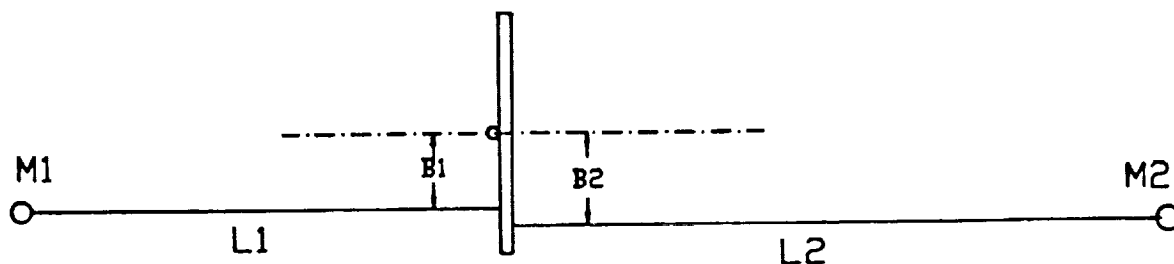
This configuration is made by two fixed centered tethers, on one of which (the downward one) a mobile mass, henceforth called elevator, is present. This mobile mass accomplishes the same function of the mobile tether but the elevator configuration is intrinsically more stable than the double tethered centered one; in fact the end mass on the tether on which the elevator is placed acts as a stabilizing device for the tether in plane librations.

A E R I T A L I A
societa'
aerospaziale
italiana
SPACE SYSTEMS GROUP

TETHERED
GRAVITY LABORATORY STUDY

DOC. : TG-RP-AI-021
ISSUE : 01
DATE : 15/NOV/89
PAGE : 27 OF 38

DOUBLE TETHER SHIFTED CONF.



	MOBILE TETHER SYSTEM					FIXED TETHER SYSTEM			
	END MASS	TET. LEN.	TET.MASS	SHIFT	RANGE	END MASS	TET. LEN.	TET.MASS	SHIFT
	M_1 (KG)	L_1 (m)	M_{T1} (KG)	B_{10} (m)	ΔB_1 (m)	M_2 (KG)	L_2 (m)	M_{T2} (KG)	B_2 (m)
PHASE I (OF2)	3044	8305	2473	29.84	± 1.43	5388	5919	1175	30

TABLE 4 - DOUBLE TETHER SHIFTED CONFIGURATION DATA

The study of this system is analytically more complex than that of the other ones as an added degree of freedom is present. To simplify the dimensioning process it has been assumed that the elevator mass and the end mass of the tether on which the elevator moves are equal. This is reasonable as the elevator mass could not be much greater than the end mass otherwise the stabilizing effect would be too small; on the other hand an end mass much greater than the elevator mass does probably not represent an efficient mass distribution.

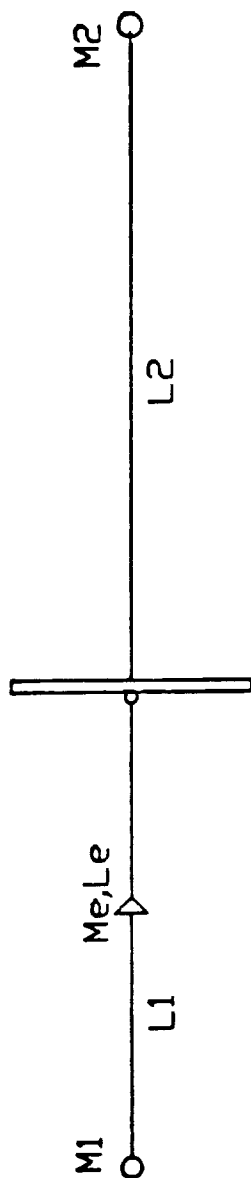
The average position of the elevator was determined assuming that the minimum distance between the elevator and the Space Station is 500 m.

From those conditions and from the knowledge of the possible excursions of the elevator the system was dimensioned with the same criteria used in the previous configurations.

The numerical results (see table 5) show that elevator configurations, quite similar in the two phases, are noticeably smaller and lighter than the other double tether systems and further optimization appears possible. The same clearance problem found in the double tether centered configuration is present while the elevator design causes a big increase in system complexity. Again as in the double tether shifted configuration, an enhancement on certain properties of the system leads to an increase in complexity which questions its worthiness.

Other tether configurations are possible, for instance a shifted elevator system or an increase to three or four of the tethers number are thinkable, but these solutions were judged too complex and full of uncertainties to be investigated at this stage.

DOUBLE TETHER + ELEVATOR



	TETHER SYSTEM 1			TETHER SYSTEM 2			ELEVATOR	
	ENDMASS M_1 (KG)	TET. LEN. L_1 (m)	TET. MASS M_{T1} (KG)	END MASS M_2 (KG)	TET. LEN. L_2 (m)	TET. MASS M_{T2} (KG)	MASS M_e (KG)	STATIC POS. L_e (m)
PHASE I (OF2)	2250	5711	1087	3463	5024	823	2250	1642
PHASE II (MB16)	2500	6505	1444	4091	5414	968	2500	1801

TABLE 5 - DOUBLE TETHER + ELEVATOR CONFIGURATION DATA

5.0 OVERALL CONSIDERATIONS

5.1 SPACE STATION IMPACTS

The side effects of the presence of tethered systems on the Space Station are to be assessed with care as they can be decisive on an evaluation of the concept soundness. Four are the main categories on which tethered system impacts can be classified (see table 6).

- a) Operational. In this category fall all the problems related to tether clearance which will increase the difficulties on proximity manoeuvres, Shuttle docking, rendezvous and EVA. Furthermore Space Station reboosting will probably require careful monitoring to avoid exceedingly large tether oscillations. Tether deployment and retrieval are, per se, major operations which will require dedicated hardware, software and crew time. The clearance problem is crucial during phase 1 for the configurations with two centered tethers being all the zone near the lab of limited accessibility.

The problem is somewhat lessened on the single tether configuration where only half of the space is interested by tether presence and on the double tether shifted configuration where the zone near the lab is free from tether interference. In phase 2 the situation betters for all the configuration given that the T.A.P.'s are on the upper and lower booms.

- b) Disturbances. The disturbances included in this category are due to tethers acting on the Space Station and on the U.S. module in particular. In fact, even if tether systems can reduce the accelerations due to forces acting on the Space Station, they can be sources of dynamic noise. Possible causes of these noises are, for instance, the quick tether length variations due to thermal expansion at local dawn and sunset. In the SAO report it is shown that adopting a careful choice of vibration dampers it is possible to reduce the value of these accelerations to 1 micro-g for the double tether centered system, to 0.6 micro-g for the elevator configuration and to a mere 0.01 micro-g for the single tether configuration.

In any case these disturbances would have a relatively high frequency (0.5 Hz) and short duration (few minutes). Another source of noise is the atmospheric drag which is not negligible in so long tethers.

Obviously the effect of these disturbances is rather low when the T.A.P.'s are on the upper and lower booms. During phase 1 only average importance could be annexed to disturbances in the case of the single tether configuration, thank to its lightness, and in the case of the shifted configuration where the distance between the T.A.P. and the lab. damps the mechanical noise. The worst cases are again the two configurations with centered double tethers during phase 1 where heavy systems are attached quite near to the lab's.

- c) Tether severage. The probability of tether severage due to meteoroids hits is imposed to be equal for all the tethers but the consequences are quite different in the various configurations. The position of the T.A.P. far from the lab during phase 2 reduces the risk of the severed tether hitting the Space Station core. In phase 1 the single tether, light and low tensioned, presents a reduced risk compared to the heavy double tether systems. Possibly the worst case is the double tether shifted configuration.
- In that case, the main problem is due to the fact that in case of rupture a large torque (of the order of thousands of $N \cdot m$) acts around the roll axis unless the surviving one is immediately severed. This requires continuous monitoring of tether tension and swift decision and action (under this torque the Space Station can roll of 45 degrees in five minutes).
- d) Attitude control. The tether influence on attitude control has many aspects and not all of them are negative. Basically two are the tether effects:
- if the T.A.P.'s are not on the C.o.G. there is an increase in the stiffness of the system around pitch and roll axis. If the Space Station departs from its nominal attitude, the tethers give rise to a restoring torque proportional to T.A.P. distance from C.o.G. so this stiffness enhancement is more pronounced in phase 2. Tether generated torques can be beneficial in stabilizing the Space Station against environmental torques, but, at the same time, they hinder the possibility of large attitude manoeuvres. These torques are proportional to tether length and mass so they are lower in the case of the single tether;
 - the tethers can cause a change in the distance between C.o.G. and center of pressure as they modify the mass and area distribution. This fact can be used to change the aerodynamic torque.

TETHER SYSTEM CONFIGURATION									
IMPACT CATEGORIES	SINGLE TETHER		DOUBLE CENTERED TETHER		DOUBLE SHIFTED TETHER		DOUBLE TET. + ELEVATOR		
	PHASE I	PHASE II	PHASE I	PHASE II	PHASE I	PHASE II	PHASE I	PHASE II	
OPERATIONAL	MEDIUM	LOW	HIGH	MEDIUM	MEDIUM	N.A.	HIGH	MEDIUM	
DISTURBANCES	MEDIUM	LOW	HIGH	LOW	MEDIUM	N.A.	HIGH	LOW	
TETHER SEVERAGE	MEDIUM	LOW	HIGH	MEDIUM	HIGH	N.A.	HIGH	MEDIUM	
ATTITUDE CONTROL (MAY BE BENEFICIAL)	LOW	MEDIUM	HIGH	HIGH	HIGH	N.A.	HIGH	HIGH	

TABLE 6 - TETHER SYSTEMS IMPACTS ON SPACE STATION

5.2 CONFIGURATIONS TRADE-OFF

A summary of the leading dimensions of the four tether configurations in the two phases is reported in table 7. The single tether configuration, which is able to counteract steady accelerations, is smaller and lighter by an order of magnitude than the others, whereas the elevator configuration is smaller and lighter than the other double tether configurations by some ten percent.

In phase 1 the C.o.G. appears to be close enough to U.S. lab. so that the 1 micro-g level is attained in nearly the whole lab.

Periodic accelerations of low frequency seem to be within the 1 micro-g level. This fact and the number of problems due to the position of T.A.P. near the lab. (especially clearance problems) lessen the worthiness of double tether systems in phase 1. The double tether shifted configuration appears too complex (and dangerous in case of tether severage) to be a sensible solution given the limited results which can be achieved. The single tether seems to be the only configuration with a limited impact on the Space Station but its usefulness is limited given the already low level of steady acceleration in phase 1.

During phase 2 the steady accelerations are higher than 1 micro-g in the most part of the lab and could be reduced to 0.5 micro-g using tethered systems. The T.A.P. is placed on the upper or lower boom reducing greatly the clearance problem and the disturbance transmitted by tethers to the labs.

In general the phase 2 appears a more adequate environment for C.o.G. control by tether systems. The use of a single tether is advisable to counteract steady accelerations and will be required if large mass distribution changes (due for instance to large payloads placed on the upper boom) take place.

The dynamic control of periodic disturbances of the assumed magnitude requires long and heavy systems. Only if it can be demonstrated that the actual disturbances are much lower than the assumed ones, more manageable systems can be used, but in that case tether usefulness would cease. A possible application of double tether configurations is a multipurpose tethered system which accomplishes the function of C.o.G. control among others.

A E R I T A L I A
societa'
aerospaziale
italiana
SPACE SYSTEMS GROUP

TETHERED
GRAVITY LABORATORY STUDY

DOC. : TG-RP-AI-021
ISSUE : 01
DATE : 15/NOV/89
PAGE : 34 OF 38

TET. CONFIGURATION	PHASE I SPACE ST.		PHASE II SPACE ST.	
	TOTAL MASS (KG)	TOTAL LENGHT (m)	TOTAL MASS (KG)	TOTAL LENGHT (m)
SINGLE TETHER	149	1660	365	2766
DOUBLE CENTERED TETHER	12080	14224	14196	15227
DOUBLE SHIFTED TETHER	12080	14224	-	-
DOUBLE TETHER + ELEVATOR	9873	10735	11503	11919

TABLE 7 - TETHER CONFIGURATIONS OVERALL MASS AND LENGTH DATA

A possible additional function of the tether systems could be to damp the structural vibrations of the main boom during phase 1. This could be accomplished (as shown in SAO report) tuning the longitudinal vibrations of the tether to the first mode of flexural vibration of the Space Station. To avoid loss of tension in the tether, long (5 to 10 km) and massive (15000 to 20000 kg) systems are required to control an oscillation at 0.1 Hz with an amplitude of 0.01 meters.

5.3

MAJOR FINDINGS AND RECOMMENDATIONS

A summary of the previous discussions is reported in table 8.

The overall tether systems impact on the Space Station assessment was derived from what is reported in para 5.1. On the basis of the analysis reported in appendix B it can be said that the expected disturbances due to thermal effects are quite low and can be minimized through an adequate choice of tether material, thermal properties and damping devices.

The possible benefits achievable by implementations of the various solution were judged comparing the capabilities of the systems with the expected disturbances. Due to the low level of the gravity gradient acceleration during phase 1 the usefulness of tether systems is lower in this case than in phase 2. The ability of the double tether configurations to deal with significant dynamic disturbances is important, but, as the size of the dynamic disturbances is still uncertain, no configuration can be judged as surely highly beneficial.

The cost was assessed mainly on the basis of the development risks and expected hardware complexity. The mobile T.A.P. required by the double tether shifted configuration will cause a big cost increase whereas the elevator design is also a complex task.

- During phase 1 the difficulties due to the tether systems are very likely greater than the problems they are required to solve. The cost/benefit figure of tethered systems for C.o.G. control is low in phase 1 and further studies are not recommended.
- On MB16 the simple and light single tether configuration can lead to a significant improvement on the steady accelerations environment.

TETHER SYSTEM CONFIGURATION									
SINGLE TETHER		DOUBLE CENTERED TETHER		DOUBLE SHIFTED TETHER		DOUBLE TET. + ELEVATOR			
PHASE I PHASE II		PHASE I PHASE II		PHASE I PHASE II		PHASE I PHASE II		PHASE I PHASE II	
MAIN FEATURES	SMALL NO	SMALL NO	LARGE YES	LARGE YES	LARGE YES	LARGE YES	LARGE YES	LARGE YES	LARGE YES
	SIZE DYNAMIC CONTROL								
SPACE STATION IMPACTS		MEDIUM	LOW	HIGH	MEDIUM	MEDIUM	N.A.	HIGH	MEDIUM
BENEFIT		VERY LOW	LOW	LOW	MEDIUM	MEDIUM	N.A.	LOW	MEDIUM
COST		LOW	LOW	MEDIUM	MEDIUM	HIGH	N.A.	HIGH	HIGH

TABLE 8 - TETHER CONFIGURATIONS MAIN FEATURES

A E R I T A L I A
societa'
aerospaziale
italiana
SPACE SYSTEMS GROUP

TETHERED
GRAVITY LABORATORY STUDY

DOC. : TG-RP-AI-021
ISSUE : 01
DATE : 15/NOV/89
PAGE : 37 OF 38

- The use of a double tether centered configuration on MB16 makes sense only if a relevant function is found for the end masses. The situation is slightly different for the elevator configuration where the elevator, even if it increases system complexity, can offer a wide range of opportunities to exploit.
- In summary further study on the dynamic C.o.G. control is opportune but it is so only if pictured in a wider scenario of enhanced Space Station capabilities where C.o.G. control is only one of the functions accomplished by tethers.

A E R I T A L I A
societa'
aerospaziale
italiana
SPACE SYSTEMS GROUP

TETHERED
GRAVITY LABORATORY STUDY

DOC. : TG-RP-AI-021
ISSUE : 01
DATE : 15/NOV/89
PAGE : 38 OF 38

REFERENCES

- REF. 1 from "The perfectly ideal accelerometer" by Ermit Stanlinger - Teledyne Brown Engineering - Workshop Proceeding on "Measurement and characterization of the acceleration environment on board the Space Station" - August 1986.
- REF. 2 "Meteoroid Environment Model - 1969 (Near Earth to Lunar Surface)" NASA SP-8013, March 1969, by COUR-PALAIS, B.G.
- REF. 3 "Orbital Debris Environment for Space Station" by KESSLER D.J. SSC-20001, 1986.

APPENDIX A

PADUA UNIVERSITY FINAL REPORT

TETHEPED GRAVITY LABORATORY STUDY

CONTRACT NAS9-17877

FINAL REPORT

University of Padua Tasks:

- Force Field Characterization
- Mathematical Models Review

prof. Silvio Bergamaschi

FORCE FIELD CHARACTERIZATION

prof. Silvio Bergamaschi
Institute of Applied Mechanics
University of Padua, Italy

Introduction

As it is well known, a point mass in a keplerian orbit is in a condition of free fall. This is because conic sections are the results of the assumptions made in the "one-body problem". In fact, in this classical problem of Celestial Mechanics, it is assumed that:

- a point mass P is subject to the attraction induced on it by a center O of gravitational force
- O is also a point and is fixed in an inertial reference system
- other forces on P are negligibly small

In this case, the horizontal (both in plane and out of plane) components of the acceleration at P are zero, while, in the direction of the local vertical, the gravitational and centrifugal accelerations balance each other, being equal in magnitude and opposite in direction.

However, it is also well known that the one-body problem, though very useful for computational purposes, is an idealization. As a consequence, an analysis intended to characterize the acceleration field at points close to the center of mass (c.o.m.) of the Space Station (S.S.) must evaluate quantitatively the discrepancies between real conditions and the ones assumed in the one-body problem. This is the purpose of the present work package; in particular, the attention is focused on:

- the departure of real orbits from conic sections and their related perturbations
- the finite extension in the euclidean space of the S.S., its attitude motion and structural vibrations

In addition, an attempt is made to assess the order of magnitude of the perturbation induced on points not coincident with c.o.m. by the gravitational field originated by the S.S. itself.

The characterization of the perturbations made above implies that the usual approach is used, where orbit and attitude dynamics are considered to be uncoupled, so that, dealing with attitude motion, a reference, unperturbed (by attitude) orbit is used. Strictly speaking, when the dimensions of the spacecraft are considerable, as is the case of the S.S., the degrees of freedom (d.o.f.) which describe the motion around c.o.m. can have a bearing in modifying the orbit. However, it has been shown (1) that such perturbations usually are, for practical engineering purposes, very small. Only in resonant, or quasi resonant conditions, i.e. when the frequencies associated to attitude are coincident, or very close to the mean motion of a near circular orbit, can orbital motion be appreciably affected by attitude dynamics. In the S.S. case, attitude is controlled actively, so that near resonant conditions can easily be avoided. In any case, the order of magnitude of the orbital perturbations induced by attitude control is smaller, or at most comparable, to the discrepancy between the nominal circular orbit and the one allowed by the orbital control deadband. Since this last orbital features are taken into account in the analysis to follow, it seems justifiable to neglect spin-orbit coupling. The authors of this report are aware that the acceleration field acting on the S.S. has already been studied in recent years. In particular, in the following, reference will be made to the excellent work made by Teledyne Brown (2) and by dr. Naumann (3). However, both the analyses above can be updated or deepened because:

- The S.S. configuration has been changed from the Power Tower to the Dual Keel and, more recently, to the initial (in the assembling sequence) Dual Keel configuration. Therefore, many characteristic parameters (mass, inertia tensor, cross sectional area) have been subject to change, thus causing also some discrepancies between the results of the studies mentioned above. In this respect, of particular importance are the values of the semimajor axis and of the cross

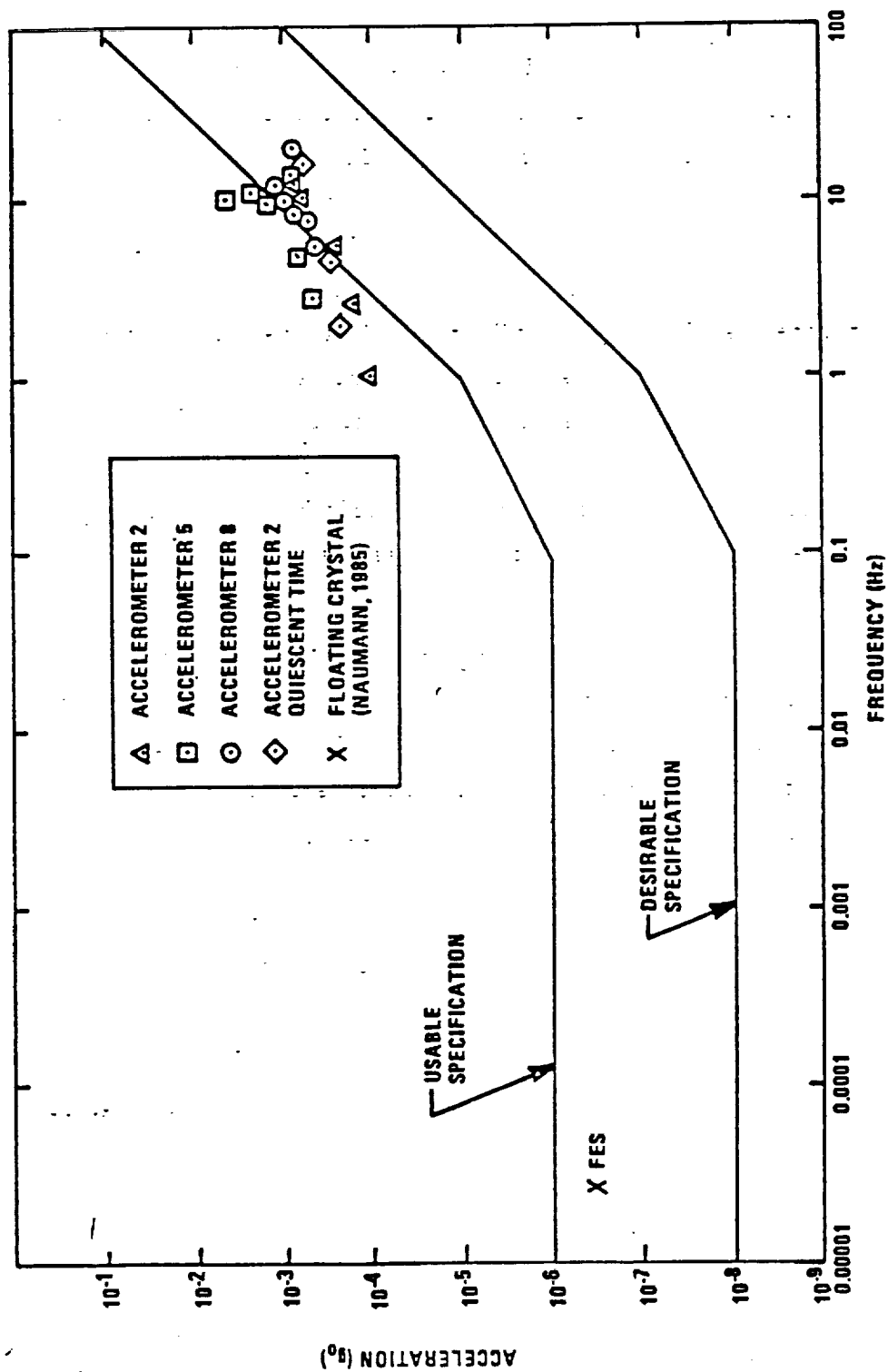


FIGURE 1. PROPOSED ACCELERATION LIMIT SPECIFICATIONS AND MEASURED ENVIRONMENT FROM THE FLUID EXPERIMENT SYSTEM (FES) ON SPACELAB 3

section for the evaluation of drag induced acceleration.

- Some restrictive assumptions can be somewhat relaxed. For instance, the perturbing effect of a small orbital eccentricity can be taken into account. Moreover, the order of magnitude of the perturbations induced by attitude dynamics can be assessed without excessive simulation effort.

The refinement of the models adopted in previous studies is not expected to alter significantly their results, but, on the contrary, to complement them. In fact, the S.S. specification of $10^{-5}g$ disturbance, independent from frequency, has been criticized on the grounds that acceleration levels better than $10^{-5}g$ at frequencies lower than 10^{-1} Hz are required by many processes to take place in the scientific labs. It has also been found that the $10^{-5}g$ requirement can be relaxed at higher frequencies. Fig. 1 shows one of the results published in (2): two curves have been drawn, related to "usable" and to "desirable" acceleration levels. Thus, while it is felt that slightly more sophisticated mathematical models cannot modify the results already obtained in the acceleration range around $10^{-6}g$, it is believed that they can be useful to characterize (also in the frequency domain) the perturbation field at very low levels as $10^{-8}g$.

Orbit Perturbations

In general, the differences between the path of an Earth artificial satellite and a keplerian orbit are caused by:

- a) upper harmonics of the Earth gravity field
- b) third body gravitational attractions
- c) orbital energy dissipation by the atmosphere
- d) solar radiation pressure
- e) spacecraft orbit and attitude active control

As currently planned, the International Space Station will be injected into a nominally circular orbit with an inclination of about 28.5 deg with respect to the Earth equatorial plane, at an average altitude around 400 km (possibly depending on the assembly process phase). In a low Earth orbit (LEO) like this, the luni-solar attraction is too small, in comparison to the Earth field, to provide sensible perturbations; for this reason, point b) will be neglected.

On the other side, the departure of the Earth shape from a perfect sphere and the non homogeneity of its mass distribution are known to affect LEO-s, modifying their osculating elements. In the expansion of the Earth gravitational potential in spherical harmonics, the term proportional to J_2 , describing Earth oblateness, is three orders of magnitude smaller than the fundamental term, while the other contributions have amplitudes (normalized to the fundamental) of the order of 10^{-6} or less. For this reason, only the perturbations caused by J_2 will be examined in the following.

For what concerns point e), the evaluation of the acceleration induced by

active control depends on:

- nominal orbit parameters
- mission requirements
- S.S. reaction control system (RCS) characteristics

At the present time, all the points above are not known with accuracy sufficient to justify a detailed, time expensive analysis. Therefore, it has been decided to assume that out of plane perturbations, usually small if the orbit plane has not to be changed, are negligible, while in plane thrusters are fired only for altitude make-ups, or when orbit eccentricity exceeds 10^{-3} . This seems reasonable, being the Space Shuttle case, hence, in the following, when dealing with gravitational perturbations, the S.S. orbit will be considered to be eccentric, with $e = 10^{-3}$.

Gravity induced Perturbations: The Mathematical Model

The purpose is to evaluate the acceleration field induced by gravity gradient on a point P of the S.S., fixed in it, but not coincident with c.o.m.

This kind of analysis is not new, having already been done in (2) and (3).

The extension proposed herein consists to include in the models the effect of a slight orbit eccentricity and to take into consideration the effect of

the Earth oblateness. As both the orbital eccentricity and J_2 are of the

order of 10^{-3} , it is intended, as written above, to analyze the perturbing

field at levels comparable to $10^{-6}g$. The S.S. is assumed to be a rigid body

The geometry of the model is shown in fig. 2, where:

- (O,X,Y,Z) is an inertial reference system, centered at the Earth c.o.m., with Z toward the geographic North Pole and the X-Y axes in the equatorial plane
- (G,x,y,z) is the orbital reference frame, with its origin at the c.o.m. of the S.S., x is in the direction of the upper local vertical and z points to the orbit pole, while y completes a counterclockwise triad
- $(\vec{e}_1, \vec{e}_2, \vec{e}_3)$ are the unit vectors of the inertial frame
- $(\vec{c}_1, \vec{c}_2, \vec{c}_3)$ are the unit vectors of the orbital frame
- \vec{r} and \vec{r}_p are, respectively, the radii vectors from O to G and to a point P fixed in the S.S.
- i is the orbit inclination, Ω the longitude of the ascending node and u the argument of the latitude

In order to evaluate the acceleration level at P, the Lagrangian formalism is adopted. The kinetic energy per unit mass is:

ORIGINAL PAGE IS
OF POOR QUALITY

$$T = \frac{1}{2} \dot{\vec{r}}_r \cdot \dot{\vec{r}}_r \quad (1)$$

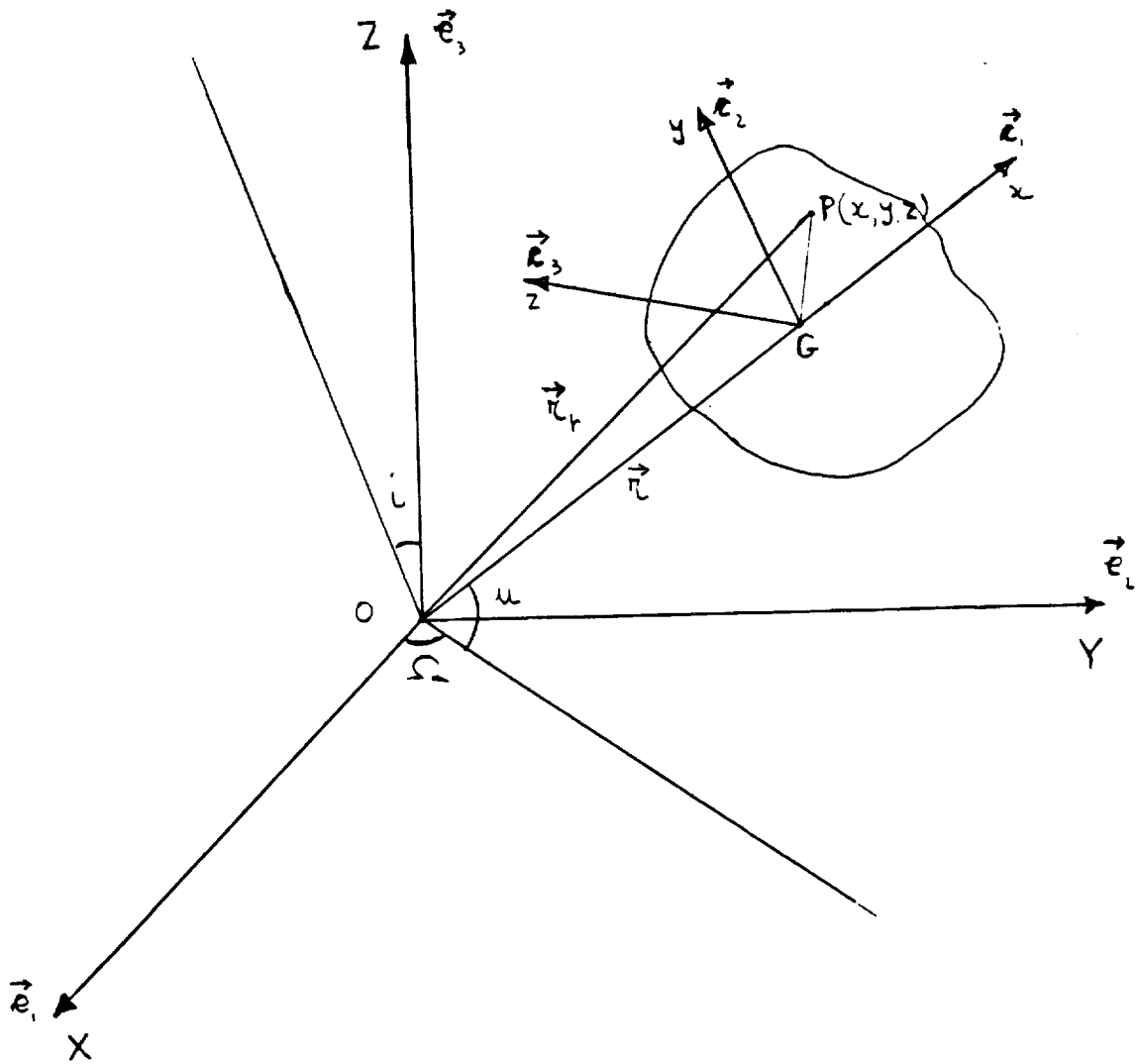


Fig 2

Now:

$$\vec{r}_r = (R+x) \vec{e}_1 + y \vec{e}_2 + z \vec{e}_3 \quad (2)$$

so that:

$$\dot{\vec{r}}_r = (\dot{R}+\dot{x}) \vec{e}_1 + \dot{y} \vec{e}_2 + \dot{z} \vec{e}_3 + (R+x) \vec{\omega} \times \vec{e}_1 + y \vec{\omega} \times \vec{e}_2 + z \vec{\omega} \times \vec{e}_3 \quad (3)$$

where:

$$\vec{\omega} = \omega_1 \vec{e}_1 + \omega_2 \vec{e}_2 + \omega_3 \vec{e}_3 \quad (4)$$

is the angular velocity of the orbital reference frame. Since the model is intended to take into account also the perturbations caused by J_2 , the time variations of Ω and i cannot be neglected, so that the explicit expressions of the components of $\vec{\omega}$ are:

$$\begin{cases} \omega_1 = \Omega \sin i \sin u + \dot{i} \cos u \\ \omega_2 = \Omega \sin i \cos u - \dot{i} \sin u \\ \omega_3 = \Omega \cos i + \dot{u} \end{cases} \quad (5)$$

Thus, the kinetic energy can be written as:

$$T = \frac{1}{2} \left\{ (\dot{R}+\dot{x} + z\omega_2 - y\omega_3)^2 + [\dot{y} + (R+x)\omega_3 - z\omega_1]^2 + [\dot{z} + y\omega_1 - (R+x)\omega_2]^2 \right\} \quad (6)$$

The potential energy is:

$$V = - \frac{\mu}{r_r} \left[1 + \frac{J_2 R^2}{2 r_r^2} (1 - 3 \sin^2 \beta) \right] \quad (7)$$

where:

- R is the equatorial radius of the Earth
- β is the latitude of P , so that:

$$\sin \beta = z_r / r_r$$

- $\mu = 3.986008 \cdot 10^{14} \text{ m}^3 \text{ s}^{-2}$ is the Earth gravitational constant

Since Z_p has to be expressed in function of x, y, z , the matrix transformation:

$$\begin{bmatrix} \vec{e}_1 \\ \vec{e}_2 \\ \vec{e}_3 \end{bmatrix} = \begin{bmatrix} \cos \Omega \cos u - \sin \Omega \sin u \sin i & -\cos \Omega \sin u - \sin \Omega \cos u \sin i & \sin \Omega \sin i \\ \sin \Omega \cos u + \cos \Omega \sin u \sin i & -\sin \Omega \sin u + \cos \Omega \cos u \sin i & -\cos \Omega \sin i \\ \sin i \sin u & \sin i \cos u & \cos i \end{bmatrix} \cdot \begin{bmatrix} \vec{e}_1 \\ \vec{e}_2 \\ \vec{e}_3 \end{bmatrix} \quad (9)$$

is used. After some algebraic manipulations, eq. (7) can be rewritten as:

$$\begin{aligned} V = & -\frac{\mu}{r} \left\{ 1 - \frac{x}{r} + \frac{x^2 - y^2 - z^2}{2r^2} + \frac{J_2 R^2}{2r^2} \left[\left(1 - \frac{3x}{r} \right) (1 - 3 \sin^2 i \sin^2 u) + \right. \right. \\ & \left. \left. - \frac{6}{r} (y \sin^2 i \sin u \cos u + z \sin i \cos i \sin u) \right] \right\} \quad (10) \end{aligned}$$

Where, in the J_2 dependent terms, the power expansion of the modulus of has been stopped to the linear terms in x/r (and similar), because the quadratic contributions are three orders of magnitude smaller than any of the ones retained in (10).

Slightly Eccentric Orbit

Let us apply the formulas derived in the previous chapter, to compute the acceleration at P when the orbit of the c.o.m. is slightly eccentric. J_2 perturbations are not taken into account at this point. In this case, the usual expression of the radius vector in an elliptic orbit is simplified to:

$$r = a (1 - e \cos nt) \quad (11)$$

where:

- a is the semimajor axis
- e is the eccentricity
- $n = (\mu/a^3)^{1/2}$ is the orbit mean motion

Further, since u is the sum of the argument of perigee ω and the true anomaly w , we can assume in this case that the apsidal line of the orbit is coincident with the line of nodes, so that the argument of the latitude can be attributed the same time dependence of the true anomaly; i.e., at the first order in the expansion of the eccentricity:

$$u = nt + 2e \sin nt \quad (12)$$

Also, the osculating elements are constant, so that eqs. (5) are simplified in:

$$\omega_1 = \omega_2 = 0 \quad \omega_3 = \dot{u} \quad (13)$$

and the lagrangian is:

$$L = \frac{1}{2} \{ (\dot{r} + \dot{x} - y\dot{u})^2 + [\dot{y} + (r+x)\dot{u}]^2 + \dot{z}^2 \} + \frac{\mu}{r} \left(1 - \frac{\lambda}{r} + \frac{2x^2 - y^2 - z^2}{2r^2} \right) \quad (14)$$

from which the components of the acceleration of P with respect to G can easily be derived. They are:

$$\begin{vmatrix} a_x \\ a_y \\ a_z \end{vmatrix} = n^2 \cdot \begin{vmatrix} 3+10e \cos mt & -2e \sin mt & 0 \\ 2e \sin mt & e \cos mt & 0 \\ 0 & 0 & -1+3e \cos mt \end{vmatrix} \begin{vmatrix} x \\ y \\ z \end{vmatrix} \quad (15)$$

It is seen immediately that (15) reduces to the well known result in case of a circular orbit. It is also seen that orbit eccentricity causes the in plane horizontal component of the acceleration to be different from zero, contrary to the circular orbit case; thus, in principle, a_x and a_y are coupled, so that a point on the local horizontal containing the c.o.m., but displaced forward or backward with respect to it, is subject to a time varying vertical acceleration, the period of which is equal to the orbital period.

Let us now assume:

$$\begin{aligned} a &= 6778 \text{ km} & e &= 10^{-3} \\ x &= -2 \text{ m} & y &= 10 \text{ m} & z &= 4 \text{ m} \end{aligned} \quad (16)$$

The values given to the orbital elements are reasonable, corresponding to an orbit at an average altitude of 400 km, having an eccentricity equal to the residual e allowed by the Space Shuttle control. Moreover, the dependence of the acceleration on e is very clear from the structure of (15), while the value chosen for a is not critical, in the sense that different altitudes in the range 350-450 km would cause only minor changes in the corresponding n^2 values.

On the contrary, some comments are pertinent to justify the choice of the coordinates. The S.S. configuration considered in this study is similar to the one shown in fig. 3. From the data available on geometrical features

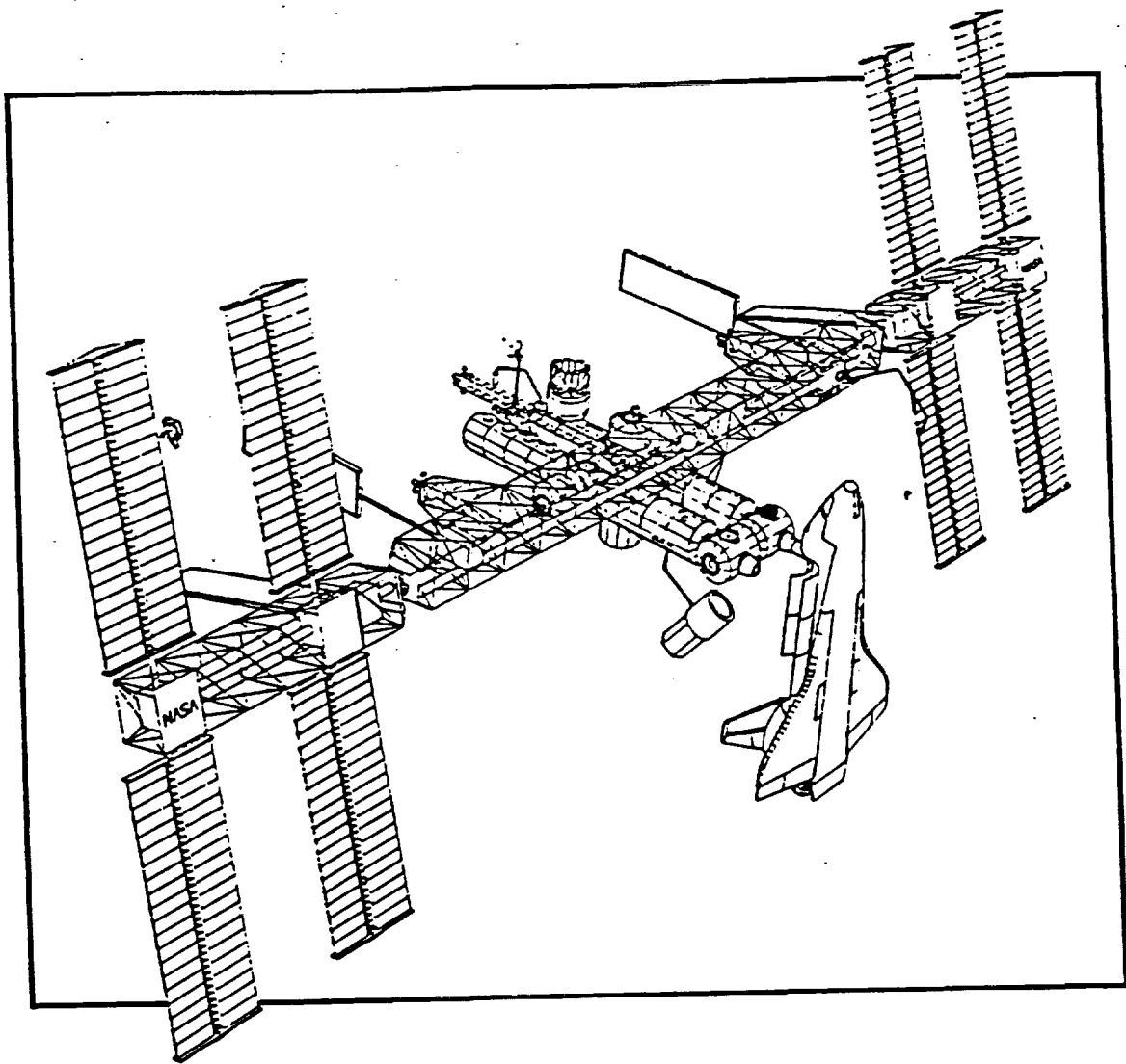


Fig. 3

and mass distribution, it is seen that the vertical offset between the c.o.m. and the symmetry axis of the labs is close to 1m, with c.o.m. upward. Thus, points have been selected which are displaced 1m downward with respect to the axis of the labs. This choice is considered to be both reasonable and slightly conservative. The same arguments apply to y and z. Points have been chosen which are rather close to the airlocks and relatively far from the ideal orbit plane of c.o.m., with respect to which the labs are assumed to be in symmetrically opposite positions.

With the data above, one has:

$$\begin{cases} a_x = -7.68 \times 10^{-6} - 2.56 \times 10^{-8} \cos nt - 2.56 \times 10^{-8} \sin nt \\ a_y = -5.12 \times 10^{-9} \sin nt + 1.28 \times 10^{-8} \cos nt \\ a_z = 5.12 \times 10^{-6} + 1.54 \times 10^{-8} \cos nt \end{cases} \quad (\text{m/sec}^2) \quad (17)$$

As expected, the main acceleration component is the vertical constant term. In this case, it does not exceed $10^{-6}g$, because of the choice made on x. It is noted, however, that the evaluation of c.o.m. location has necessarily been approximated, so that the possibility exists that points with x close to -3m be still inside the labs; at such points the field can reach values close to, or slightly larger than $10^{-6}g$.

The amplitudes of the terms originated by eccentricity are smaller than $10^{-8}g$; even in more extreme conditions, the "desirable" limit is not exceeded. This is because the comparatively large y terms are multiplied only by matrix coefficients depending on e.

J₂ Perturbations

Using the method adopted above, but starting from the complete expression of the lagrangian, as given by eqs. (6) and (10), J₂ perturbations can be evaluated. In this case, the acceleration components are:

$$\begin{pmatrix} a_x \\ a_y \\ a_z \end{pmatrix} = \begin{pmatrix} \omega_3^2 + 2\mu/n^3 & \dot{\omega}_3 & -\dot{\omega}_2 - \omega_1\omega_3 \\ -\dot{\omega}_3 & \omega_3^2 - \mu/n^3 & \dot{\omega}_1 - \omega_2\omega_3 \\ \dot{\omega}_2 - \omega_1\omega_3 & -\dot{\omega}_1 - \omega_2\omega_3 & -\mu/n^3 \end{pmatrix} \cdot \begin{pmatrix} x \\ y \\ z \end{pmatrix} \quad (18)$$

which reduces to (15) if the J₂ dependent terms are dropped. In writing explicitly the coefficients of (18), only the terms linear in J₂ have been retained. This is for two reasons:

- Since J₂ is of the order of 10⁻³, its square is as small as the contributions of the upper harmonics of the Earth gravity field, which have been ignored since the beginning. Moreover, J₂ is small in itself.
- The functions written in (18) contain the osculating elements and their derivatives. In the following, a theory is used where the changes of the orbital elements are calculated to the first order in J₂.

The explicit expressions of the terms in (18) are lengthy, so that they are not reported here for sake of brevity, and also because, fortunately, they are not essential for the evaluation of the amplitude and frequency content of the acceleration. After some algebra, it is seen that the main contributions to (18) come from a, e, Ω, i and their time derivatives. From first order perturbation theory, the changes of such elements, with

respect to their unperturbed values, are, for an initially circular orbit (4):

$$\left\{ \begin{array}{l} \Delta a = \frac{3J_2 R^2}{2a_0} \sin^2 i_0 \cos 2nt \\ \Delta e = \frac{3J_2 R^2}{2a_0^2} \left[\left(1 - \frac{5}{4} \sin^2 i_0\right) \cos nt + \frac{7}{12} \sin^2 i_0 \cos 3nt \right] \\ \Delta \Omega = - \frac{3J_2 R^2}{4a_0^2} \cos i_0 (2nt - \sin 2nt) \\ \Delta i = \frac{3J_2 R^2}{8a_0^2} \sin 2i_0 \cos 2nt \end{array} \right. \quad (19)$$

where n is the mean motion of the unperturbed orbit and the subscripts $_0$ denote unperturbed quantities. In this case, with the same values used above, one has:

$$\left\{ \begin{array}{l} \Delta a = 2.2 \cos nt \quad (\mu m) \\ \Delta e = 1.44 \times 10^{-3} (0.71 \cos nt + 0.13 \cos 3nt) \\ \dot{\Omega} = -1.43 \times 10^{-6} (1 - \cos 2nt) \quad (\text{rad/sec}) \\ \dot{i} = -6.8 \times 10^{-7} \sin 2nt \quad (\text{rad/sec}) \end{array} \right. \quad (20)$$

From (20) it is seen that:

- the amplitude of the semimajor axis change is very small
- the amplitude of the eccentricity change is of the order of 10^{-3}
- $\dot{\Omega}$ and \dot{i} cause the angular velocity of the motion of the S.S. to change both in magnitude and in direction. The amplitude of the change is in the range of 10^{-6} rad/sec.

From the point of view of the evaluation of the accelerations, the change of a is negligible. The e variation has the same order of magnitude of the case analyzed above, so that the same results apply. Finally, the changes induced in $\vec{\omega}$ by $\dot{\Omega}$ and \dot{i} are three orders of magnitude smaller than the

mean motion. In conclusion, the perturbations induced by Earth oblateness do not reach $10^{-6}g$ in amplitude. This result is confirmed by the explicit computation of (18).

Aerodynamic Acceleration

In general, the modelization of the interaction between a spacecraft and a planetary atmosphere is a complex problem. The air resistance of a body has six components, three being forces and three moments of forces, which tend to make the motion of an asymmetric body very complex; this is the reason why, quite often, drastic simplifying assumptions are adopted (5).

In our case, the S.S. attitude is actively controlled, so that the aerodynamic torque is balanced by the action of control moment gyros and/or the reaction control system. In any case, this aspect of the aerodynamic interaction affects attitude motion, which will be examined later.

Thus, we are left with the force components, the magnitude of which depends, apart from any other consideration about the features of the model being adopted, on the orientation of the normal to each interested element of area with respect to the direction of the velocity relative to the atmosphere. Now, the extension of the S.S. cross sectional area is largely due to the presence of the solar panels, which can be rotated with respect to the rest of the S.S., in order to maximize the incoming flux of solar energy. Thus, the area to be taken into account in the computations changes with time not only in magnitude, but also in orientation, depending on the performance capabilities of the panels attitude control and on the optimization strategy being adopted. Both these characteristics are largely unknown to the authors of this report, so that it has been decided to:

- assume worst case conditions, in the sense that, in the numerical computations, the whole area of the solar panels will be considered

to be coincident with the cross section

- assume the lift equal to zero, so that drag is maximized. The value obtained in this way is conservative with respect to drag and can also be used to obtain upper limits for the lift components
- In the analysis, the model given in (6) is used, where the atmosphere is assumed to rotate rigidly with the Earth and advantage is taken from the smallness of its velocity with respect to the S.S. orbital velocity. The unperturbed orbit is assumed to be circular. Thus, the components of the aerodynamic acceleration in the inertial frame are:

$$\begin{cases} a_x = C \left(1 - \frac{2\delta}{n_0} \omega i_0 \right) \sin n_0 t = C \cdot D_1 \sin n_0 t \\ a_y = -C \left[\cos i_0 - \frac{\delta}{n_0} (1 + \omega^2 i_0) \right] \cos n_0 t = -C \cdot D_2 \cos n_0 t \\ a_z = -C \left(1 - \frac{\delta}{n_0} \cos i_0 \right) \sin i_0 \cos n_0 t = -C \cdot D_3 \cos n_0 t \end{cases} \quad (21)$$

where:

- $C = C_D A \rho a_0^2 m_0^2 / 2 m$
- the subscript 0 refers to quantities pertaining to the unperturbed orbit. Since no confusion is possible, from now on it will be dropped
- δ is the Earth rotation rate
- the other symbols are self explaining

Using (9) with the assumption that $\Omega = \omega = 0$, the acceleration components are transformed in the orbital frame. The result is:

$$\vec{a}_D = 0 \cdot \vec{e}_1 - \frac{1}{2} (D_1 + D_2 \cos i + D_3 \sin i) \vec{e}_2 + (D_2 \sin i - D_3 \cos i) \cos n t \vec{e}_3 \quad (22)$$

Let us now consider the same orbit as above and take:

$$C_D = 2.3 \quad A = 1368 \text{ m}^2 \quad m = 1.4 \cdot 10^5 \text{ kg} \quad \rho = 6.5 \cdot 10^{-12} \text{ kg/m}^3 \quad (23)$$

With these data, one has:

$$\vec{a}_g = 0 \cdot \vec{e}_1 - 3.8 \cdot 10^{-6} \vec{e}_2 - 1.3 \cdot 10^{-7} \sin \alpha \vec{e}_3 \quad (\text{m/sec}^2) \quad (24)$$

from which it is seen that the drag has no component in the vertical direction, because of the assumptions made on the atmospheric motion and on the S.S. orbit; further, the main component does not reach $10^{-6}g$ and the out of plane acceleration amplitude is one order of magnitude smaller.

The numbers above have to be considered with some care. In fact, the results of (2) and (3), where the same problem has been analyzed, show some discrepancies. The differences are not due to the models, which seem to be similar to the one adopted herein, but to the assumptions made in the numerical computations about the S.S. ballistic coefficient, orbit altitude and atmospheric density. In this report, mass and area of the S.S. are consistent with the configuration selected at the beginning, but it is evident that both these parameters, and in particular m , are subject to change during the assembly process. Moreover, and even more important, ρ changes dramatically with altitude; finally, the value of the atmospheric density adopted has to be considered as an average, 100% differences with respect to the actual value being possible. At present, it seems that the altitude of the orbit has still to be frozen, being probably closer to 350 km in the initial phase, and to 400 km later on. If so, in the initial orbit, the drag acceleration would be close to $10^{-6}g$, even in average conditions, due to air density increase. Thus, while orbital characteristics are not important in the evaluation of gravity induced accelerations, they are crucial for a reliable estimate of the aerodynamic perturbations.

Radiation Pressure Acceleration

The evaluation of the perturbation induced by the pressure of the solar radiation is subject to some of the same uncertainties encountered in the case of atmospheric drag. Radiation pressure direction is contrary to the Sun vector, i.e. the vector from the S.S. to the Sun, so that the direction of the force acting on the S.S. is dependent on the orientation of the solar panels with respect to the Sun vector, which, in turn, is not fixed in the orbital reference frame. Thus, no attempt is made here to evaluate the force direction and only its magnitude is computed in a conservative case.

The assumptions made are:

- The solar panels surfaces are always orthogonal to the Sun vector
- The incident radiation is specularly reflected by the panels. This is not true, because part of it is likely to be absorbed, or diffusely reflected; however, specular reflection maximizes the momentum transferred from the radiation to the S.S., so that this assumption is conservative (7)

The mean momentum flux, P , acting on a surface normal to the Sun vector is:

$$P = F_e / c \quad (25)$$

where:

- $F_e = 1358 \text{ W/m}^2$ is the solar constant
- c is the velocity of light

Strictly speaking, F_e is not constant, since it undergoes a small annual variation because of the eccentricity of the Earth orbit. However, due to the more drastic simplifications made above, such slight time dependence is here ignored.

Hence, in virtue of the assumptions made above, the S.S. acceleration in the direction opposite to the Sun vector is:

$$a_r = \frac{2 F_e A}{c m} \quad (26)$$

With the same values used above, one has: $a_r = 8.85 \cdot 10^{-8} \text{m/sec}^2$, which is almost two orders of magnitude smaller than drag induced acceleration and dependent only on the area on mass ratio. It is noted, however, that the value obtained is close to $10^{-8}g$, so that the previously mentioned desirable acceleration level can possibly be perturbed even by radiation pressure. If the acceleration field has to be characterized to such very low levels, more sophisticated models have to be implemented.

Attitude Motion and Structural Dynamics

In addition to perturbations caused by the departure of real orbits from conic sections, accelerations at points fixed in the S.S. can be originated by attitude control and structural vibrations.

Structural vibrations are not taken into account in this study for a variety of reasons. First, scarce information is available on the S.S. elastic properties, so that the methods of harmonic analysis cannot be used.

Second, from (8) it is seen that the lower natural vibration modes of the Power Tower configuration have frequencies from 0.1 to 1 Hz. Now, it is reasonable to assume that the Dual Keel frequencies be in the same range, or higher. On the other side, this perturbation analysis is a preliminary to the study of what one or more masses tethered to the S.S. can do to decrease the residual acceleration level. Thus, although in the past it has been suggested to use tethers "tuned" to the frequencies of their main body, in order to act as vibration dampers, this somewhat remote possibility is not taken into account here and tethers will be considered to be means to compensate only steady, or low frequency perturbing actions. In this respect, it is noted that, in the present context, "low frequency" means frequencies comparable to the mean motion of the S.S. orbit, as is the case of orbital perturbations.

Further, the analysis in the frequency domain of the acceleration levels at the location of the experiments is complicated by two causes:

- Uncertainty in the features of the perturbing forces. Structural vibrations can be excited in a variety of manners, including pumps, fans, crew motion, AOCs, Shuttle dock and undock. Some of such forces are random in nature; others, though deterministic, are known only poorly.

- Uncertainty in the S.S. dynamic response. The energy of an external impulse is shared between the different vibration modes and transmitted to points far from the excitation source. In this process, part of the mechanical energy is lost because of structural damping, the features of which are unknown to the authors. In addition, in order to decrease, or impede the transmission of vibrations all around the S.S., isolation devices will be used both at subsystem level, to isolate the scientific labs from perturbations originated at different locations, and at rack level, to eliminate the dynamic noise possibly originated by other experiments in the same lab. Again, to the authors knowledge, the configuration of the isolation system has not yet been defined completely at this point in time, so that any attempt to evaluate the g-jitter level at the experiments location is likely to be meaningless.

From the considerations above, it can be concluded that the analysis of the accelerations caused by structural vibrations is well beyond the scope of this limited effort. Moreover, some disturbance components in the real system might not even have been anticipated in the harmonic analysis, so that post flight evaluation of accelerometer data seems to be the only viable method to obtain a reliable estimate. This kind of approach has already been used in connection with Spacelab flights (9).

Lastly, from fig. 1 it is seen that it is expected that μ -g experiments be increasingly tolerant to perturbations having increasing frequency; therefore, the effects of at least some of them could be small.

Attitude Control Acceleration

S.S. attitude is simulated more easily than structural vibrations, because elasticity can be neglected and rigid body assumptions apply. What follows is the justification and the results of a two-dimensional model developed to analyze the acceleration generated by S.S. rigid body rotation. The model is two-dimensional both for sake of simplicity and because of the S.S. geometry. Simplicity, i.e. the reduction from the three to the two dimensional ambient space, is appropriate here because, again, only incomplete information is available on the characteristics of the attitude control laws, thus making any more sophisticated model meaningless. The importance of S.S. geometry, and in particular of the position of the scientific laboratories with respect to c.o.m., stems from the feature, already mentioned above, that the points at which the experiments are likely to be located are relatively close to c.o.m. both in the vertical and in the out of plane directions, while the offset can be larger (up to $\approx 10\text{m}$) along the y horizontal axis, thus causing larger linear accelerations for a given angular velocity.

Thus, it has been decided to simulate only pitch and to use, in the numerical calculations, what is presently known from the requirements on attitude control laws. The c.o.m. of the S.S. is assumed to be in a circular orbit. The vertical and horizontal components of the acceleration of a point the motion of which differs only slightly from uniform circular are given by the left sides of Hill's equations.

They are:

$$\begin{cases} a_x = \ddot{x} - 2n\dot{y} - 3n^2x \\ a_y = \ddot{y} + 2n\dot{x} \end{cases} \quad (27)$$

The geometry of the model is shown in fig. 4, where:

- \bar{G} is the c.o.m. of the S.S.
- ϑ is the pitch angle. It is assumed that the configuration with $\vartheta = 0$ is of equilibrium
- P is a point, fixed in the S.S., the coordinates of which, with respect to the S.S. principal inertia system, are:

$$\begin{cases} u = d \cos \gamma \\ v = d \sin \gamma \end{cases} \quad (28)$$

The coordinates of P in the orbital (G, x, y) reference frame are:

$$\begin{cases} x = d \cos(\gamma + \vartheta) \\ y = d \sin(\gamma + \vartheta) \end{cases} \quad (29)$$

Introducing (29) in (27), taking into account that P experiences an acceleration equal and opposite to the one written in (27), assuming that ϑ is small while γ is arbitrary and retaining only first order terms in ϑ , one has:

$$\begin{vmatrix} a_x \\ a_y \end{vmatrix} = \begin{vmatrix} 2m\ddot{\vartheta} + 3m^2 & \ddot{\vartheta} - 3m^2\vartheta \\ -\ddot{\vartheta} & 2m\ddot{\vartheta} \end{vmatrix} \cdot \begin{vmatrix} u \\ v \end{vmatrix} \quad (30)$$

Since the details of the attitude motion are not known, some assumptions based on the requirements (8) are to be made; they are:

- the deadband of attitude control is 5 deg
- the maximum allowed rotational velocity is $\omega = 0.02$ deg/sec

Further, it is assumed that pitch motion is harmonic, so that:

$$\vartheta = 8.7 \cdot 10^{-2} \sin 4 \cdot 10^{-3} t \quad (\text{rad}) \quad (31)$$

therefore, (30) becomes:

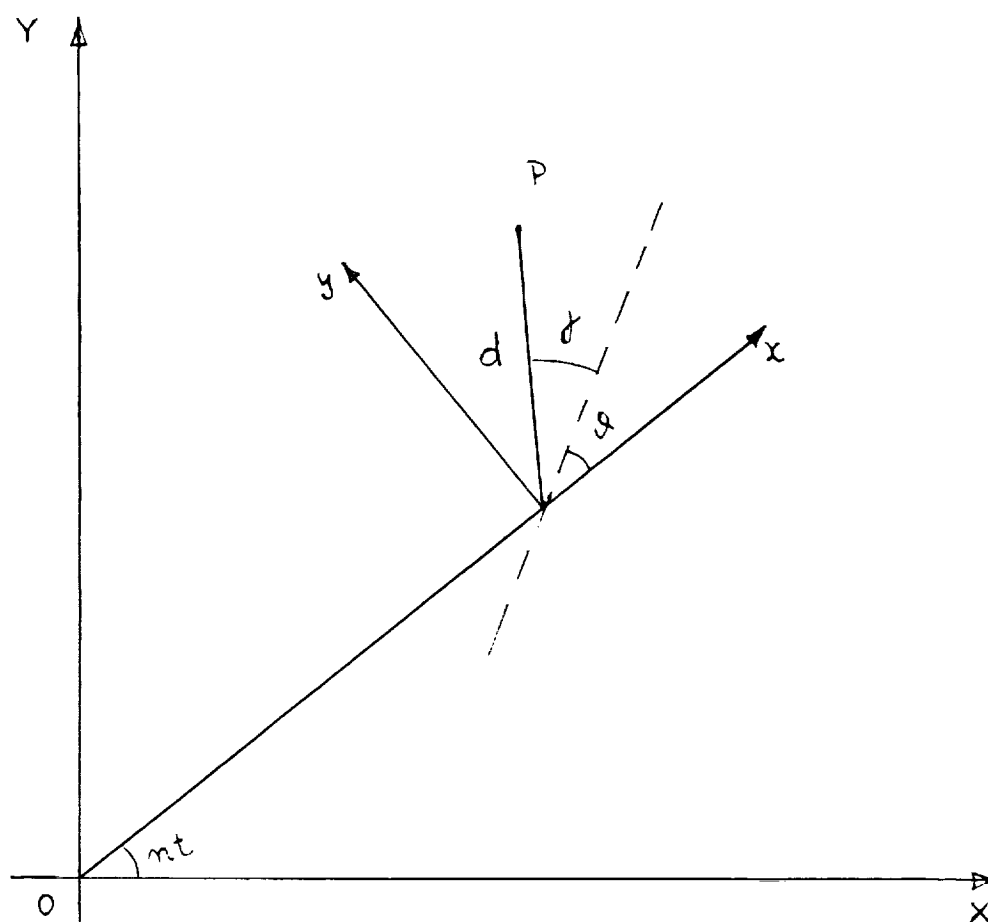


Fig. 1.

$$\begin{vmatrix} a_x \\ a_y \end{vmatrix} = \begin{vmatrix} 7.9 \cdot 10^{-7} \cos \omega_f t + 3.24 \cdot 10^{-6} & -1.7 \cdot 10^{-6} \sin \omega_f t \\ 1.4 \cdot 10^{-6} \sin \omega_f t & 7.9 \cdot 10^{-7} \cos \omega_f t \end{vmatrix} \cdot \begin{vmatrix} u \\ v \end{vmatrix} \quad (30)$$

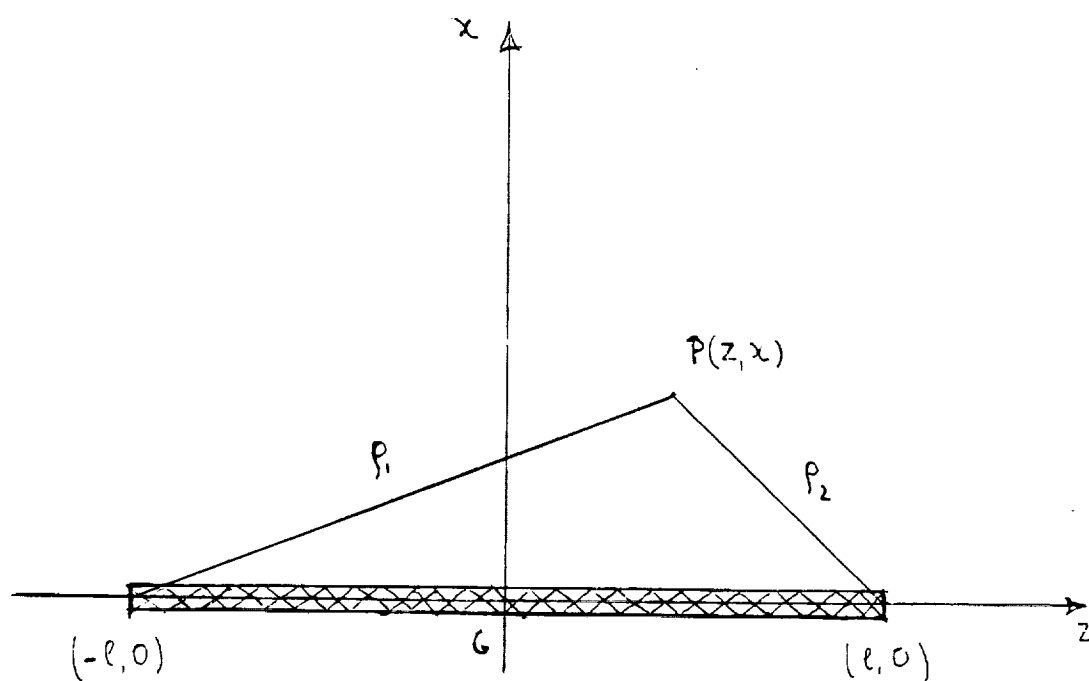
It has already been stated that it is believed that vertical distances from the experiments locations to c.o.m. are likely to be less than 2m, so that the "usable" limit of $10^{-6}g$ is not exceeded because of excessive vertical offsets. On the contrary, the horizontal distance of the points close to the airlocks can be of the order of 10 m, thus inducing an harmonic vertical component of the acceleration of about $1.7 \cdot 10^{-6}g$ in amplitude. The horizontal component can have a peak value of $0.8 \cdot 10^{-6}g$.

It is seen that low frequency attitude motion can induce vertical accelerations larger than $10^{-6}g$, at least in part of the scientific labs. Since the period of such motion is close to half an hour, it is conceivable, at least in principle, to use variable length tethers, in order to originate an equal and opposite acceleration at the labs. It is also noted that the acceleration amplitude could be reduced by decreasing the deadband amplitude (which formerly was 1 deg); this reduction, however, is likely to have an impact on c.m.g. performances and energy consumption.

ORIGINAL PAGE IS
OF POOR QUALITY

Gravitational Attraction of the Space Station

The attraction of a spacecraft on a point on board is usually neglected in ordinary perturbation analysis because of its smallness. In this case, however, the S.S. mass is considerably larger than that of a more conventional spacecraft and, further, it will be dedicated, at least in part, to scientific activity potentially very sensitive, even to very small accelerations. Therefore, it has been decided to adopt a model, as simple as possible, to have a feeling of the order of magnitude of this perturbation. The simplicity of the model is dictated both by the expected smallness of the induced acceleration, and by the changes of the S.S. geometry and mass distribution, which cause a more detailed study to be futile at this point in time. For this reason, the S.S. has been assumed to be a straight rod and a two-dimensional model has been adopted in the x - z plane in virtue of cylindrical symmetry.



The attraction of a rod with length $2l$ and mass per unit length μ , located as shown in fig. 5, on a point P is:

$$\begin{cases} a_x = \frac{G\mu}{x} \left[\left(\frac{1}{p_2} - \frac{1}{p_1} \right) z - \left(\frac{1}{p_2} + \frac{1}{p_1} \right) l \right] \\ a_z = G\mu \left(\frac{1}{p_1} - \frac{1}{p_2} \right) \end{cases} \quad (33)$$

where $G = 6.67 \cdot 10^{-11} \text{ m}^3 \text{ kg}^{-1} \text{ sec}^{-2}$ is the gravitational constant and the meaning of the other symbols is shown in fig. 5. For points close to c.o.m. one has: $p_1 \approx p_2 = l$ so that (33) are simplified in:

$$a_x = - \frac{2G\mu}{x} \quad a_z = 0 \quad (34)$$

Assuming $m = 1.4 \cdot 10^5 \text{ kg}$, as before, and $2l = 100 \text{ m}$, the first of eqs. (34) becomes: $a_x = -1.87 \cdot 10^{-7} / x \text{ m/sec}^2$, i.e.: $a_x = -1.87 \cdot 10^{-7} \text{ m/sec}^2$ for points 1 m above c.o.m..

Two comments are to be made to the result above. First, it is seen from the first of (34) that the vertical component is not defined for points belonging to the rod itself, which, in the model, has no thickness. Thus, the formula cannot be applied to points excessively close to the rod. Second, real points on board the S.S. are inside the labs, so that the attraction of the walls is averaged to a value probably less to the one just given, which, for this reason, must be considered as an upper limit.

Conclusions

At the end of this study, it can be concluded that the major source of dynamic perturbations on board the S.S. is likely to be the controlled attitude motion. This disturbance has to be considered steady, because the inertia distribution is such that the reference attitude is unstable with respect to the gravity gradient torque, so that active control is needed on a continuous basis.

Such perturbation can induce accelerations larger than the "usable" limit of $10^{-6}g$ at points in the labs which are located relatively far from c.o.m. in the in-plane horizontal direction. If so, the problem can be solved, or alleviated, by positioning the most disturbance sensitive experiments closer to c.o.m..

Apart from the constant gravity gradient term, the other main source of disturbance is air drag. The 10^{-6} limit is not exceeded, but since the larger component is horizontal, the addition of a tethered system cannot be of any help. It is noted again that the value above is critically dependent on the assumptions made on the orbit altitude and the S.S. ballistic coefficient. Drag induced acceleration at different steps of the assembling sequence can differ appreciably from this value.

The other accelerations analyzed so far are smaller. In some cases, what has been done has been to obtain an order of magnitude evaluation. For more precise estimates, if needed, more sophisticated models have to be implemented.

At the purpose of avoiding confusion due to the discrepancy of the results of this and other analyses with the post flight evaluations of the accelerometer data taken mainly from Spacelab missions, it is stated explicitly that the g-jitter originated by on board sources is expected to

be, by far, the major source of dynamic noise at the labs. g-jitter has not been taken into account because excessively dependent on parameters, operating modes, subsystem features, etc.; to the authors knowledge, some of the features needed for a reasonable estimate have still to be frozen, as is the case of the isolation subsystem, from which dynamic noise transmissibility depends. In any case, in absence of isolation, g-jitter amplitude can easily reach the m-g range, or even more. In this case, when sufficient information will be available, particular attention must be devoted to the distinction between steady and transient sources of perturbation.

References

- (1) S. N. Mohan et al.: "Interaction between Attitude Libration and Orbital Motion of a Rigid Body in a Near Keplerian Orbit of Low Eccentricity". Celestial Mechanics. Vol. 5. n. 1. 1972. pp. 157-173.
- (2) Teledyne Brown Eng.: "Low Acceleration Characterization of Space Station Environment". Final Report. Contract NAS8-36122. October 1985.
- (3) R. I. Naumann: "Gravity Level Estimates and Effects". MSFC. 14 August 1985.
- (4) T. E. Sterne: "An Introduction to Celestial Mechanics". Interscience Publishers. 1960. Ch. 5.
- (5) J. O. Cappellari (Editor): "Mathematical Theory of the Goddard Trajectory Determination System". GSFC. April 1976.
- (6) F. T. Geyling, H. R. Westerman: "Introduction to Orbital Mechanics". Addison-Wesley. 1971. Ch. 5.
- (7) J. R. Wertz (Editor): "Spacecraft Attitude Determination and Control". D. Reidel. 1978. Ch. 17.
- (8) V.V. A.A.: "Space Station Program Definition and Requirements". Section 3: Space Station System Requirements. NASA. S.S.P.D.. JSC 30000. Sec. 3. Rev. A. October 1985.
- (9) H. Hamacher et al.: "The Environment of Earth-Orbiting Systems". In: "Fluid Sciences and Materials Science in Space". H. U. Walter Editor. Springer-Verlag. 1987. Ch. 1.
- (10) W. D. MacMillan: "The Theory of the Potential". Dover. 1958. Ch. 2.

MATHEMATICAL MODELS REVIEW

prof. Silvio Bergamaschi
Institute of Applied Mechanics
University of Padua, Italy

Introduction

The purpose of this work package is twofold:

- to look at the specialized literature, at the purpose to find already developed mathematical models capable of simulating the motion of a system composed by the S.S. and by one or more masses tethered to it, and hence of evaluating the accelerations at points close to c.o.m.
- to survey the features desirable in such a model, in order to give suggestions about the most efficient way to implement it in a form amenable to computer use. In this respect, the first problem to be addressed is an old one, i. e.: is it preferable to have a general purpose computer code, or a library of more specialized, but independent routines?

The task is not so simple, because a number of models have been proposed since 1974. Thus, it has been decided to begin with an historical overview, intended to clarify what has been done in the field of the simulation of the motion of tethered systems and what is still to be done. For further details, the reader is addressed to the recent, excellent survey by Misra and Modi (1).

Dynamics Simulation Models Historiography

It has been found that the history of tethers in space can be traced back at least to 1895, when Tsiolkowskii, possibly amazed by the slenderness of the Tour Eiffel, conceived a space tower with its center of mass at geostationary altitude (2).

In the space era, however, the concept of a satellite to be tethered to the Space Shuttle was first proposed in a S.A.O. report of 1974, where its possible scientific uses were also outlined (3).

That report included the equations resulting from a two-dimensional model of tether dynamics, but no results were presented. In any case, the novelty of the concept stimulated other studies and in 1975 both NASA (MSFC) (4) and ESA (ESTEC) (5) sponsored independent research efforts intended, "inter alia", to investigate tether dynamics, with particular attention devoted to the feasibility of deployment and retrieval manoeuvres. For our purposes, it is interesting to recall the most important assumptions, common to both the models:

- Shuttle (or, in any case, main body) in circular, unperturbed orbit
- system c.o.m. coincident with Shuttle c.o.m.
- tether mass included, but elasticity neglected or masked
- satellite simulated as a point mass (as well as the Shuttle)

In synthesis, both the models simulated the system as a peculiar, variable length (three dimensional in the case of the NASA model) pendulum, attached to a point moving in a circular path, and subject to perturbations. In other words, they were as general as required by the need of demonstrating the feasibility of manoeuvres, but no more than that.

In the second half of the seventies, NASA sponsored the Phase B study for the TSS (Tethered Satellite System) and, at the same time, a number of

investigators, attracted by the intricacy of the problem, dedicated their efforts to the simulation of the motion of tethered satellites. The intent was to remove some of the simplifying assumptions mentioned above and/or to study particular aspects of the motion, of particular relevance for other applications of tethers which were being proposed in the same years. Some of them (e.g. gravity gradiometry) postulated very well known, or very clean from perturbations, acceleration levels at the platform where the experiments were supposed to take place, so that more refined models were needed.

The results of such simulation efforts were summarized at the beginning of the eighties by Misra and Modi (6) in a paper from which Table 1 is taken. The table reports the authors of implemented models vs. the features of the motion being simulated. The trend toward generality, as time goes on, is evident from the capability of some of them to simulate such characteristics as tether elasticity, attitude motion of the end bodies and offset of the tether attachment point at the Shuttle (with respect to c.o.m.).

Unfortunately, the penalty to be paid for the addition of such new capabilities, and in particular for the simulation of tether elasticity was a big one. The rigid body librations of a constant length tether are characterized by frequencies comparable to the orbital mean motion. In the small angle approximation, they are $\approx \sqrt{3}$ and 2ω , respectively, for the in plane and the out of plane components, corresponding to periods of about 52 and 44 min in LEO. The frequencies of tether elastic vibrations, both longitudinal and transverse, are much higher. To assess their order of magnitude, let us consider the TSS-1 case. From the results of (7) it is seen that the fundamental mode of the longitudinal vibrations (the so called spring-mass mode) has a period close to 45 sec, while the first harmonic of out of plane taut string vibrations has a period shorter than 7 min. These values depend on tether length, elastic properties and end

mass inertia, but are characteristic in the sense that, for any given configuration, the frequencies of elastic vibrations (in particular the longitudinal ones) are much higher than the mean motion; the same applies to the attitude motion of the end mass, the periods of which, for systems not excessively large, are likely to be in the minutes range or shorter.

As a consequence, the equations of motion are "stiff", so that, when using numerical methods for their solution, very short time steps have to be adopted. This was the reason why the most general computer codes reported in tab. 1 were excessively time consuming, frequently requiring integration times considerably larger (even 10 times) than the physical time. This was also the reason why most of them were abandoned and substituted by semianalytical models, less general in scope, but also extremely cheaper; (7) is an example of this generation of models.

It is noted that, in any case, the general purpose codes just mentioned were not sufficiently general to simulate the motion of the S.S. with two masses tethered to it, with the accuracy degree required by the present study; in fact, for instance, none of them included structural dynamics.

Also, the configurations considered were essentially dumb-bells. In more recent years, however, this last limitation was considerably relaxed.

Applications of tethers requiring systems considerably different from TSS had been proposed since the seventies, but in 1986, when the National Commission On Space (NCOS) released its report and included tethers as one of the areas deserving further attention in the future U.S. space policy, new ideas were proposed. NASA and PSN (the National Space Plan of Italy) established a joint task group at the purpose of coordinating the efforts in the two countries in the field of tether applications studies and demonstrations, with particular attention devoted to those of interest for S.S. operations. Without going into undue detail, it can be mentioned that some of these applications foresee:

- new scientific and technological goals

	Ebner ¹	Stulver and Bainum ²	Rupp ³	Baker et al. ⁴	Kulla ⁵	Buckens ⁶
Three dimensional motion	No	No	No	Yes	No	Yes
Tether mass	Yes	No	Yes	Yes	Yes	Yes
Longitudinal vibration of the tether	No	No	Yes	Yes	No	No
Longitudinal strain variation along the tether	No	No	No	No	No	No
Transverse vibrations of the tether	Yes	No	Steady state only		Yes	Yes
Torsional stiffness of the tether	No	No	No	No	No	No
Anisotropy of the tether	No	No	No	No	No	No
Discretization procedure	Galerkin	—	—	—	Finite difference	Galerkin
Rotational motion of end masses	No	Yes	No	Yes	No	No
Offset of the point of attachment at the Shuttle	No	Yes	No	No	No	No
Aerodynamic drag	No	No	Yes	Yes	Yes	No
Rotating atmosphere	No	No	No	Yes	No	No

Table 1 (continued)

	Kalaghan et al. ⁷	Modi and Misra ⁸	Modi and Misra ⁹	Misra and Modi ¹⁰	Kohler et al. ¹¹	Bainum and Kumar ¹²
Three dimensional motion	Yes	Yes	Yes	Yes	Yes	Yes
Tether mass	Yes	Yes	Yes	Yes	Yes	No
Longitudinal vibration of the tether	Masked	Yes	Yes	Yes	Yes	No
Longitudinal strain variation along the tether	Masked	No	No	Yes	Yes	No
Transverse vibrations of the tether	Masked	Yes	Yes	Yes	Yes	No
Torsional stiffness of the tether	No	No	No	No	Yes	No
Anisotropy of the tether	No	No	No	No	Yes	No
Discretization procedure	Point elements	Galerkin	Galerkin	Galerkin	Finite difference and Finite elements	—
Rotational motion of end masses	No	Yes	Yes	Yes	No	No
Offset of the point of attachment at the Shuttle	No	No	No	Yes	No	No
Aerodynamic drag	Yes	No	Yes	Yes	Yes	Yes
Rotating atmosphere	Yes	No	Yes	Yes	Yes	Yes

- configurations different from TSS
- new dynamical regimes for tether motion

Therefore, new simulation models have been implemented, or are under development to gain deeper insight into the motion of such systems. The models are new in two respects:

- They consider different configurations of tethered systems, as is the case of the work done at S.A.O. for constellations
- They study aspects of the dynamics not present in TSS. An example is the evaluation of the orbital decay or evolution of free tethers, after separation from both the end bodies

The result is that the already existing trend in favor of a library of relatively simple computational routines, as opposed to general purpose models, has been further extended. At the Tether Dynamics Simulation Workshop held in 1986, the question was posed whether a universal simulation program should be developed or not (8). The general consensus of the attending dynamicists was no. The reasons for this answer were different, including the crucial point that such a program might even not exist, because various applications could require their own "best" program. Therefore, what can be concluded on the basis of past experience is that, on account of the complexity intrinsic in the motion, different applications of tethers in space usually require dedicated and often highly specialized simulation models. This is the most important reason why acceleration levels at the scientific labs of the S.S. cannot be evaluated by means of already existing computer codes. For the same reason, this study has been started with a characterization of the force and torque fields which has made use of simple, but dedicated models, tailored to the desired degree of accuracy of the present purposes.

A Dedicated Computer Code

In the preceding chapter, as a result of the survey about the state of the art of dynamics simulations, it has been shown that the acceleration levels to be expected at the experiments locations on board the S.S. cannot be derived from the outputs of any existing computer code.

Therefore, the problem is now to examine the features desirable in a mathematical model to be possibly developed for that purpose and to decide which is the best choice between a single model and a set of more specialized ones.

The features of a computer code, necessary to predict with a good degree of accuracy the perturbation field at points fixed in the S.S. result from:

- the analysis of the perturbing field
- the mechanical features of the S.S. itself
- the accuracy of the micro-g level simulation to be achieved

Should the goal be to reach an accuracy of $10^{-9}g$, the majority of the perturbations considered in the force field characterization would have to be taken into account. This, of course, originates serious problems. To mention some of them:

- Air drag (a more refined model is needed) causes the orbit to decay, so that the usual simplifying assumptions of a given circular, or near circular orbit cannot be made. Further, orbital motion is coupled to attitude dynamics
- Since the attitude motion of the S.S. is likely to be the major source of perturbation, detailed information is needed about the control law and the actuators; otherwise, the simulation effort is physically meaningless

- A structural vibrations model should be included. The problem here is: how reliable such a model can be before in flight testing?

In addition, the code would suffer from the shortcomings common to the models mentioned above and pointed out in (8); in synthesis, the quality of a simulation depends not only on the mathematical method being used, but also on the accuracy of the input, both initial conditions and parameters. Inaccurate initial conditions can excite parasitic components of the motion, absent in real dynamics. In some cases such components are amplified as time goes on, thus causing the simulation to diverge asymptotically from real motion.

More serious seem to be the problem of parameters. In absence of sufficient information, some of them are usually given "reasonable" values, or even ignored. The classic example is the one concerning material damping. As is well known, the inclusion of damping in the dynamical models usually increases the amount of computations needed to obtain a solution. For this reason, whenever possible, mechanical systems are considered as conservative.

This assumption has been frequently used also in the simulation of tethered systems dynamics. However, in some problems, as the evaluation of the transient acceleration caused by the Orbiter docking to the S.S., damping must be taken into account. In this case, the simulation quality depends on the accuracy to which the damping matrices of the S.S. and of the tether(s) are known. In the tether case, some experimental work on damping has already been done, but the dispersion of data is large and, moreover, in flight conditions are considerably different; thus, the amount of uncertainty is also large. It is not known, at present, if energy dissipation on board the S.S. has been evaluated or not.

In conclusion, it is believed that:

- The task of implementing a model to simulate the motion of a system composed by the S.S., one or two tethered masses and, possibly, an

elevator, is a big one if such features as environmental forces, ADCS and structural vibrations are to be included

- The quality of simulations, or at least of some of them, might be lowered by lack of precision in the assignment of initial conditions and numerical values of parameters affecting the motion

Conclusions

In this section, it has been seen that previously developed general purpose computer codes cannot help in the evaluation of the perturbing acceleration inside the scientific modules.

The problem of the cost-effectiveness of implementing a new code, dedicated specifically to the present space system has also been examined. It is concluded that the effort is not advisable, because the possibility exists that some inputs can be evaluated with the desired degree of accuracy only by measurements made in situ.

As a consequence, the only viable approach to the problem seems to be the one being used in the present study. If, in the future, better accuracy will be needed, some of the models used herein can be substituted without impact on the others.

References

- (1) A. K. Misra, V. J. Modi: "A Survey on the Dynamics and Control of Tethered Satellite Systems". AAS paper n. 86-246. In: "Tethers in Space". Vol. 62 of the Advances in the Astronautical Sciences. Univelt Inc. 1987. pp. 667-719.
- (2) G. Von Tiesenhausen: "Tethers in Space. Birth and Growth of a New Avenue to Space Utilization". NASA TM-82571. MSFC. February 1984.
- (3) G. Colombo et al.: "Shuttle-borne "Skyhook". A New Tool for Low Orbital-Altitude Research". S.A.O. Report. September 1974.
- (4) W. P. Baker et al.: "Tethered Subsatellite Study". NASA TMX-73314. MSFC. March 1976.
- (5) P. Kulla: "Dynamics of Tethered Satellites". Proceedings of the Symposium of Dynamics and Control of non rigid Spacecraft. Frascati. Italy. May 1976.
- (6) A. K. Misra, V. J. Modi: "Deployment and Retrieval of a Satellite Connected by a Tether to the Space Shuttle". AIAA paper n. 80-1963. AIAA/AAS Astrodynamics Conference. Danvers . Ma. August 1980.
- (7) S. Bergamaschi et al.: "A Continuous Model for Tether Elastic Vibrations in TSS". AIAA paper n. 86-0087. AIAA 24-th Aerospace Sciences Meeting. Reno. Ne. January 1986.
- (8) C. C. Rupp: "Summary of the September 16 Tether Dynamics Simulation Workshop". AAS paper n. 86-247. In: "Tethers in Space". Vol. 62 of the Advances in the Astronautical Sciences. Univelt Inc. 1987. pp.721-724.

APPENDIX B

SMITHSONIAN ASTROPHYSICAL OBSERVATORY

TASK 1 REPORT

Analytical Investigation of
Tethered Gravity Laboratory

Aeritalia Contract 8864153

TASK 1 Report
Active Center of Gravity Control

Principal Investigator
Dr. Enrico C. Lorenzini

Co-Investigators

Dr. Mario Cosmo
Mr. David A. Arnold

November 1989

Prepared for
Aeritalia, Società Aerospaziale Italiana
Space System Group, Torino, Italy

Smithsonian Institution
Astrophysical Observatory
Cambridge, Massachusetts 02138

<p>The Smithsonian Astrophysical Observatory is a member of the Harvard-Smithsonian Center for Astrophysics</p>

CONTENTS

	Page
Summary	1
Figure Captions	2
SECTION 1. INTRODUCTION	5
2. TASK 1 TECHNICAL ACTIVITY	5
2.1 Introductory Remarks	5
2.2 Acceleration Noise And Tethered Systems' Dynamics	7
2.3 Simulation Model	8
2.4 Double Tether Centered System	11
2.4.1 Acceleration Noise	14
2.4.2 Noise Abatement Through Longitudinal Dampers	20
2.5 Single Tether System	24
2.5.1 Acceleration Noise	26
2.6 Double Tether System With Space Elevator	31

CONTENTS

	Page
SECTION 2.6.1 Acceleration Noise	33
2.7 Tethered Dynamic Absorber	43
2.7.1 Equivalent System	43
2.7.2 System Dynamics	48
2.7.3 Numerical Results	51
2.8 References	55
3. CONCLUSIONS	56

Summary

This Task 1 Report deals with the investigation of the dynamics of each one of the three tethered configurations proposed by Aeritalia for controlling the acceleration level on board the space station. Specifically the dynamic response and the apparent acceleration level on board the station are evaluated for each tethered system acted upon by environmental and gravitational perturbations. The effects of longitudinal dampers on the acceleration levels are also shown and the important role of the dampers is demonstrated through numerical simulation. The criteria followed for designing effective longitudinal dampers are also dealt with.

Furthermore the report assesses the capability of a tethered system in damping the first flexural mode of the single-transverse-boom space station.

Figure Captions.

- Figure 1. Reference frames and coordinates.
- Figure 2. Schematic of Double Tether Centered System (DTCS) and its discretization model.
- Figures 3(a)-3(f). Dynamic response of Double Tether Centered System (DTCS). Orbital parameters: 28.5° inclination, 180° initial anomaly, initially circular orbit, Sun at the Summer Solstice. Environmental and gravitational perturbations: thermal fluxes in and out of tethers, dynamic atmospheric density model (Jacchia's 1977), J_2 -gravity-term. Initial tether temperature equal to 380°K . Tether longitudinal dampers are deactivated.
- Figures 4(a)-4(b). Dynamic response of the DTCS like in Figures 3 except for the fact that two longitudinal dampers, each one tuned to the bobbing frequency of the associated tether segment, are activated.
- Figure 5. Schematic of Single Tether System (STES) and its discretization model.

Figures 6(a)-6(f). Dynamic response of STES. The assumptions are like in Figures 3. One longitudinal damper, tuned to the bobbing frequency of the only tether, is activated.

Figure 7. Schematic of Double Tether System with Space Elevator (DTSSE) and its discretization model.

Figure 8. Schematic of the 2-DOF system which models the bobbing oscillations of the lower tether. The station is modelled by the wall, m_1 is the elevator and m_2 is the lower-end-platform.

Figures 9(a)-9(i). Dynamic response of the DTSSE. The assumptions are like in Figures 3. Three longitudinal dampers, each one tuned to the bobbing frequency of the associated tether, are activated.

Figure 10. (a) Schematic of Tethered Dynamic Absorber for abating the first flexural mode the single-transverse-boom station.

(b) Schematic of the equivalent system of Tethered Dynamic Absorber.

Figure 11.

(a) Effective static moment required to a Tethered Dynamic Absorber for avoiding tether slackness vs. modal frequency. The flexural modal amplitude is assumed equal to 0.1m.

(b) Masses of end-platform, tether, and total mass of Tethered Dynamic Absorber vs. tether length for both steel and kevlar tether materials. The effective static moment is 10^8 kg-m and the frequency of the first flexural mode is 0.1 Hz.

1. INTRODUCTION

This is Task 1 Report submitted by the Smithsonian Astrophysical Observatory (SAO) under Aeritalia contract 8864153, "Analytical Investigation of Tethered Gravity Laboratory," Dr. Enrico C. Lorenzini, Principal Investigator. This Task 1 Report covers all the technical activity carried out at SAO on the *Active Center of Gravity Control*.

2. TASK 1 TECHNICAL ACTIVITY

2.1 Introductory Remarks

The analysis performed by Aeritalia (AIT) has identified four different configurations of tethered systems to be attached to the initial IOC (transverse boom only) configuration of the space station (SS). These four tethered systems were designed not only to provide alternative ways of controlling the acceleration levels on board the SS but also for providing additional capabilities such as the variable gravity laboratory and the damping of flexural modes of the station.

The control of the static position of the center of gravity of the overall system and hence of the acceleration bias on board the SS has been carried out by Aeritalia. The results of the analysis, shown in the AIT Quarterly Progress Report #1, have been used by Aeritalia to design the four different tethered configurations. The four tethered configurations are:

1. Double Tether Centered System (DTCS0
2. Single Tether System (STS)
3. Double Tether System with Space Elevator (DTSSE)
4. Shifted Double Tether System (SDTS)

In particular system 4 had been designed to control the attitude of the station (directly related to the acceleration levels) but has later been discarded by Aeritalia based on considerations of operational constraints.

Out of the three configurations left two must be selected at the end of this contractual task as the most promising for controlling the acceleration levels on board the station and optionally for providing additional capabilities to the station. Before making such a selection a fundamental topic had to be addressed, namely the evaluation of the acceleration noise produced on board the station by each one of the three tether configurations.

2.2 Acceleration Noise And Tethered Systems' Dynamics

On one hand a tethered system attached to the space station provides some unique capabilities for the station as briefly mentioned in the previous section. On the other hand since a tethered system has a large exposed area and covers long distances it is affected by several environmental perturbations such as aerodynamic drag, thermal disturbances, and non-spherical gravity effects of which the J_2 term is the most important. The effects of these perturbations are small but non-negligible when we consider acceleration levels as low as 10^{-6} g. For this reason each one of the three tethered configurations, which passed the first selection by Aeritalia, were further investigated by SAO to assess the acceleration noise level transmitted to the space station when each tethered system is acted upon by environmental perturbations.

Based upon previous experience with tethered systems for microgravity applications, we know that longitudinal (along the tethers) dampers are necessary for achieving a microgravity level well below 10^{-5} g. The thermal perturbations, in fact, cause quasi-impulsive variations of the tether lengths each time the system crosses the terminator. Consequently the longitudinal component of the acceleration on board the SS builds up over several orbits exceeding the 10^{-5} g level, unless longitudinal dampers are added to the system.

2.3 Simulation Model

The analysis of the dynamics of the three tethered systems attached to the space station has been carried out by means of one of the SAO computer code, developed under a different contract. The code models a tethered system with a number of massive, point-like lumps connected by springs and dashpots. The lumps are either tether lumps or platform lumps and their masses are consequently very different. A numerical integrator, which can be a variable-step 4th-order Runge-Kutta or a predictor-corrector, integrates the acceleration components of each lump with respect to a rotating orbiting frame ORF (see Figure 1). ORF rotates on a circular orbit at the constant orbital rate Ω for that altitude. The origin of ORF is selected by the user at the beginning of the simulation run. Usually it is chosen to coincide with the system center of mass (CM) or the system orbital center (CO) or the space station itself. As the simulation progresses the origin of ORF and the tethered system depart from one another owing to the environmental and orbital perturbations.

The cartesian coordinates of the lumps are the integration variables of the computer code. We also use another set of variables to provide a more pictorial and to some extent physical description of the system dynamic. This set of coordinates is formed by (see Figure 1): the distances ℓ_i between successive lumps, the deflections ϵ_0 's of the inner lumps with respect to the line through the end-platforms, and the in-plane and out-of-plane libration angles of the overall

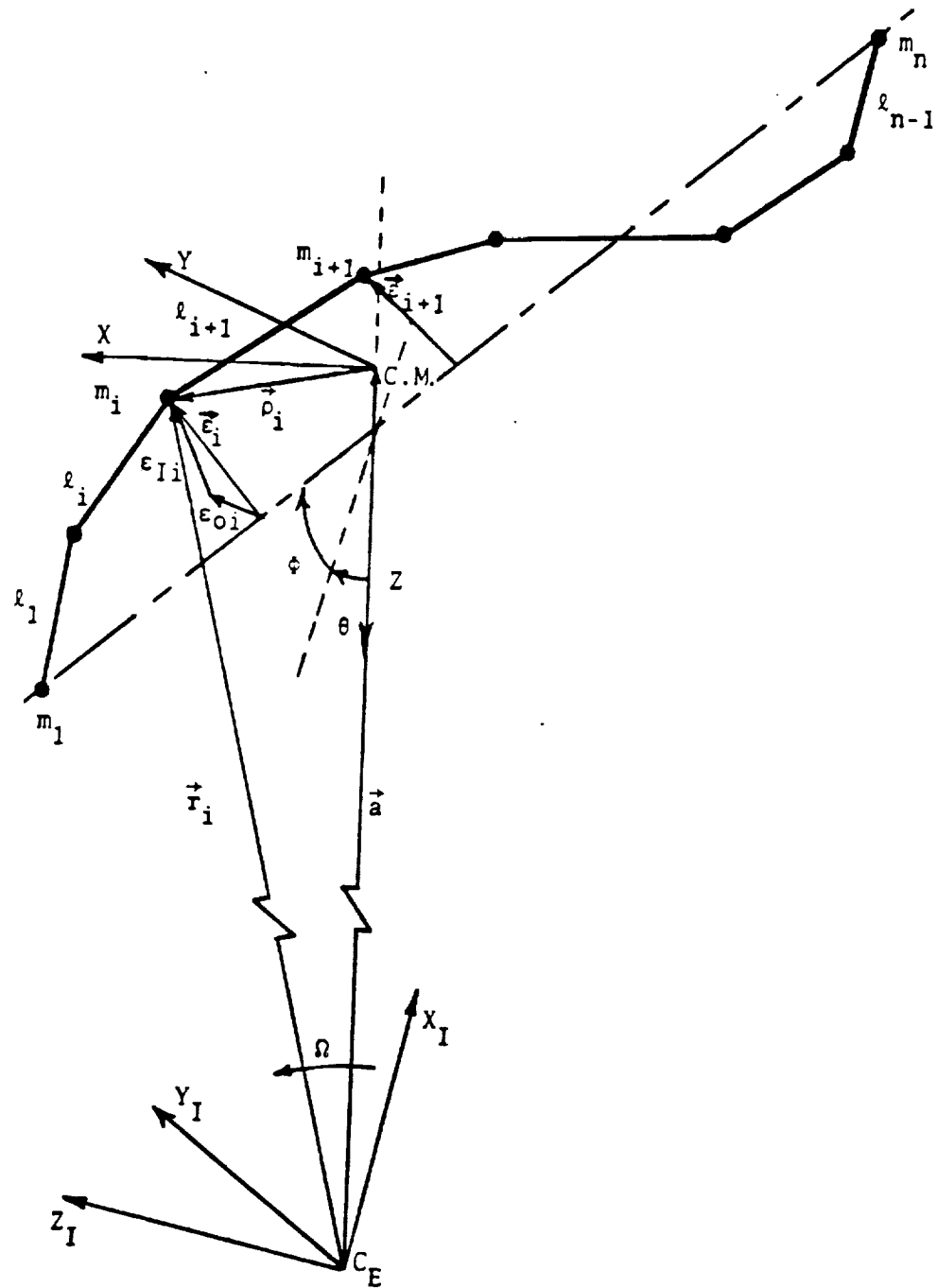


Figure 1.

system with respect to the local vertical (LV). The deflections ϵ_i 's are then projected onto the in-plane components ϵ_I 's and the out-of-plane components ϵ_O 's. This new set of variables will be used extensively in the next sections.

The simulation code is also equipped with subroutines which model aerodynamic forces, gravity forces, and thermal fluxes.

Because of the very low acceleration levels in which we are interested, an accurate model of external forces is necessary in order to simulate with high enough fidelity the effects of the environment on the system dynamics. The main external perturbations are: the gravitational forces F_g the aerodynamic forces F_d , and the thermal effects on the tensional forces F_T .

The gravity model of the computer code is not linearized and takes into account zonal harmonic of the gravity field (J_2 -term). The J_2 -term has a secular effect on such orbital parameters of the system as mean anomaly, argument of perigee, and right ascension of the ascending node. The J_2 -term also affects the librations and lateral oscillations (see next sections) of long tethered systems like those under analysis.

The drag model is an analytical fit of Jacchia's 1977 density model. The atmospheric density varies as a function of the altitude (the Earth's oblateness is also considered) and the local exospheric temperature. The latter takes into account the diurnal variation, which is a function of the argument of longitude and

solar activity.

The thermal inputs on the tether segments are: the solar illumination, the Earth's albedo, and the IR Earth radiation. The only cooling process is the emitted radiation. The position of the terminator is computed as a function of the Sun's position along the ecliptic. As the system crosses the terminator, the tether temperature varies abruptly; consequently the tether segments expand or contract and the tethers' tensions exhibit steep variations. The $N-1$ equations of the thermal balance of the tether segments are added to the equations of motion and integrated numerically by the integrator.

2.4 Double Tether Centered System

The Double Tether Centered System (DTCS) proposed by Aeritalia is the first one that we analyzed. We simulated the dynamics of this configuration both with and without longitudinal dampers to show the different acceleration levels for the two cases.

The DTCS has been modelled by 9 lumps: 3 lumps for the platforms and 3 lumps for each one of the tethers as shown in Figure 2. We rounded off the values of the masses of the platforms and of the length of the upper tether adopted by Aeritalia. We also computed again the length of the lower tether which provides the equilibrium of the forces (or zero apparent acceleration) at the space station. For a long tether system, in fact, the point of zero net force

(orbital center) does not coincide neither with the CM nor with the center of gravity CG. The gravity force is non-linear and its departure from linearity has a non-negligible effect for long tethered systems if we are interested in micro-gravity acceleration levels. The design parameters of the DTCS, with the orbital center at the space station, is therefore as follows (see Figure 2):

$$M_1 = 3050 \text{ kg}$$

$$M_2(SS) = 200 \times 10^3 \text{ kg}$$

$$M_3 = 5400 \text{ kg}$$

$$\ell_1 = 8360 \text{ m}, m_{T1} = 2490 \text{ kg}, \text{dia}_1 = 0.012 \text{ m}$$

$$\ell_2 = 6000 \text{ m}, m_{T2} = 1191 \text{ kg}, \text{dia}_2 = 0.010 \text{ m}$$

where m_{T1} and m_{T2} are the masses of the lower and upper tether respectively. If we adopt aluminum tethers, as proposed by Aeritalia, the stiffness coefficients of the two tethers are $EA_1 = 8,482,300 \text{ N}$ and $EA_2 = 5,890,486 \text{ N}$ respectively. We also adopt a viscous damping model for the longitudinal oscillations of the tethers. This implies that the ratio between the axial tether viscosity EA' and its stiffness EA is constant; consequently the critical viscosity is a linear function of the longitudinal wavelength. This damping model is not agreed upon by all the investigators. Nevertheless, it is a conservative model and is therefore a prudent choice before any other experimentally tested damping model of tether material is produced. For the simulation runs, shown later on, we assume a critical

Double Tether Centered System (DTCS)

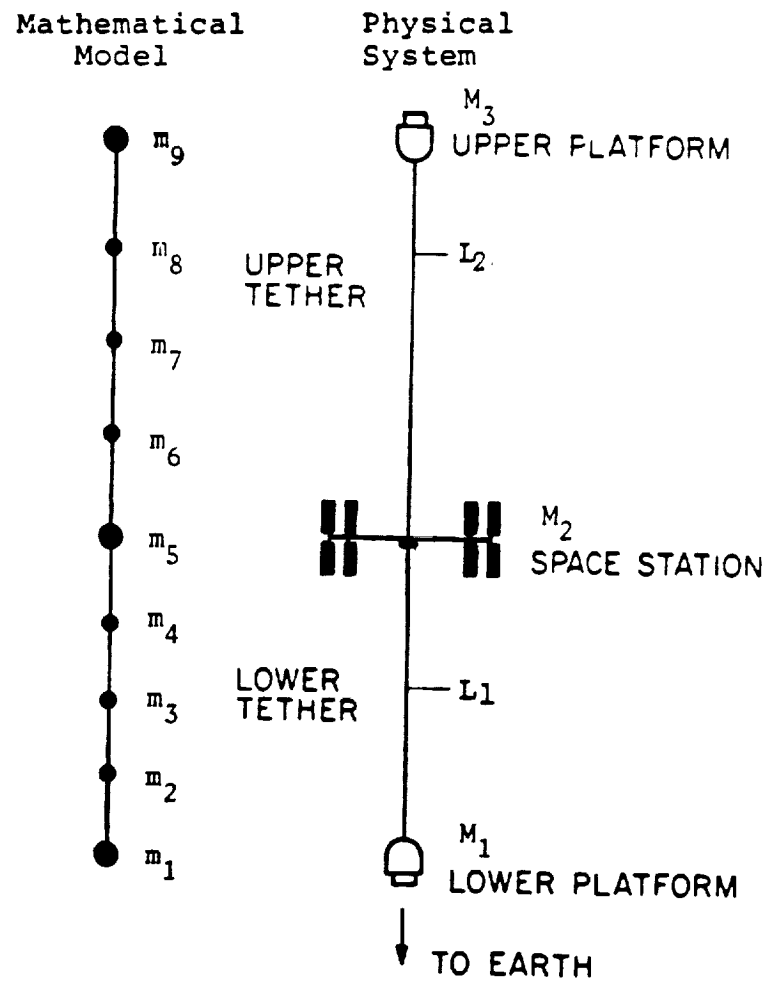


Figure 2.

wavelength of longitudinal waves of about 60 m. This means that any longitudinal wave, propagating along the tether, with a wavelength shorter or equal to 60 m is asymptotically damped. The values of axial tether viscosities for the DTCS, consistent with the above critical wavelength, are $EA'_1 = 30,000$ N-sec and $EA'_2 = 20,000$ N for the lower and upper tether respectively. The orbital altitude of the system is 352 km and the inclination 28.5° . These values are the same for the three configurations under analysis.

2.4.1 Acceleration Noise -

For the first simulation run of the DTCS we assume that the system has no longitudinal dampers. The simulation starts with the system aligned with the local vertical. The initial conditions are equilibrium initial conditions which means that the initial elastic stretches have been appropriately computed to balance the external forces. The initial orbital anomaly is equal to π on a 28.5° inclination orbit with the space station initially at 352 km of altitude. The Sun is at the Summer Solstice and the initial tether temperature T is the equilibrium temperature of an aluminum tether which is steadily exposed to Sun rays perpendicular to its longitudinal axis. The thermal characteristic of the aluminum tether are summarized below:

$$c = \text{specific heat} = 962 \text{ J/Kg-}^\circ\text{K}$$

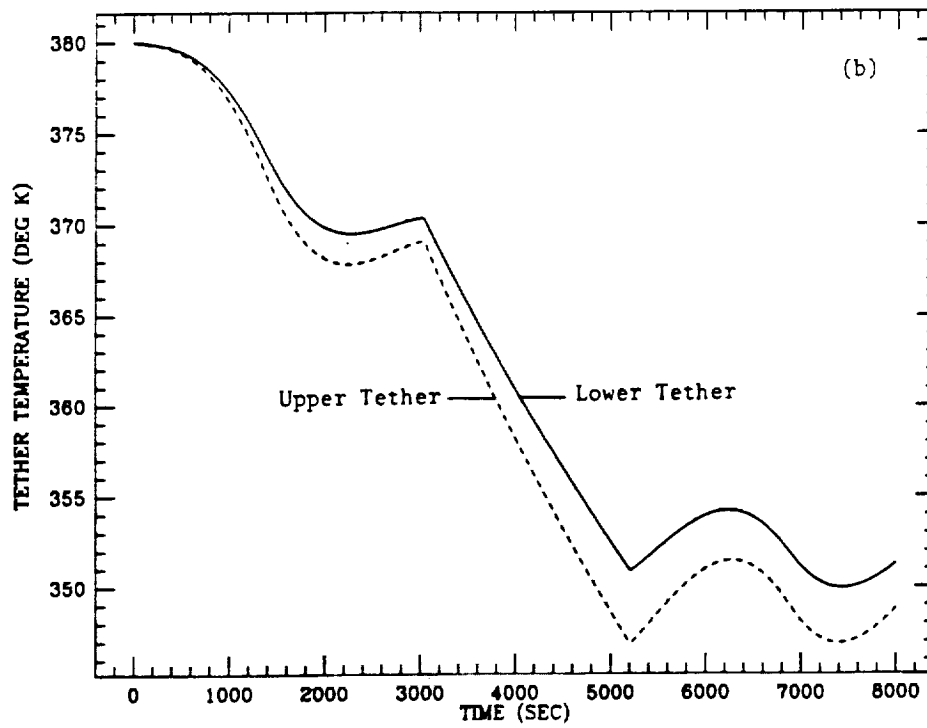
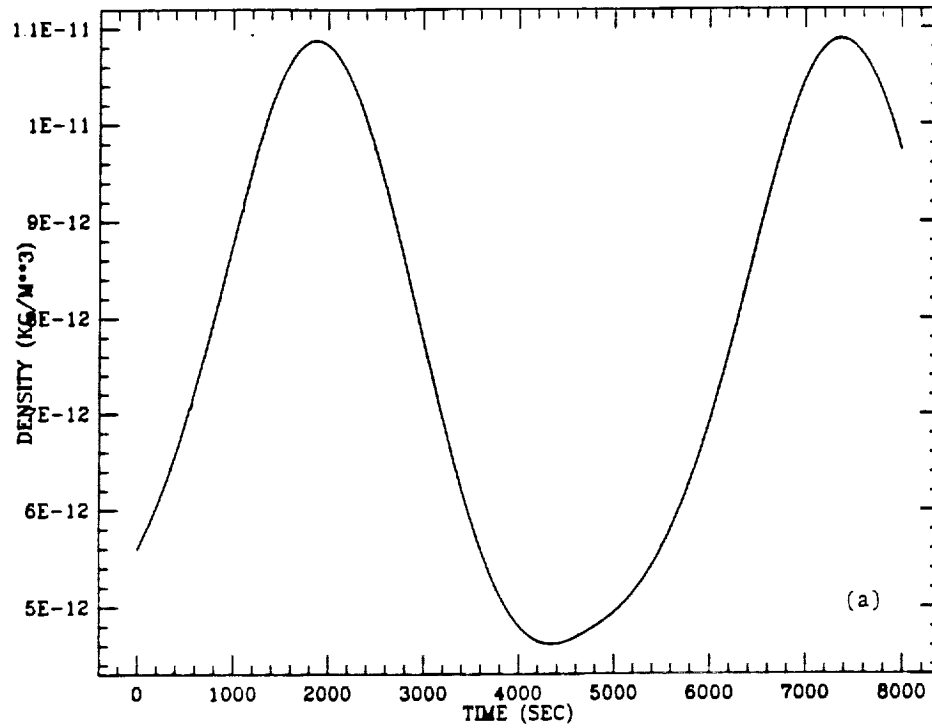
$$\begin{aligned}
\rho &= \text{volume density} = 2700 \text{ kg/m}^3 \\
\epsilon &= \text{emissivity} = -0.01 + 6.6 \times 10^{-7} T^2 \\
\alpha &= \text{absorptivity} = 0.2 \\
\alpha_{\text{IR}} &= \text{IR absorptivity} = 0.05 \\
\delta &= \text{coefficient of thermal expansion} = 1.3 \times 10^{-5} \text{ } ^\circ\text{K}^{-1}
\end{aligned} \tag{1}$$

The drag model, described briefly in Section 2.3, has an average exospheric temperature of 900 °K (the local exospheric temperature in the model depends on the argument of longitude). The gravity model is described in Section 2.3. The duration of the simulation run is 8000 sec or 1.5 orbits since the orbital period is equal to 5495 sec.

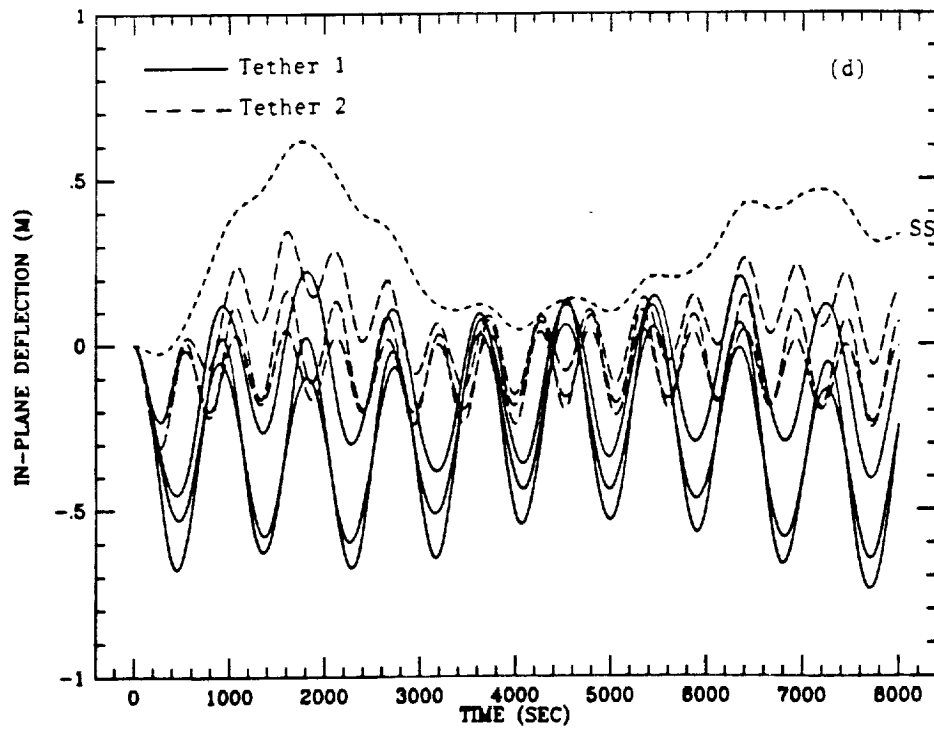
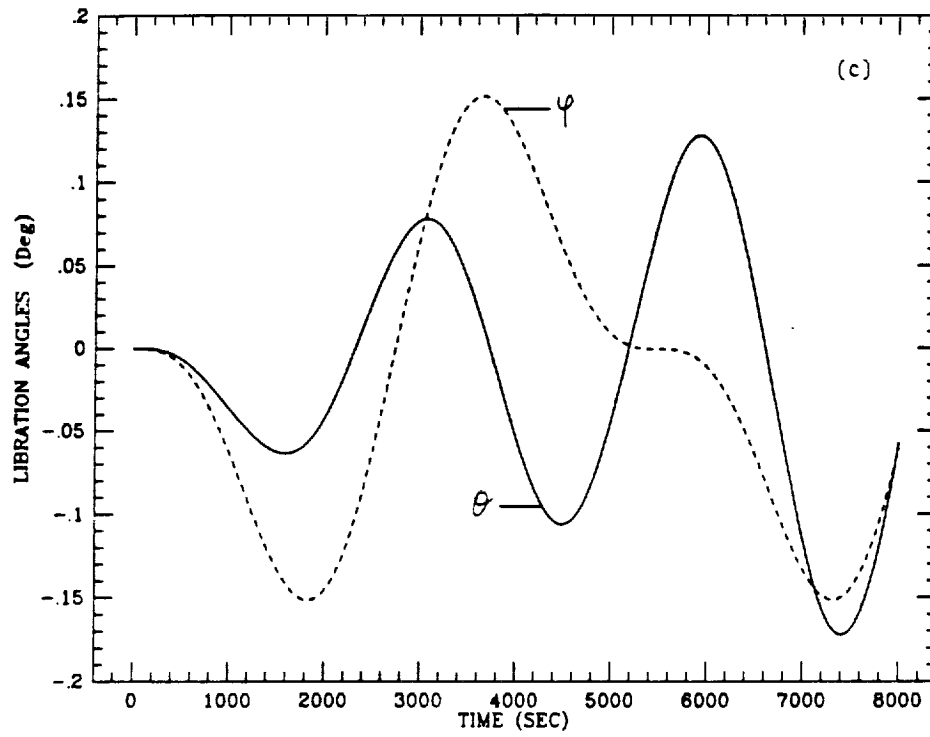
The relevant features of this simulation run are shown in Figures 3(a)-3(f). Specifically Figure 3(a) shows the atmospheric density profile at the SS over 1.5 orbits according to the model implemented in our simulation code. The density profile is valid for all the simulation runs shown in this report. Figure 3(b) depicts the temperatures of the lower and upper tether respectively. The two temperature profiles are slightly different from one another owing to the different tether diameters. Since the lower tether is thicker and more massive its thermal inertia is larger than the upper tether. From the temperature profiles it is easy to see the effect of the changing view factor and the eclipse. In particular the derivative of the temperature is discontinuous at each crossing of the terminator.

Figures 3(c) and 3(d) show the in-plane θ , the out-of-plane φ libration angles and the in-plane tether deflections ϵ_I 's respectively. The out-of-plane tether deflections are negligible. The magnitudes of the libration angles and in-plane deflections are small which implies that the drag and J_2 gravity perturbations have a relatively moderate effect upon the system dynamics. Specifically the librations are excited primarily by the J_2 and the tether deflections by the atmospheric drag. It is worth noticing that in Figure 3(d) the two tethers trail the SS (lump 5). The two tethers, moreover, vibrates as a violin string with two different frequencies, as shown in Figure 3(d), owing to their different linear densities.

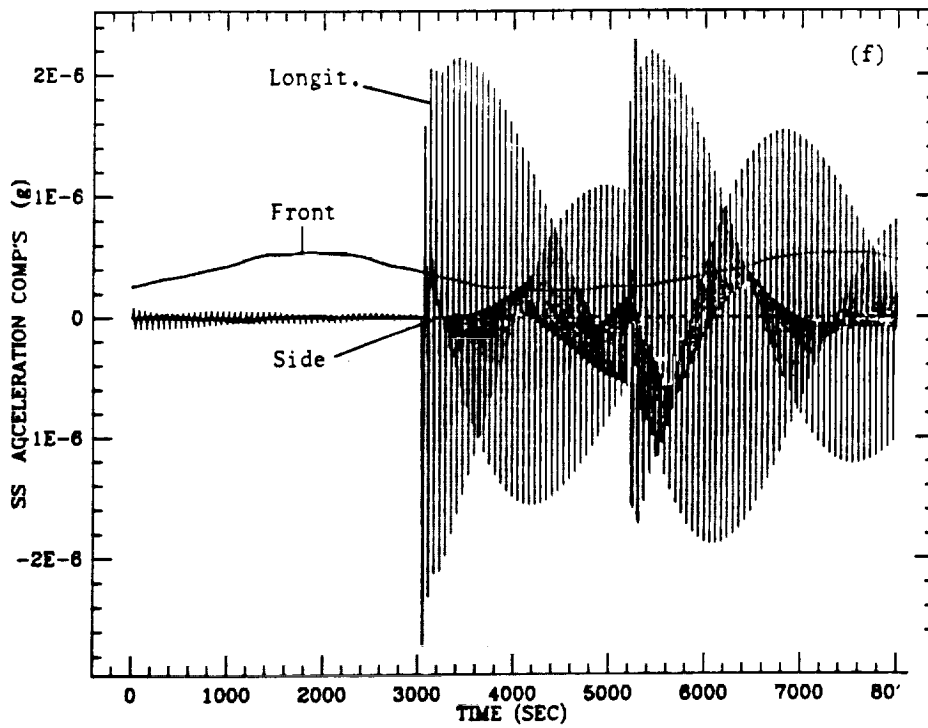
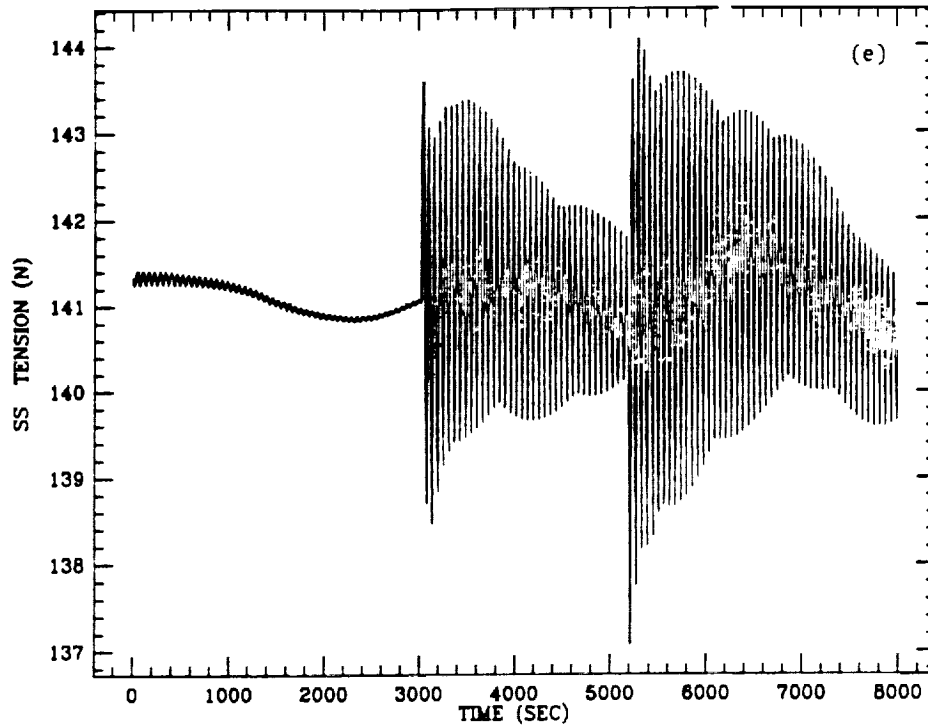
Figure 3(e) shows the tether tension at the SS attachment points; the upper and the lower tether tensions at the SS are very close because the SS is at the orbital center. The low frequency oscillation, caused by system librations which are driven by the J_2 gravity term, is clearly shown in the figure. The effects of the thermal shocks at the crossings of the terminator are also shown in the figure. The thermal shocks excite tether longitudinal oscillations which perturb the acceleration level on board the SS. In the absence of tether longitudinal dampers (consistent with the assumptions for this run) the tether tension, and consequently the acceleration level, builds-up reaching the maximum value around the 10th-orbit as we learned from longer simulation runs of other tethered systems. The effect of all the environmental perturbations is clearly shown in Figure 3(f) which depicts the longitudinal, front and side components of the acceleration measured on board the SS. These components are referred to the



Figures 3(a) and 3(b).



Figures 3(c) and 3(d).



Figures 3(e) and 3(f).

tether-body reference frame which provides an accurate representation of the SS body-reference-frame (our model does not have the rotational dynamics of the platforms) since it is reasonable to assume that, for small angles, the SS librates like the overall system. The front component is generated by the air drag acting upon the SS (cross section $A = 1400 \text{ m}^2$), the end platforms ($A = 10 \text{ m}^2$ for each platform), the lower tether ($A = 100.3 \text{ m}^2$), and the upper tether ($A = 60 \text{ m}^2$). The side acceleration component is negligible. The longitudinal component is affected primarily by the thermal shocks. The shocks force the system to ring, in particular they excite the longitudinal tether oscillations which, in the absence of longitudinal dampers, are only moderately abated by the tether material damping.

2.4.2 Noise Abatement Through Longitudinal Dampers -

The longitudinal tether oscillations triggered by the thermal shocks can be abated by adding a longitudinal damper for each tether. The damper can be a passive device in the form of a spring-dashpot system placed in series to the tether, or it can be active. In the latter case each reel controls the associated tether according to a proportional-derivative control law. Since the tethers of the DTCS are relatively stiff and consequently the elastic stretches are only a few centimeters long, passive dampers can be easily implemented by inserting spring-dashpot devices between the tethers' tips and the attachment points to the end-platforms.

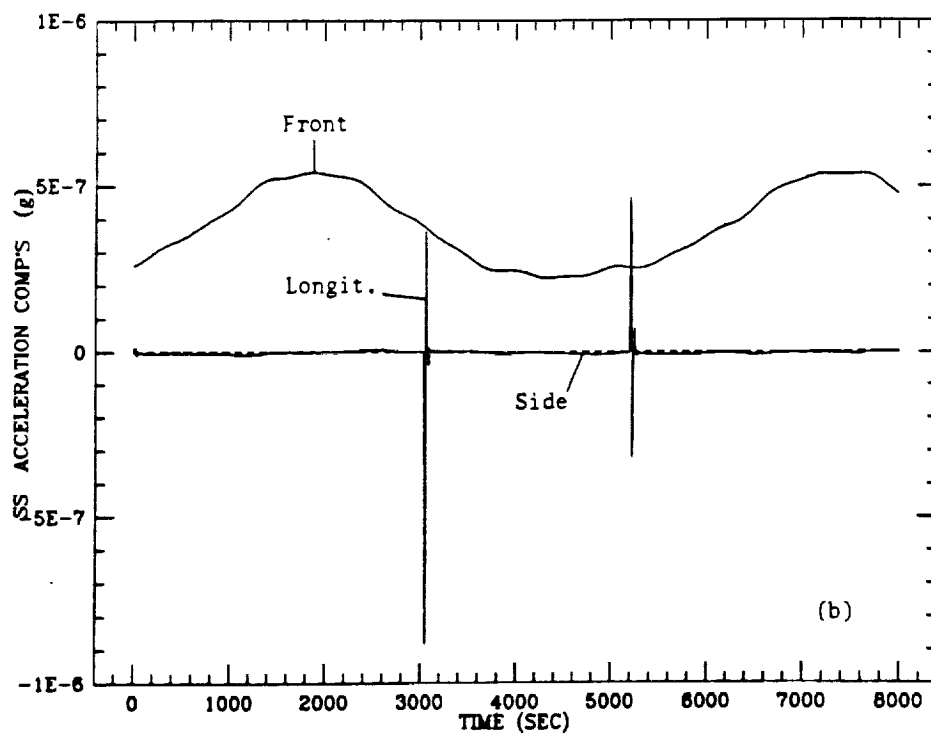
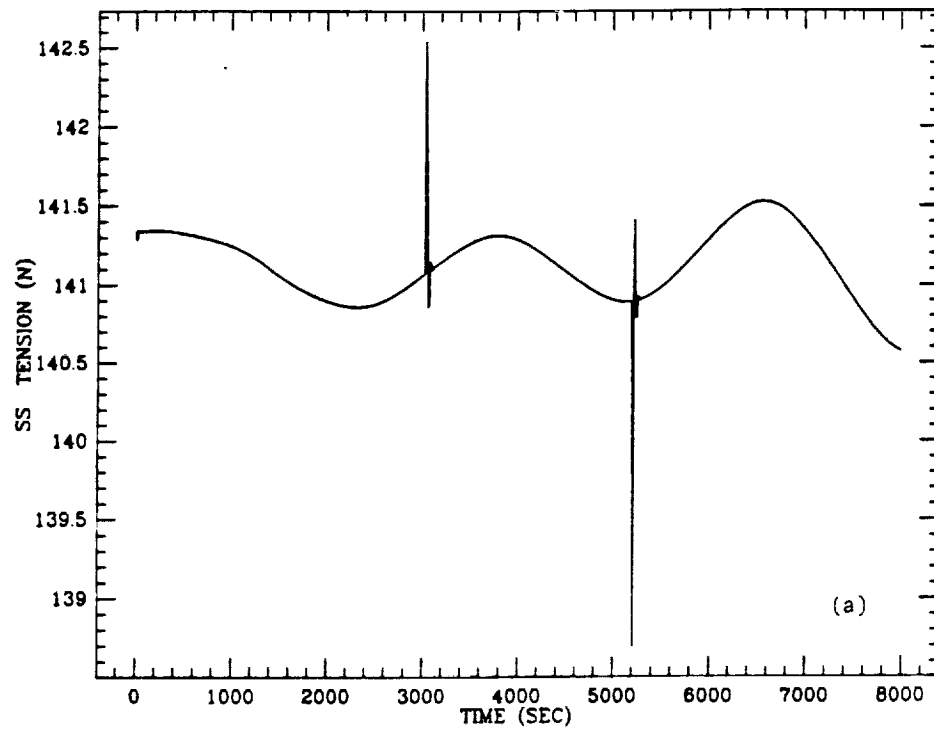
In reference [1] an optimization of the dynamic response of a longitudinal damper in series with a tether has been carried out. The damper-plus-tether system is a third order oscillating system if the intrinsic mass of the damper is neglected. The damper parameters, ω_d = angular frequency and b_d = damping coefficient, which provide the fastest decay time after the action of an impulsive perturbation, have been computed in reference [1]. The results indicate that a damper tuned to the tether bobbing frequency is a sub-optimal solution. The decay time may actually be faster for a detuned damper at the expenses, however, of a larger elastic tether stretch and hence a larger fluctuation of the acceleration. We have therefore opted for the sub-optimal tuned damper. Reference [1] also indicates the best value of damping coefficient for a tuned damper. The optimal value of b_d is consistent with a damping ratio equal to 0.9 for the response of the hypothetical 1-DOF damper system (the damper is assumed to be directly connected to the end-platform in this hypothetical system). The value of b_d is therefore given by:

$$b_d = 1.8 EA/(\ell\omega_o) \quad (2)$$

where ω_o is the bobbing frequency of the tether which is also equal to the damper frequency ω_d since the damper is tuned. After carrying out the computations we obtain:

$$\begin{aligned}
\omega_{d1} &= \omega_{01} = 0.4927 \text{ rad/s} && (\text{lower tether}) \\
b_{d1} &= 3,707 \text{ N/(m/s)} \\
\omega_{d2} &= \omega_{02} = 0.4113 \text{ rad/s} && (\text{upper tether}) \\
b_{d2} &= 4,297 \text{ N/(m/s)} && (3)
\end{aligned}$$

We run a second simulation of the DTCS like the one shown in the previous chapter except for the addition of the two longitudinal dampers defined above. The results of this simulation are shown in Figures 4(a)-4(b). The libration angles and the tether deflections, as expected, are not affected by the longitudinal dampers. The longitudinal dynamics, on the contrary, is strongly affected. As shown in Figures 4(a) and 4(b), the tether tension at the SS and the longitudinal component of the acceleration have been strongly abated. The longitudinal oscillations are rapidly reduced to zero after the terminator's crossings. The values of the peaks are reduced to a value comparable to the front acceleration component. Furthermore, based on our experience with longer simulation runs of tethered systems, the build-up of longitudinal oscillations is avoided with the longitudinal dampers. The maxima shown in Figures 4(a) and 4(b) are, therefore, absolute maxima. The maximum acceleration on board the SS, in this case, is always smaller than 10^{-6} g.



Figures 4(a) and 4(b).

2.5 Single Tether System

The second configuration proposed by Aeritalia is a Single Tether System (STES) designed to compensate for the static position of the system orbital center. We have simulated the dynamic of this system in order to evaluate its acceleration noise. Following a path similar to that of the previous section we model the system with a number of lumps. This time we adopt 4-lumps: two for the platforms and two for the tether. Since this system is quite stiff a higher number of lumps would result in very long CPU times. 4-lumps provide, however, enough resolution for the purpose of our analysis. The design parameters of STES, proposed by Aeritalia, are shown below (see Figure 5):

$$M_1 = 70.4 \text{ kg}$$

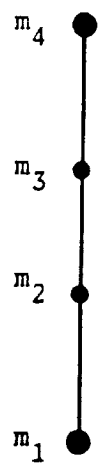
$$M_2(SS) = 200 \times 10^3 \text{ kg}$$

$$\ell_1 = 1660 \text{ m}, m_T = 79 \text{ kg}, \text{dia} = 0.005 \text{ m}$$

which result in a tether stiffness coefficient $EA = 1,472,622 \text{ N}$ and an axial tether viscosity $EA' \simeq 5000 \text{ N-sec}$ if we assume tether material characteristics like those of the DTCS. The tether material is as suggested by Aeritalia, aluminum with the thermal properties given by equations (1) of Section 2.4.1.

Single Tether System (STES)

Mathematical
Model



Physical Model

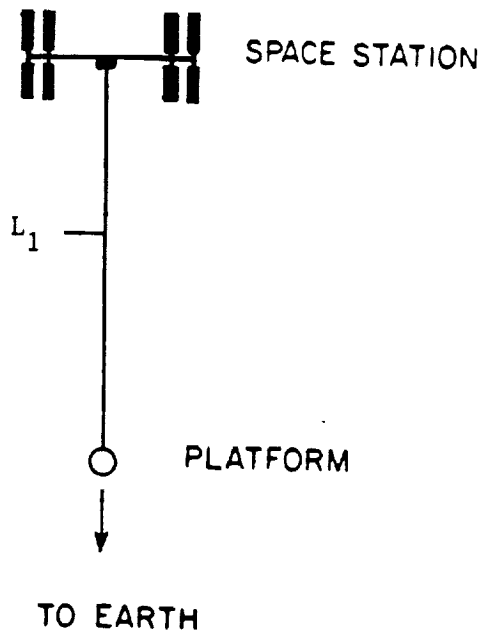


Figure 5.

2.5.1 Acceleration Noise -

A simulation of STES has been run according to the same assumptions described in Section 2.4.2. Specifically one longitudinal damper with the following characteristics

$$\omega_d = \omega_{01} = 2.842 \text{ rad/s}$$

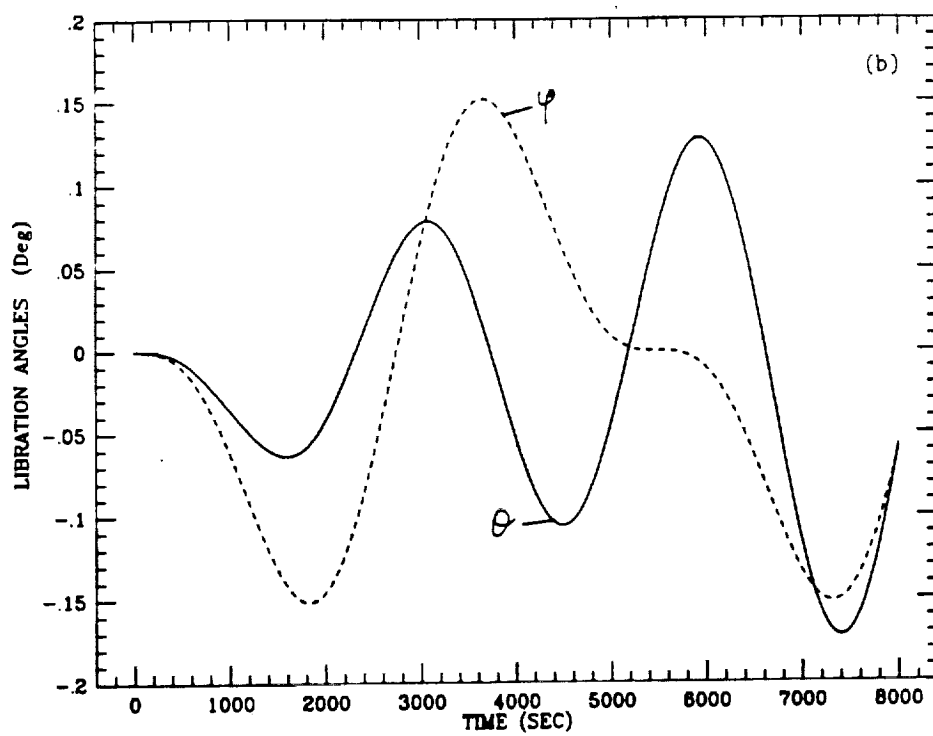
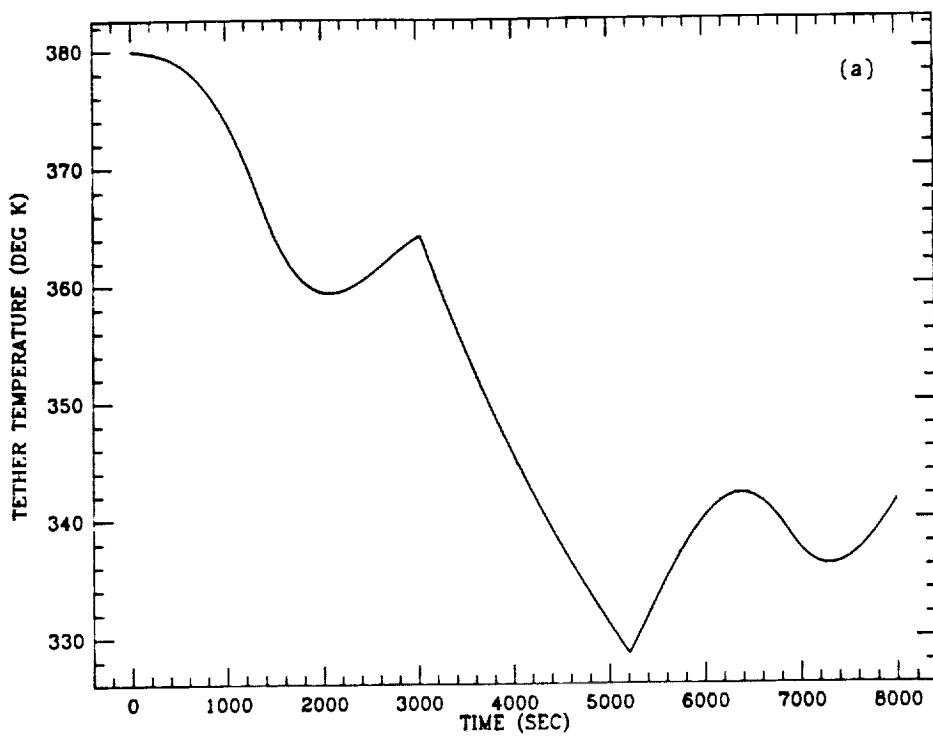
$$b_d = 562 \text{ N/(m/s)}$$

is placed in series to the tether. It is worth mentioning that since our simulation code models the platforms as point masses the simulation model does not reflect the offset between the space station's CM and the geometrical center of the microgravity laboratory on board the station. In other words when the simulation code computes the acceleration level on board the station it views the station as a point.

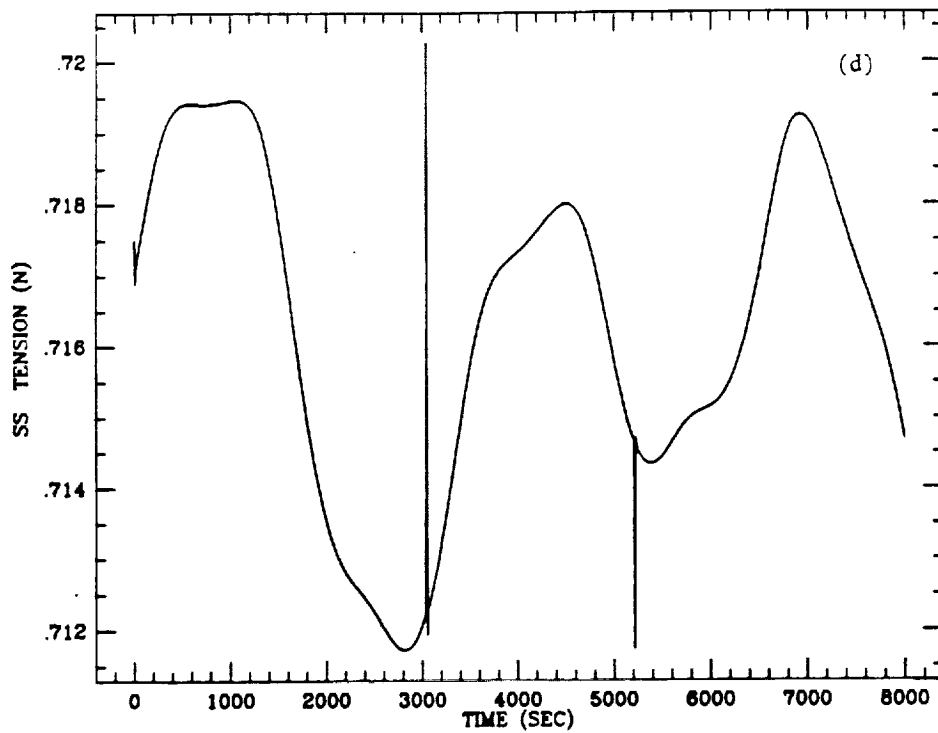
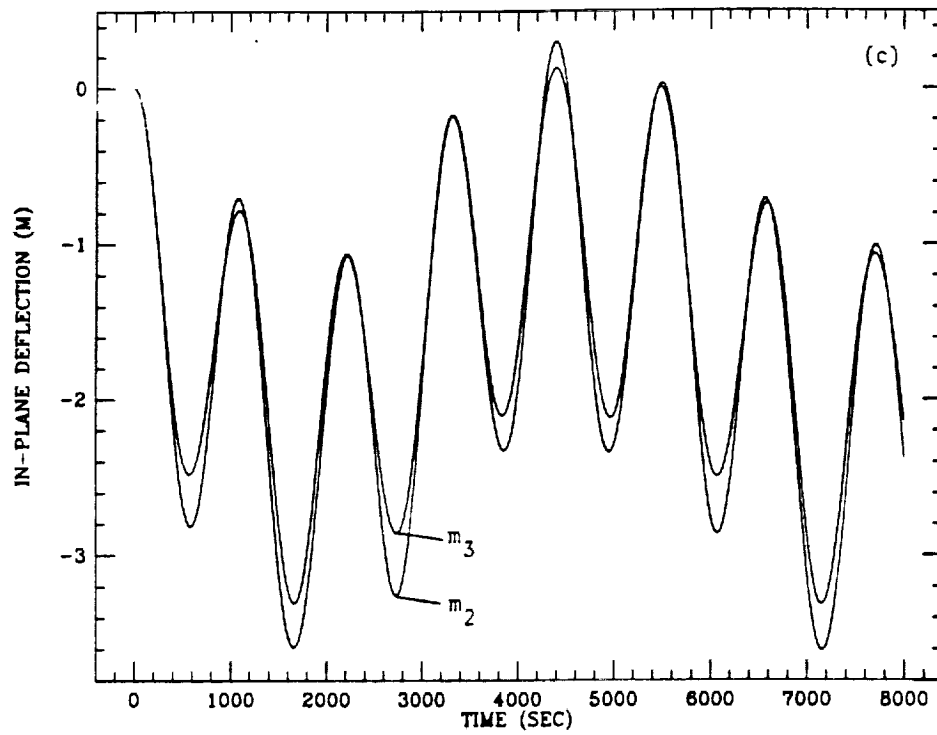
The results of this simulation run are shown in Figures 6(a)-6(e). The atmospheric density profile is like that of Figure 3(a). The tether temperature is shown in Figure 6(a). The temperature profile resembles that of Figure 3(b). The magnitude is slightly different owing to the different tether diameter. The in-plane θ and out-of-plane φ libration angles are shown in Figure 6(b) while the in-plane tether deflections are depicted in Figure 6(c). The deflections are bigger than for the DTCS because of the lower tension of STES [see Figure 6(d)] which,

therefore, provides a smaller restoring force. Finally Figure 6(e) shows the components of the acceleration measured on board the SS. The front component, which is primarily related to the air drag acting upon the SS frontal section, is the largest component. The side component is negligible. The longitudinal component is also relatively smooth [see also the enlargement in Figure 6(f)]. This is most probably due to the shorter tether length, with respect to the DTCS, and also to the lighter end-platform. A lighter end-platform allows the tether to shorten or lengthen more freely following a temperature variation, without causing a large fluctuation of the tension, and hence of the apparent acceleration.

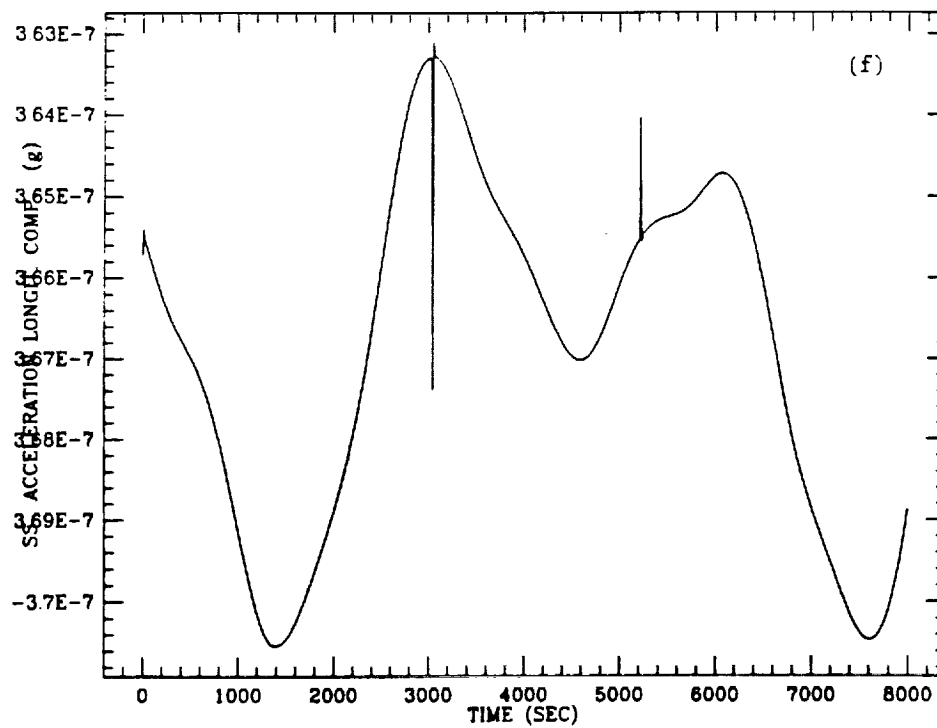
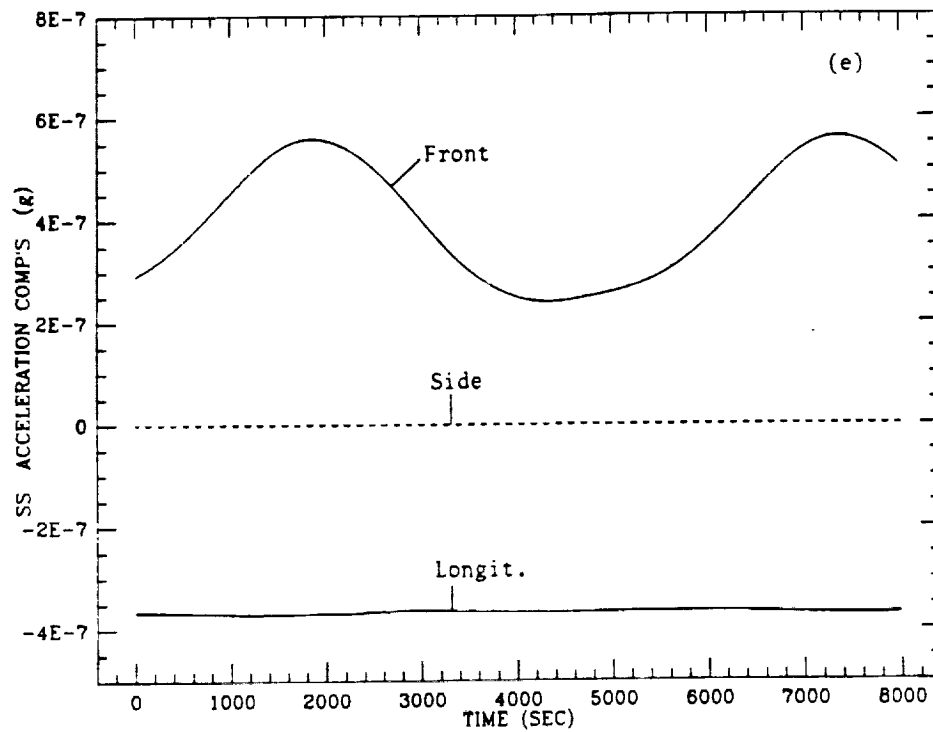
The longitudinal acceleration component, as explained before, is not computed at the location of the microgravity laboratory. Actually, the bias of the longitudinal acceleration corresponds to a 1-m-offset between the station CM and the microgravity lab. Consequently the bias at the microgravity lab is close to zero. In conclusion the STES appears to be less noisy than the DTCS. Both the STES and the DTCS are well within the 10^{-5} g microgravity requirement on board the station. In particular the tether-related acceleration fluctuations around the DC value on board the SS are of the order of 10^{-8} g for STES.



Figures 6(a) and 6(b).



Figures 6(c) and 6(d).



Figures 6(e) and 6(f).

2.6 Double Tether System With Space Elevator

The third configuration proposed by Aeritalia is a Double Tether System with Space Elevator (DTSSE). Like for the first configuration we adopt the rounded-off design parameters, indicated by Aeritalia, for the upper side of the system (where the elevator is located) and we compute the tether length of the lower side in order to have the orbital center at the SS. With reference to Figure 7 the design parameters of the DTSSE are

$$M_1 = 2250 \text{ kg}$$

$$M_2(EL) = 2250 \text{ kg}$$

$$M_3(SS) = 200 \times 10^3 \text{ kg}$$

$$M_4 = 3460 \text{ kg}$$

$$\ell_1 = 4060 \text{ m}, \quad m_{T_1} = 774 \text{ kg}, \quad \text{dia}_1 = 9 \text{ mm}$$

$$\ell_2 = 1640 \text{ m}, \quad m_{T_2} = 313 \text{ kg}, \quad \text{dia}_2 = 9 \text{ mm}$$

$$\ell_3 = 4977 \text{ m}, \quad m_{T_3} = 949 \text{ kg}, \quad \text{dia}_3 = 9 \text{ mm}$$

The three tether segments have therefore the same stiffness coefficient $EA = 4,771,294 \text{ N}$ and the same axial viscosity $EA' \simeq 16,500 \text{ N-sec}$ consistent with the values adopted in the previous sections. The tethers are made of aluminum as proposed by Aeritalia. The discretization model for the DTSSE is a 10-lump-model: 2 evenly spaced lumps for each of the three tether segments and 4 lumps for the 4 platforms.

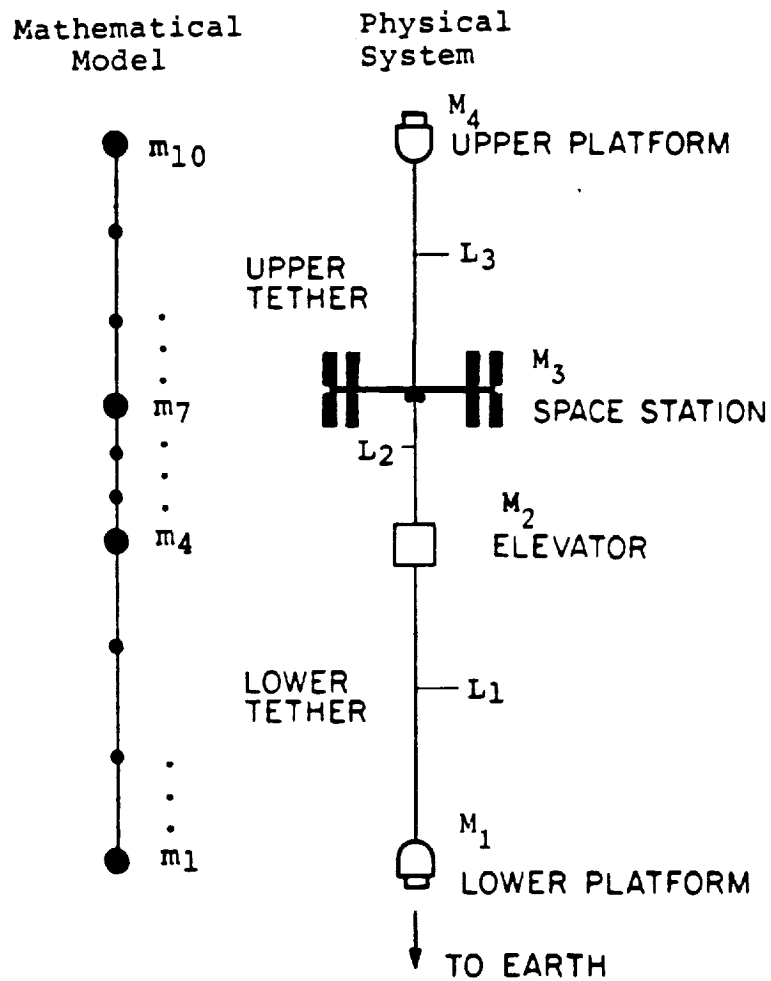


Figure 7.

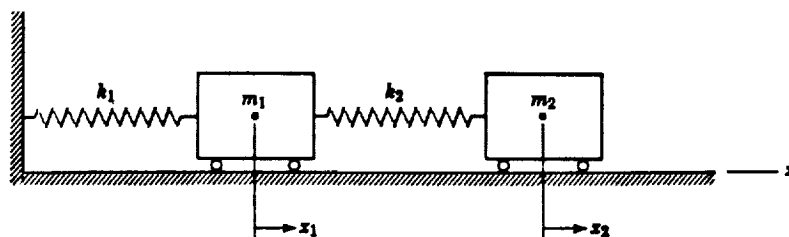


Figure 8.

2.6.1 Acceleration Noise –

A simulation of the DTSSE has been run according to the same assumptions described in Section 2.4.2 with the exception of the initial temperature which has been reduced from 380°K to 335°K in order to be closer to the equilibrium value. In particular, three longitudinal dampers have been added to the system: one for each tether segment. This time, however, it is more complex to compute the bobbing frequencies of the two tether segments above and below the elevator because these two longitudinal DOF's are coupled. Since the station is two orders of magnitude heavier than the other platforms we can reasonably assume that the vibrations of the lower tether are decoupled from the vibrations of the upper tether. The bobbing frequency of the upper tether can be computed, therefore, by assuming that the upper tether is a 1-DOF system. The bobbing frequency of the upper tether is

$$\omega_{03} = \sqrt{EA/(\ell_3 m_{Q3})} \quad (4)$$

where the equivalent mass $m_{Q3} = \left(M_3 + \frac{1}{2} m_{T3}\right) \cdot M_2 / \left(M_3 + M_2 + \frac{1}{2} m_{T3}\right)$ for the mass of the upper tether. The lower tether subsystem (elevator plus end-mass plus two tether segments) can be modelled, with respect to the bobbing oscillations, as a 2-DOF system. Such a system is schematically depicted in Figure 8. The mass m_1 is the elevator and m_2 the end-platform. The stiffnesses of the two

tethers are $k_1 = EA/\ell_1$ and $k_2 = EA/\ell_2$, respectively. The eigenfrequencies and eigenvector of this relatively simple system can be found in any book about multi-DOF-system dynamics. Specifically the eigenfrequencies are given by:

$$\omega_{o,i}^2 = \frac{-b \pm \sqrt{b^2 - 4ac}}{2a} \quad i = 1, 2 \quad (5)$$

where

$$\begin{aligned} a &= m_1 m_2 \\ b &= - \left[m_1 k_2 + m_2 (k_1 + k_2) \right] \\ c &= k_1 k_2 \end{aligned} \quad (6)$$

After solving equation (5) for our system we obtain

$$\begin{aligned} \omega_{o1} &= 0.5395 \text{ rad/s} \\ \omega_{o2} &= 1.3611 \text{ rad/s} \end{aligned} \quad (7)$$

The amplitude ratios between the two components A_i (first DOF) and B_i (second DOF) of the eigenvectors associated with the eigenfrequencies $\omega_{o,i}$ are given by

$$\begin{aligned} r_1 &= \frac{A_1}{B_1} = \frac{k_2 - \omega_{o1}^2 m_2}{k_2} \\ r_2 &= \frac{A_2}{B_2} = \frac{k_2 - \omega_{o2}^2 m_2}{k_2} \end{aligned} \quad (8)$$

After substituting the numerical values of our system we obtain

$$\begin{aligned} r_1 &= 0.3475 \\ r_2 &= -3.1549 \end{aligned} \tag{9}$$

This result implies that the natural longitudinal oscillations of the 1st DOF (the tether segment between EL and SS) are dominated by the second eigenfrequency ω_{o2} . On the other hand, the natural longitudinal oscillations of the 2nd DOF (the tether segment between EL and the end-platform) are dominated by the first eigenfrequency ω_{o1} . In order to dissipate the energy of longitudinal oscillations it is therefore convenient to tune the damper between EL and SS to ω_{o2} and the damper between EL and the end-platform to ω_{o1} . The characteristics of the three dampers are finally as follows:

$$\begin{aligned} \omega_{d1} &= 0.5395 \text{ rad/s} \\ \omega_{d2} &= 1.3611 \text{ rad/s} \\ \omega_{d3} &= 0.4991 \text{ rad/s} \end{aligned} \tag{10}$$

$$\begin{aligned} b_{d1} &= 3,920 \text{ N/(m/s)} \\ b_{d2} &= 3,847 \text{ N/(m/s)} \\ b_{d3} &= 3,457 \text{ N/(m/s)} \end{aligned}$$

where the indexes are referred to Figure 7.

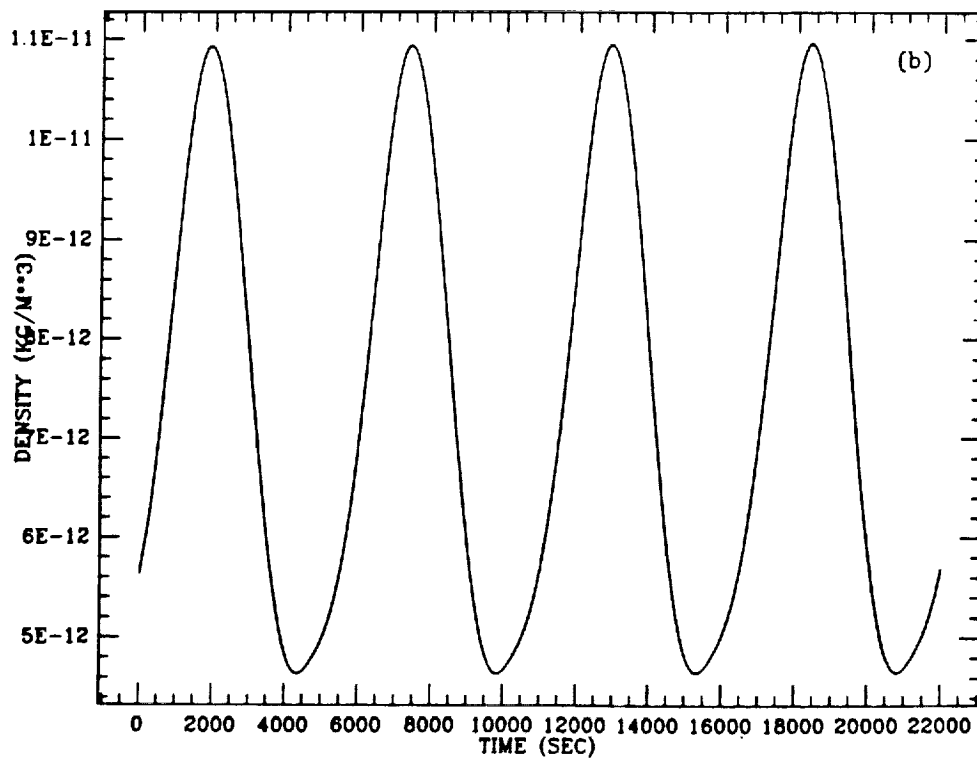
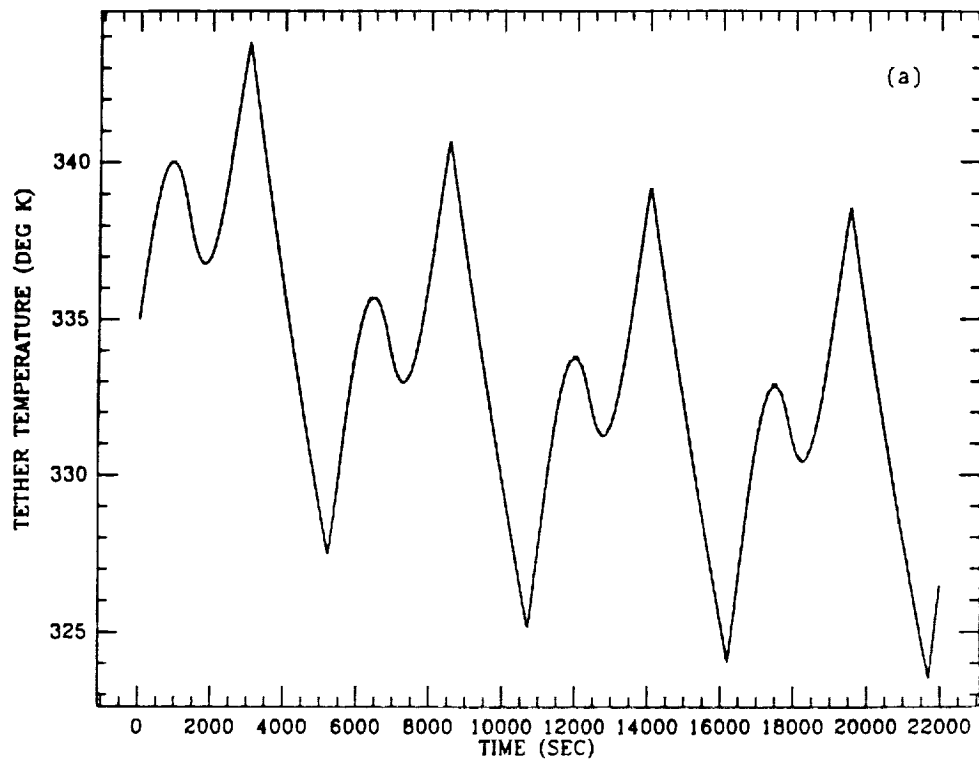
The simulation run lasts 22,000 sec (4 orbits). All the environmental and gravitational perturbations such as air drag, thermal perturbations, and J_2 gravity term are acting upon the system.

Figure 9(a) shows the variation of the atmospheric density over the four orbits caused by the Earth oblateness and by the variation of the local exospheric temperature (diurnal bulge). The latter effect, which has orbital frequency, seems to be dominant.

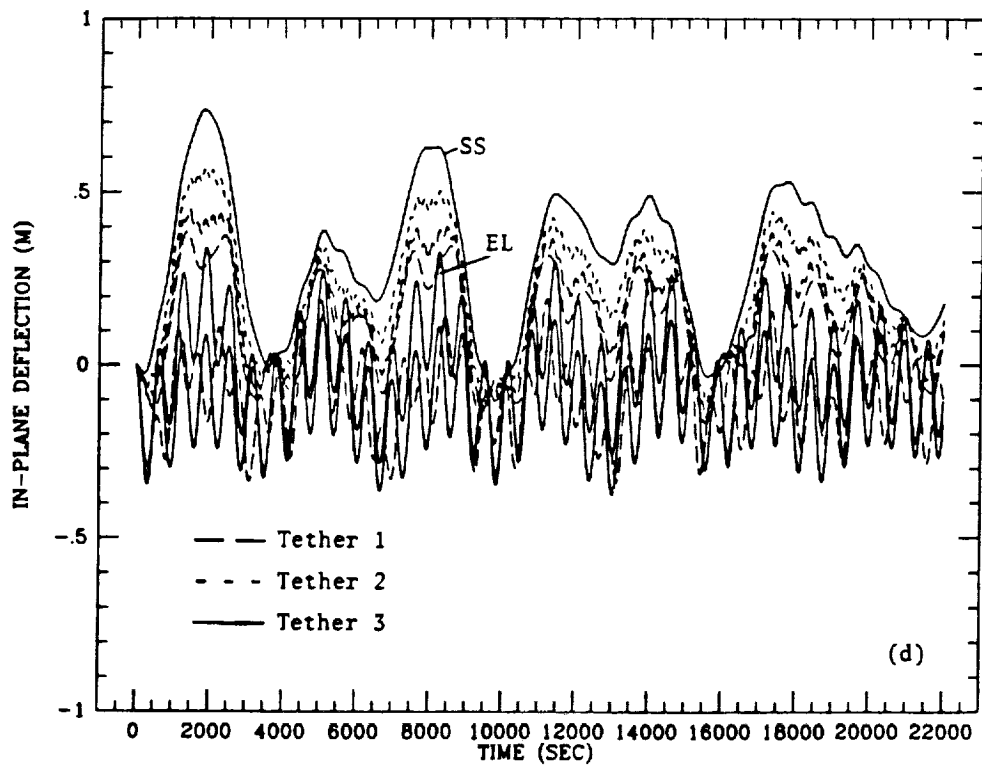
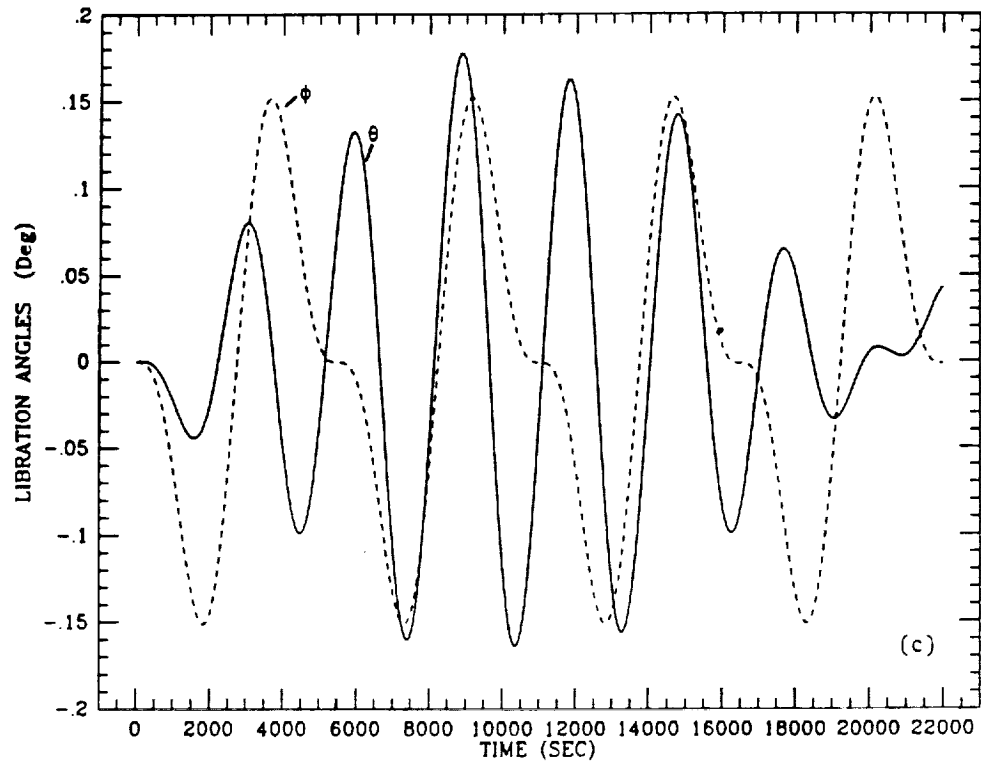
Figure 9(b) shows the temperatures, which are equal, of the three tether segments vs. time. The initial tether temperature is still slightly higher than the steady-state value but the simulation is long enough for the system to reach a thermal steady state after two orbits.

Figure 9(c) shows the in-plane (θ) and out-of-plane (φ) libration angles. Librations are small and are caused by the J_2 gravity term and by air drag. The magnitude of θ and φ are comparable. In particular θ shows an amplitude modulation with a period slightly shorter than four orbits. This is due to a beating phenomenon between the natural frequency $\sqrt{3}\Omega$ and the forcing frequency 2Ω (the angular frequency of the in-plane component of J_2 is equal to 2Ω).

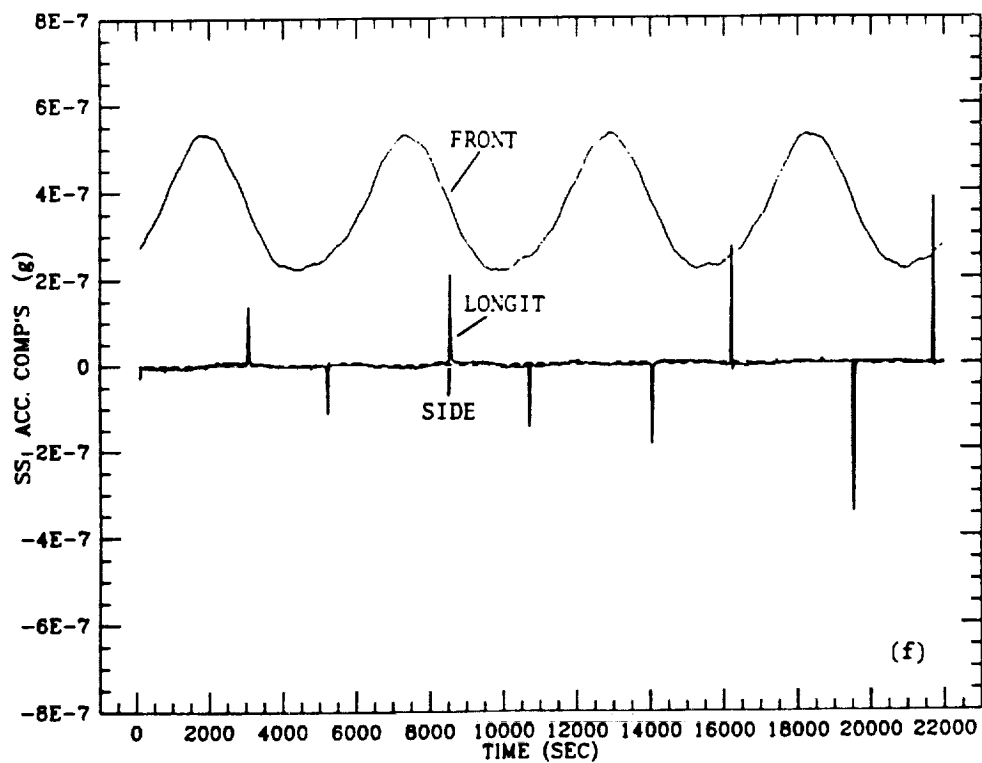
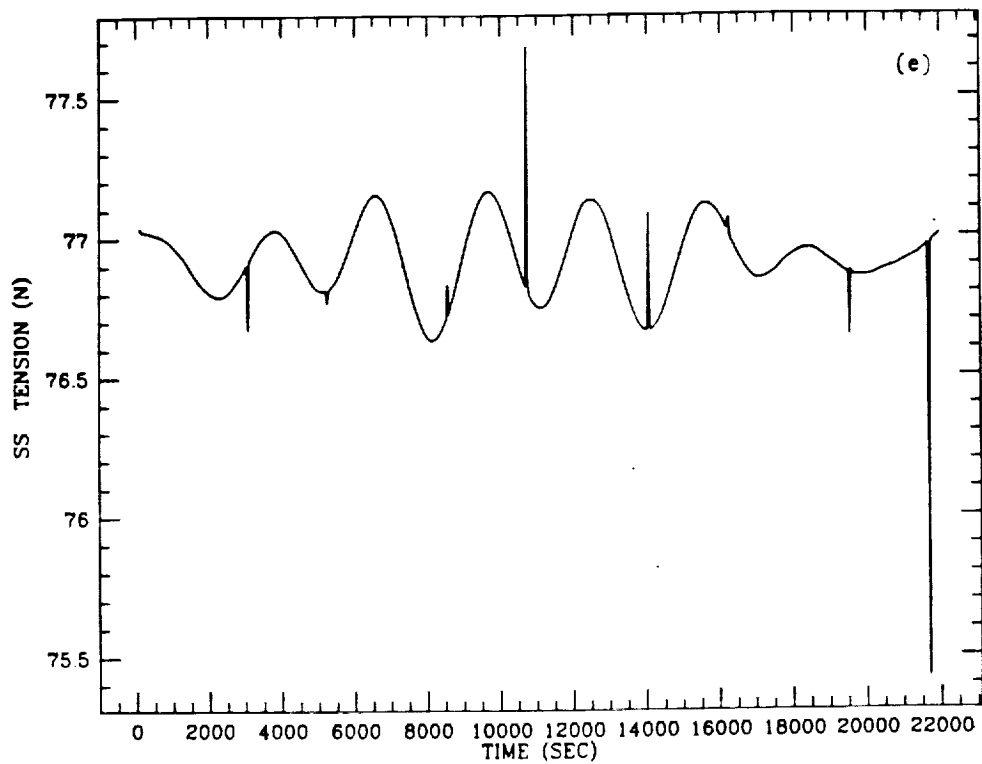
Figure 9(d) depicts the in-plane components of the deflections of the inner lumps with respect to the line through the tip-lumps. The upper and lower



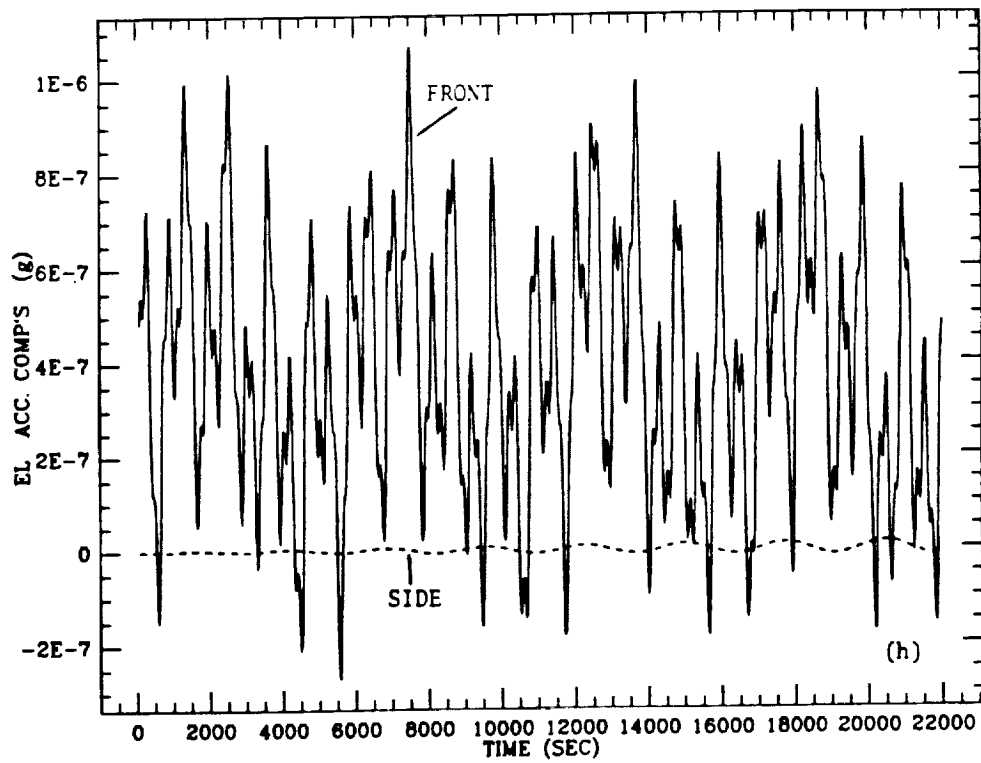
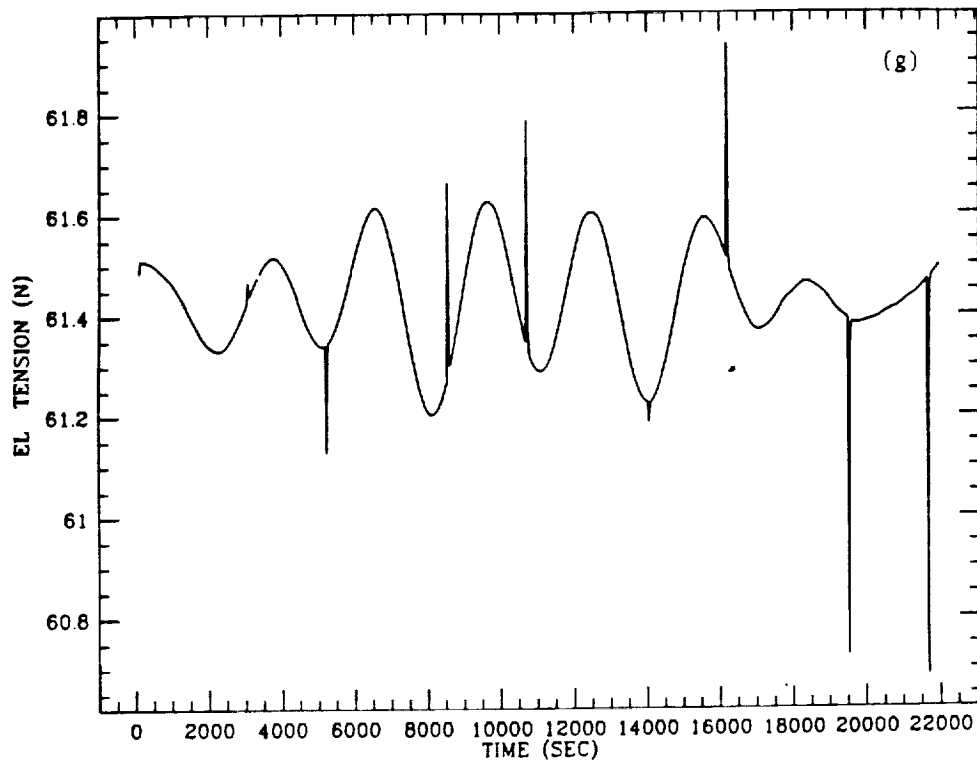
Figures 9(a) and 9(b).



Figures 9(c) and 9(d).



Figures 9(e) and 9(f).



Figures 9(g) and 9(h).

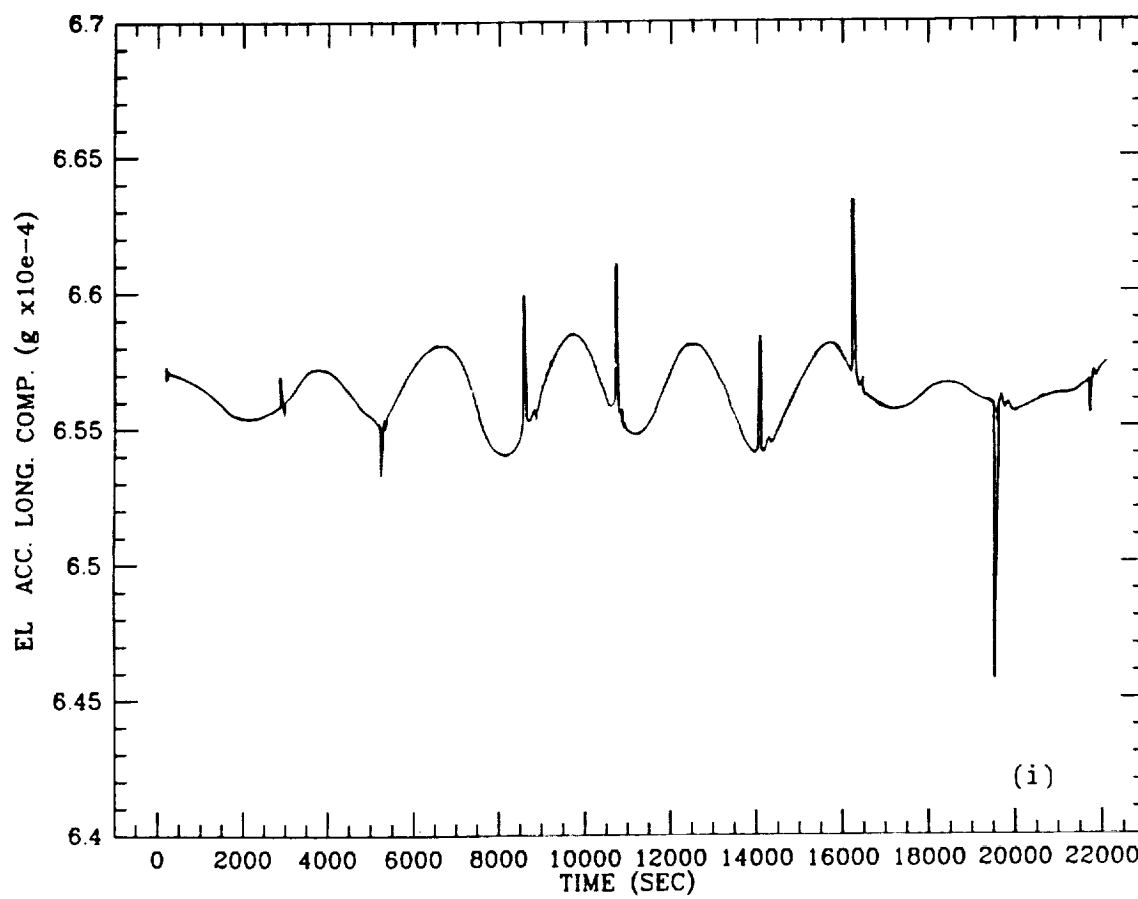


Figure 9(i).

tethers trail the SS because they have smaller ballistic coefficients than the SS. The out-of-plane components of the deflections are negligible.

Figure 9(e) shows the tension at the attachment points of the SS. The tensions at the upper and lower attachment points are almost equal because the SS is at the orbital center. The spikes caused by thermal shocks at the crossings of the terminator are clearly shown in the plot. Figure 9(f) depicts the front, side, and longitudinal components of the acceleration on board the station. The front component is primarily generated by air drag. The side component is negligible. The longitudinal (along the tether) component shows a low frequency component generated by J_2 and the usual thermal spikes. The peak-to-peak fluctuations are about 8×10^{-7} g.

Figure 9(g) shows the tension at the lower attachment point to the elevator. Figure 9(h) depicts the front and side components of the acceleration on board the elevator. Figure 9(i), finally, shows the longitudinal component of the acceleration on board the elevator. The peak-to-peak fluctuations on board the elevator are about 2×10^{-5} g which means that the acceleration fluctuations with respect to the *dc* value (sometimes called the g-quality) are about 10^{-5} g.

2.7 Tethered Dynamic Absorber

2.7.1 Equivalent System -

The acceleration level at the stationary laboratory attached to the station is significantly affected by the structural vibrations of the space station. Since the microgravity experiments are most sensitive to low frequency disturbances, flexural oscillations of the single boom station are potentially a major source of acceleration noise. The frequency of the first flexural harmonic of the station is equal to 0.1 Hz for the 3-m-truss and 0.2 Hz for the 5-m-truss space station. The first flexural harmonic is of particular importance because the through of the deformed transverse boom coincides with the location of the stationary gravity laboratory.

The magnitudes of the expected maximum amplitudes of the station's flexural modes have not been computed thus far. For the sake of our computations we have assumed a 10^{-2} m maximum deflection for the first flexural mode. The maximum values of acceleration consistent with the above amplitude are 4×10^{-4} g for the 3-m-truss and 1.6×10^{-3} g for the 5-m-truss station. It is clear from these values of accelerations that the abatement of the first flexural mode of the station is of fundamental importance for the microgravity experiments. A $\sim 10^{-3}$ g level at $\sim 10^{-1}$ Hz is strong enough to disrupt microgravity processes such as protein crystal growth, vapor crystal growth, and solution crystal growth [2].

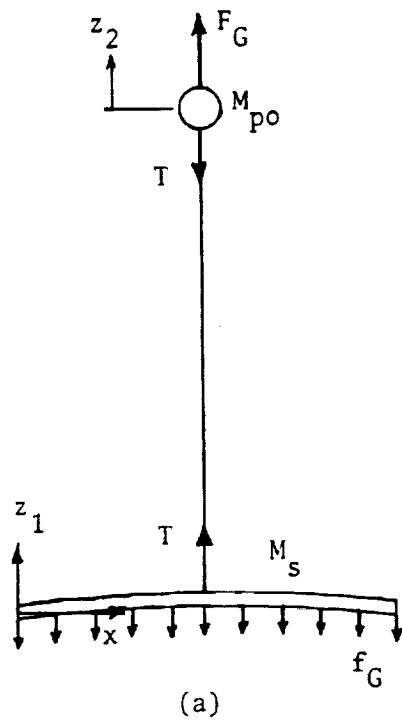
These considerations prompted us to investigate the capability of a tethered system in damping the first flexural mode of the station. Specifically the bobbing mode of the tethered system can be used to attenuate or damp the flexural mode. The system under investigation is formed by the station vibrating according to the first flexural mode in the vertical plane, a tether and an end-platform [see Figure 10(a)]. This system is a 2-DOF system which can be reduced to a classic two masses, two springs oscillating system [see Figure 10(b)]. First we must compute the equivalent mass of a point mass space station which vibrates with the same energy, frequency, and amplitude of the first flexural mode.

In order to compute the energy of the first flexural mode we assume that the station is a homogenous beam of length L vibrating freely. The modal shapes, after removing the rigid body translations, are given by [3]:

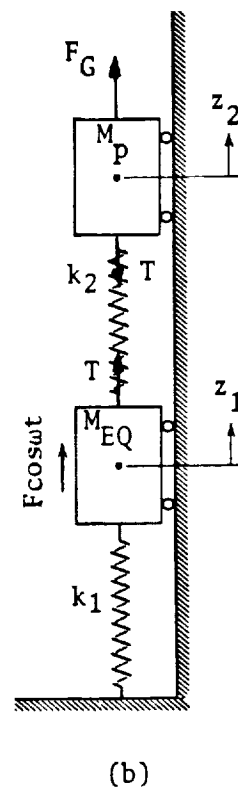
$$Z = C_1[\cos(kx) + \cosh(kx)] + C_3[\sin(kx) + \sinh(kx)] \quad (11)$$

For the first mode of a beam with free ends we have:

Physical System



Equivalent Model



Figures 10(a) and 10(b).

$$C_1/C_3 \simeq -1$$

$$k = k_1 = \frac{3\pi}{2L} \quad (12)$$

Consequently the vertical displacement of the first mode is given by

$$z \simeq C_1 [\cos(k_1 x) + \cosh(k_1 x) - \sin(k_1 x) - \sinh(k_1 x)] \sin(\omega_1 t) \quad (13)$$

where $\omega_1 = 2\pi f_1$ is the angular frequency of the first mode and where we have assumed that $t = 0$ when the beam is straight. For $t = 0$ the energy is all kinetic and it is given by

$$E = \frac{1}{2} \mu \int_0^L \dot{z}_o^2 dx \quad (14)$$

where \dot{z}_o is the velocity for $t = 0$ given by:

$$\dot{z}_o = \omega_1 Z \quad (15)$$

After substitution of equation (15) into equation (14) and after computing several integrals of trigonometric and hyperbolic functions we obtain:

$$E = \frac{1}{2} \omega_1^2 C_1^2 M_s \left(1 + 1/\pi \right) \quad (16)$$

where M_S is the total mass of the station. On the other hand, the energy of the point mass station with mass M_{EQ} vibrating at the same angular frequency ω_1 and with amplitude A is given by:

$$E_{EQ} = \frac{1}{2} \omega_1^2 A^2 M_{EQ} \quad (17)$$

The maximum oscillation amplitude at the center of the homogeneous beam $Z_{L/2}$ is given by:

$$Z_{L/2} = C_1 \left[\cos\left(\frac{3}{4} \pi\right) + \cosh\left(\frac{3}{4} \pi\right) - \sin \frac{3}{4} \pi - \sinh\left(\frac{3}{4} \pi\right) \right] = 1.32 C_1 \quad (18)$$

If we equate the energies of the two systems with equal maximum oscillation amplitudes, that is $Z_{L/2} = A$, we finally obtain

$$M_{EQ} = 0.757 M_S \quad (19)$$

Since the frequencies of the two systems are also the same we have that the stiffness of the first spring of the equivalent system [see Figure 10(b)] is:

$$k_1 = M_{EQ} \omega_1^2 = 0.757 M_S \omega_1^2 \quad (20.1)$$

and the stiffness of the second spring is

$$k_2 = M_P \omega_2^2 \quad (20.2)$$

In Figure 10(b) F_G is the gravity gradient force, which is assumed to be static, and $F = \cos(\omega t)$ is a generic perturbation force.

2.7.2 System Dynamics –

The equations of motion of the equivalent system of Figure 10(b) can be found in any book of dynamics of multi-DOF systems. In particular the displacement of the equivalent station M_{EQ} and the end-mass M_P are respectively given by:

$$z_1 = \frac{F}{k_1} \left[1 - \left(\frac{\omega}{\omega_2} \right)^2 \right] / D + \frac{F_G}{k_1} \quad (21.1)$$

$$z_2 = \frac{F}{k_1} / D + F_G \frac{k_1 + k_2}{k_1 k_2} \quad (21.2)$$

and

$$D = \left[1 + \mu \left(\frac{\omega_2}{\omega_1} \right)^2 - \left(\frac{\omega}{\omega_1} \right)^2 \right] \left[1 - \left(\frac{\omega}{\omega_2} \right)^2 \right] - \mu \left(\frac{\omega_2}{\omega_1} \right)^2 \quad (21.3)$$

where $\mu = M_P/M_{EQ}$ is the mass ratio, ω_1 is the angular frequency of the station and ω_2 of the end-platform.

For $\omega_2 = \omega$ the oscillation of the station ceases. The tethered system acts as a dynamic absorber. In this case the displacement of the end-mass is

$$z_2 = -\frac{F}{k_1} \left(\frac{\omega_1}{\omega_2} \right)^2 / \mu + \frac{F_G}{k_1} \left[1 + \left(\frac{\omega_1}{\omega_2} \right)^2 \right] / \mu \quad (22)$$

where $F/k_1 = \xi_{SF}$ and $F_G/k_1 = \xi_{SG}$ are simply the static deflections associated with the forces F and F_G .

It seems, therefore, that a tether system can in principle attenuate the first flexural mode of the station and that it can be easily tuned to the desired frequency by simply varying the steady-state tether length. In reality the avoidance of tether slackness poses a strong constraint to the design of a tethered dynamic absorber.

The tether tension T [see Figure 10(b)] is proportional to $z_2 - z_1$. Hence for $T = 0$ and for a dynamic absorber with $\omega_2 = \omega$ we must have:

$$[z_2 - z_1]_{\omega=\omega_2} = \frac{F_G - F}{k_1} \left(\frac{\omega_1}{\omega_2} \right)^2 / \mu = 0 \quad (23)$$

where

$$F_G = 3M_p \Omega^2 \ell \quad (24)$$

In equation (24) ℓ is the tether length and M_p is the effective mass of the tethered

system which takes into account the tether mass and the platform mass as follows [4]:

$$M_p = M_{p_0} + \frac{1}{2}\mu\ell \quad (25)$$

where M_{p_0} is the mass of the platform and μ the linear density of the tether.

From equation (23) we compute the minimum effective static moment $M_p\ell$ which provides a null tether tension. From equations (20.1), (23) and (24) we obtain

$$M_p\ell = \frac{0.757}{3} \xi_{SF} M_s \left(\frac{\omega_1}{\Omega} \right)^2 \quad (26)$$

where ξ_{SF} is the amplitude of the oscillations (i.e. non related to gravity gradient) of the station's first flexural mode. It is worth noticing that the minimum effective static moment $M_p\ell$ is independent of the frequency $\omega = \omega_2$.

2.7.3 Numerical Results –

An important example is the utilization of the dynamic absorber for damping the station first flexural mode at the resonant frequency ω_1 . In this case the bobbing frequency of the tethered vibration absorber ω_2 is tuned to ω_1 and we have

$$EA = \omega_1^2 M_p \ell \quad (27)$$

where EA is the tether stiffness. The tether linear density μ is also related to the tether cross section A and to the volume density ρ by:

$$\mu = \rho A \quad (28)$$

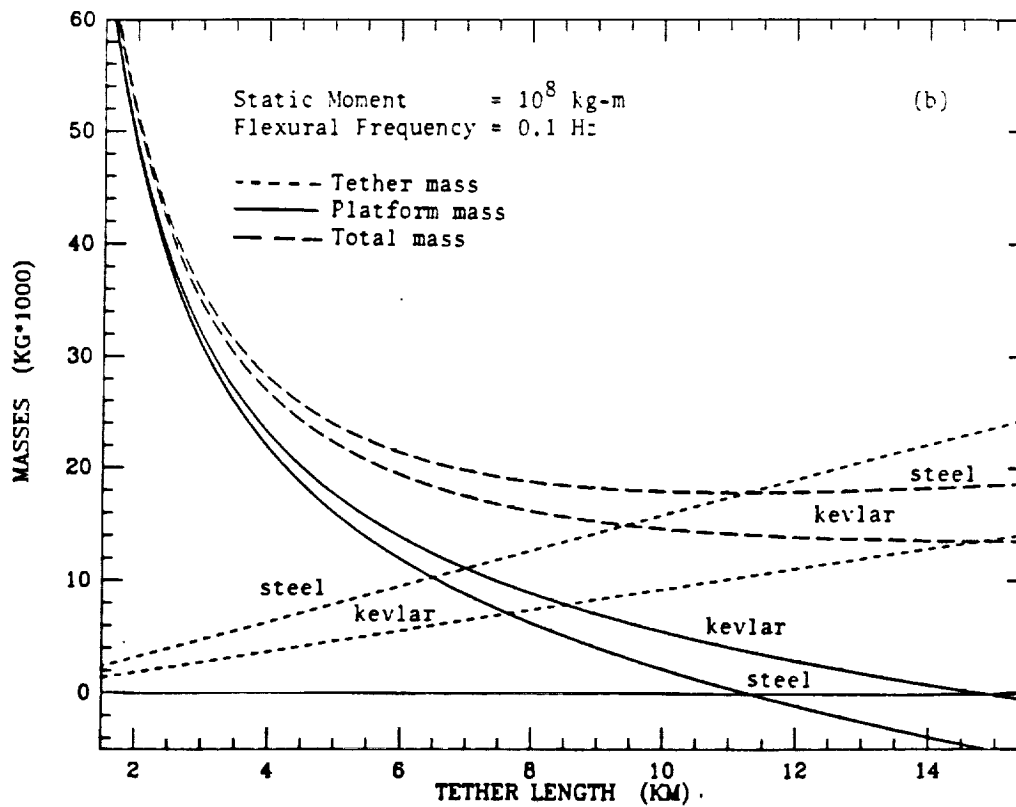
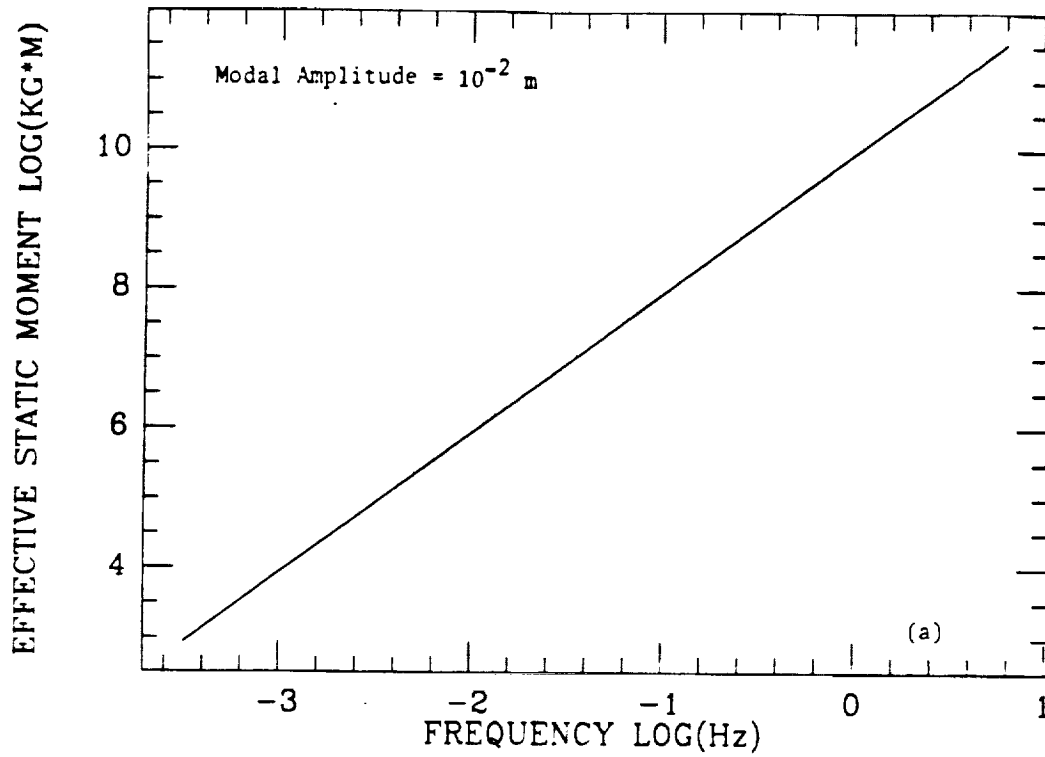
For a tether of given intrinsic characteristics E and ρ we can therefore evaluate the mass of the platform M_{po} and the tether linear density μ as a function of ω_1 and of ξ_{SF} by means of equations (25), (28), (29), and (30). For a numerical example we adopt an oscillation amplitude of the station $\xi_{SF} = 10^{-2}$ m, and an orbital rate $\Omega = 1.14 \times 10^{-3}$ rad/s (orbital altitude = 352 km).

Figure 11(a) shows the effective static moment $M_p \ell$ vs. the frequency $f_1 = \omega_1/(2\pi)$. For the resonant frequencies of the proposed configurations of the single-boom station, 0.1 Hz or 0.2 Hz, the minimum effective static moment must

be at least 10^8 kg-m. By utilizing equations (25), (29), and (30) we can design the tethered dynamic absorber. If we adopt a kevlar tether with $E = 6.2 \times 10^{10}$ N/m², $\rho = 1440$ kg/m³ from equation (29) we have that the tether diameter $d = 28.5$ mm. For a steel tether with $E = 20 \times 10^{10}$ N/m², $\rho = 8 \times 10^3$ kg/m³ we obtain $d = 15.8$ mm.

From equations (25) and (30) we compute the mass of the platform M_{po} and of the steel or kevlar tether m_T vs. the tether length. Figures 11(b) shows the mass of the platform, of the tether, and the total mass of the absorber respectively for kevlar or steel tethers. The numerical results point out that a tethered dynamic absorber for the station is quite massive. Convenient tether lengths range between 5 and 10 km with total masses ranging from 24 to 14.6 metric tons. Kevlar tethers are more convenient from a mass point of view. For a 10-km-long kevlar tether, for example, $M_{po} = 5400$ kg, $m_T = 9200$ Kg and the total mass of the dynamic absorber M_{TOT} is 14600 kg. For a 10-km-long steel tether we have, instead, $M_{po} = 2110$ kg, $m_T = 15780$ kg and $m_{TOT} = 17890$ kg.

The dynamic absorber is purely passive. Its ability to attenuate the flexural oscillations of the station is based upon an energy transfer from the vibrating station to the absorber which takes place when the device is tuned to the frequency to be abated. That energy however remains in the absorber unless a damping mechanism is added to the system. The additional damper may simply be implemented by controlling the tether length with a proportional derivative



Figures 11(a) and 11(b).

control law or by inserting a spring-dashpot system between the station and the tether. The mathematics of the system becomes more complex but the results of this analysis do not add much to the design of the absorber except for the additional computation of the damper's damping coefficient.

One final concern. Since the tethered dynamic absorber is massive, it causes a non-negligible shift of the overall system *CM* and hence a non-negligible *dc* value of the acceleration at the stationary gravity laboratory. A dynamic absorber with a 10^8 kg-m static moment produces a *CM* shift of 500 m which corresponds to a *dc* acceleration of 2×10^{-4} g. In order to neutralize this effect an equal-static-moment tethered system should be deployed on the opposite side of the station. The two systems together form a Double Tethered Centered System (*DTCS*) with dimensions somewhat different from the *DTCS* described in Section 2.4. The tethered system opposite to the dynamic absorber should be detuned from the flexural modes of the station. A lower bobbing frequency (tether softer and thinner than the dynamic absorber's tether) is recommended so that the vibrations of the station are attenuated before reaching the end-platform (on this subject see also reference [5] for further detail).

2.8 References

1. Cosmo, M., E.C. Lorenzini, S. Vetrella and A. Moccia, "Transient Dynamics of the Tether Elevator/Crawler System." In Proceedings of the 1988 AIAA/AAS Astrodynamics Conference, Minneapolis, MN, 15-17 August 1988.
2. Sharpe, A. (Ed.), "Low Acceleration Characterization of Space Station Environment." Teledyne Brown Engineering, Final Report for NASA/MSFC Contract NAS8-36122, Mod. 6, October 1985.
3. Timoshenko, S., D.H. Young, W. Weaver Jr., "Vibration Problems in Engineering." John Wiley and Sons.
4. Baker, W.P., et al., "Tethered Subsatellite Study." NASA TMX-73314, March 1976.
5. Gullahorn, G.E. and R.G. Hohlfeld, "Tether as a Dynamic Transmission Line." Space Tethers for Science in the Space Station Era, L. Guerriero and I. Bekey (Eds.), Società Italiana di Fisica, Conference Proceedings, Vol. 14, Bologna, Italy, 1988, pp. 163-168.

3. CONCLUSIONS

The analysis carried out on the proposed tethered systems for the active control of the center of gravity of the space station shows that all the three configurations meet the microgravity requirement (10^{-5} g) for the acceleration level on board the station. Specifically in order to meet that requirement over a large number of orbits each system must be equipped with longitudinal dampers in series with the tether segments. Each damper may simply be a spring-dashpot system (the dampers' stretches for the three systems are at most a few-centimeter-long) tuned to the bobbing frequency of the associated tether segment. The dampers rapidly abate the longitudinal tether oscillations excited by thermal shocks ensuing the crossings of the terminator.

The tether-related acceleration noise on board the station for the three tether systems is generated primarily by thermal shocks. On the other hand, the air drag, which is responsible for the front component of the acceleration, is mainly related to the frontal area of the station while the contributions of the tethers' cross sections are marginal.

If longitudinal dampers are adopted the maximum acceleration level on board the station for the Double Tethered System with and without the Elevator is less than 10^{-6} g. The performance of the Single Tether System with respect to tether-related acceleration noise is even better since the maximum fluctuations of the longitudinal acceleration component around the *dc* value are of the order of

10^{-5} g. A light and short tethered system is, in fact, less influenced by thermal shocks.

Finally the acceleration fluctuations (g-quality) on board the elevator of the Double Tethered System are about 10^{-5} g.

In conclusion the acceleration levels on board the station for the three proposed configurations are well within the 10^{-5} g requirement if longitudinal dampers are added to these systems. The g-quality on board the elevator for the Double Tether System with Elevator is comparable to the g-quality of the microgravity laboratory attached to the station.

From previous experience the tether-related acceleration noise on the station and the elevator can be further improved if softer tethers are used. This implies the usage of tether materials with moderate values of the Young modulus and moderate tether diameters. Since the selection of the tether diameter is driven by the survivability of the tether to micrometeoroid impacts, the evaluation of the probability of tether failure must be carefully estimated in order not to oversize the tethers.

A Tethered Dynamic Absorber can abate the space station's first flexural mode. However, for a modal frequency of 0.1 Hz (3-m-truss station) and a modal amplitude of 10^{-2} m the total mass of a 10-km-long kevlar-tether dynamic absorber is about 14.6 metric tons in order to avoid tether slackening. Since this

system has a strong static moment it requires a compensating tethered system on the opposite side of the station. The end result is a Double Tethered System in which one side, tuned to the flexural mode of the station, is the Dynamic Absorber, while the other side is detuned from the flexural oscillations.

For frequencies lower than 0.1 Hz the mass required for a Dynamic Absorber decreases strongly because the minimum static moment is inversely proportional to the square of the frequency. It seems therefore that a Dynamic Absorber becomes much more desirable if it will be proven that low frequency (< 0.1 Hz) flexural oscillations are excited during the mission of the single-boom space station.

